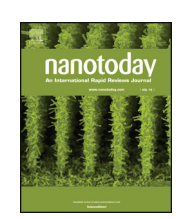
ELSEVIER

Contents lists available at ScienceDirect

Nano Today

journal homepage: www.elsevier.com/locate/nanotoday



Review

Two-dimensional transition metal dichalcogenide hybrid materials for energy applications



Nitin Choudhary^a, Md Ashraful Islam^{a,b}, Jung Han Kim^a, Tae-Jun Ko^a, Anthony Schropp^a, Luis Hurtado^a, Dylan Weitzman^a, Lei Zhai^{a,c,d,*}, Yeonwoong Jung^{a,b,c,*}

- ^a NanoScience Technology Center, University of Central Florida, Orlando, FL, 32826, USA
- ^b Electrical and Computer Engineering, University of Central Florida, Orlando, FL, 32826, USA
- ^c Materials Science and Engineering, University of Central Florida, Orlando, FL, 32826, USA
- d Department of Chemistry, University of Central Florida, Orlando, FL, 32826, USA

ARTICLE INFO

Article history: Received 20 September 2017 Received in revised form 8 January 2018 Accepted 20 February 2018 Available online 7 March 2018

Keywords:
2D transition metal dichalcogenide
2D material
TMD
Hybrid material
Energy generation
Energy storage

ABSTRACT

Two-dimensional transition metal dichalcogenides (2D TMDs) possess a rich set of extraordinary structural, chemical, electrical, and optical properties unattainable with any traditional materials. A large number of these properties are particularly suitable for energy generation/conversion applications, which renders unprecedented yet tremendous opportunities for addressing the multi-faceted demands of up-coming energy technologies. Heterogeneously integrating 2D TMDs with other energy materials is projected to improve the performance of existing energy devices and/or achieve unconventional functionalities in a highly synergic manner, which cannot be catered by stand-alone 2D TMDs. In this article, we present a comprehensive review on the up-to-date progress in the development of 2D TMD hybrid materials for a variety of energy applications. This review focuses on addressing how the incorporation of 2D TMDs can help manipulate the functionalities of conventional energy materials to achieve targeted and improved energy device performances. An overview of the recent progress in the development of various 2D TMD hybrid materials and their fabrication strategies is presented, followed by a survey on various energy devices based on these materials and their performance comparison. Current challenges associated with material developments are discussed, and forward-looking outlooks assessing unexplored research areas are also suggested.

© 2018 Elsevier Ltd. All rights reserved.

Contents

Introduction	I b
Classification and fabrication of 2D TMD hybrid energy materials	18
2D TMD-based inorganic hybrids	
2D TMD-based organic hybrids	23
Energy applications of 2D TMD hybrid materials	
Energy generation	
Energy storage	
Conclusion and outlook.	34
Acknowledgement	
References	

Introduction

Two-dimensional (2D) transition metal dichalcogenides (TMDs) extracted from their intrinsically-layered mother crystals has been known for over several decades, but their technological potential has remained unrecognized until the discovery of unique

E-mail addresses: lzhai@ucf.edu (L. Zhai), yeonwoong.jung@ucf.edu (Y. Jung)

^{*} Corresponding authors at: NanoScience Technology Center, University of Central Florida, Orlando, FL, 32826, USA.

material properties in 2D carbon allotrope 'graphene' [1-4]. Since then, 2D TMDs represented by MX₂ (M: transition metals; Ti, Zr, Nb, Mo and W. X: chalcogens; S, Se, and Te) have experienced a drastic resurgence as they were identified to possess a rich set of superior properties like graphene as well as some exotic functionalities beyond graphene and any traditional materials [5-7]. This extraordinary attribute bestows tremendous yet unprecedented opportunities for a variety of applications encompassing electronics, optoelectronic, and energy [8-11]. Unlike graphene, 2D TMDs exhibit substantial energy bandgaps and semiconducting carrier transports, allowing for large ON/OFF current ratios suitable for digital electronics [12,13]. Quantum confinement and reduced coulombic charge screenings owing to 2D dimensionality allow for unusual excitonic effects, leading to strong light-matter interactions and ultrafast optoelectronic responses [14,15]. Electronic band structures of 2D TMDs can be externally tailored by applying mechanical stress to 2D layers and/or by varying their 2D layer numbers [16,17]. Moreover, 2D TMDs display various material properties and distinct structural advantages suitable for energy applications, such as electrically/opticallyand/or thermally-driven energy generation (e.g., photovoltaics (PVs) and thermoelectrics (TEs)) and electrochemically-driven energy conversion/storages (e.g., batteries and supercapacitors) [18-22]. For example, some 2D TMDs present indirect-to-direct transitions of bandgap energies and significant photon absorptions in the near infrared-to-visible frequency regime. Such tunable optical/electrical properties coupled with their intrinsically large in-plane strain limits can project unique opportunities for mechanically deformable multi-junction PV devices of unconventional form factors [23,24]. Anisotropic 2D crystallinity accompanying strong in-plane intra-layer covalent bonding and weak inter-layer van der Waals (vdW) attraction is another critical attribute for energy applications [25,26]. Such structural uniqueness results in the large surface area of adjoining 2D TMDs with numerous sub-nanometer vdW gaps, which provides pathways to efficiently absorb charged species and intercalate ions from electrolytes in energy storage/conversions [27,28]. Additionally, 2D layer edge sites with unsaturated charge valences and dangling bonds can be utilized as highly active catalytic centers for hydrogen evolution reactions (HERs) [29,30].

Beyond the aforementioned exotic material properties and structural advantages, 2D TMDs offer great opportunities for developing unconventionally functional materials to address the multi-faceted demands of up-coming energy technologies. Rationally integrating 2D TMDs with other energy materials can improve the performance of existing energy devices and/or achieve unconventional functionalities which cannot be catered by stand-alone 2D TMDs only. 2D TMDs can be facilely exfoliated and isolated from their mother crystals owing to their weak inter-layer vdW attraction and be heterogeneously assembled with other materials of distinct dimensions/functionalities by various physical/chemical manners. For example, they can be integrated with a wide range of inorganic/organic materials including noble metals, metal oxides, and carbonaceous nanomaterials in various forms of alloyed composites and hierarchical 3D structures [31–34]. The driving motivation is to mitigate the inherent weakness of each participating material by compensating for their material properties, thus achieving novel and improved functionalities which are not attainable in their mono-component counterparts. For example, noble metals such as platinum (Pt), palladium (Pd), and ruthenium (Ru) are well known for their superior catalytic activity, but their high cost restricts practical applications. 2D TMDs with highly exposed 2D layer edges with ample dangling bonds/defective sites present high chemical reactivity which can be employed to reduce the consumption of the noble metals, circumventing the cost issue [35-37]. Carbonaceous 2D materials such as metallic graphene are gaining substantial interests in electrical and optical applications owing to their extremely high carrier mobility and mechanical flexibilities. Integrating semiconducting 2D TMDs with metallic graphene will lead to new PV Schottky junctions which can accompany the tunable optical absorption of 2D TMDs and facile charge separation from graphene [38,39]. Similarly, stacking up 2D TMDs of distinct components or modulated carrier types (p- or n-) can achieve ultrathin p-n junctions which can easily separate photo-excited electron-hole pairs (e⁻-(h)⁺) for enhanced photon energy harvesting in ultrathin PV devices [15,40,41]. Moreover, combining 2D TMDs with conjugated polymers will find niche applications in various energy storage/production, which benefits from outstanding mechanical flexibility, tunable electrical/chemical activity, and ease of material synthesis inherent to both the materials [42,43]. The scheme in Fig. 1 overviews the applications of 2D TMD hybrids in current and future energy technologies. Intrinsically exotic physical/chemical properties inherent to 2D TMD hybrids include superior optical absorption, tunable band gaps, enriched catalytic sites, and controllable charge carrier transports which are unattainable in their monolithic counterparts. These hybrid materials have already set new paradigms for the applications in energy storage (lithium-ion batteries (LIBs), supercapacitors, sodium-ion batteries) and energy generation (PVs, TEs, hydrogen storage). Moreover, hierarchically-structured large-scale 2D TMDs combined with organic/inorganic materials present an ideal combination of mechanical flexibility with tailored electrical and electrochemical properties, offering unprecedented opportunities for future stretchable, wearable and integrated energy

Considerable efforts have been devoted in developing viable synthesis/integration methodologies to achieve the optimum material properties of 2D TMD hybrids for targeted energy applications. Besides the reliable fabrication of 2D TMDs themselves, it is imperative to precisely control their dimensional and morphological coherency by incorporating new materials to ensure the structural/chemical stabilities at their interfaces. Various approaches have been explored by considering the physical/chemical natures of participating materials. Integrating 2D TMDs with carbonaceous nanomaterials (graphene or carbon nanotubes (CNTs)) were initially pursued with mechanical, liquid-assisted exfoliation and dispersions [44–46]. However, the demerits associated with these approaches such as non-uniform material coverage and uncontrolled interfacial morphologies require the development of more reliable strategies such as chemical or physical vapor deposition (CVD or PVD) which enable the sequential integration of one material onto the other [47,48]. Hydrothermal approaches such as solvothermal or one-pot/twostep hydrothermal processes were used to integrate 2D TMDs with noble metals and metal oxide nanoparticles benefiting from their intrinsic scalability of producing large quantity 2D crystals [49,50]. Hybridizations of conjugated polymers incorporating morphologysorted 2D TMDs were also pursued via in-situ and/or ex-situ manners [51–53].

In this review, we provide a comprehensive survey on up-to-date research of 2D TMD hybrid materials for energy applications. The focus of the review addresses how the incorporation of 2D TMDs can help manipulate the functionalities of conventional energy materials to achieve targeted performances in energy generation/storage applications. First, an overview of the recent progress and development of 2D TMD hybrid materials which incorporates a wide range of organic/inorganic materials as well as present their fabrication/integration methodologies. Performance comparisons are made with conventional materials in a variety of energy devices, emphasizing the opportunity and potential of these hybrid approaches in terms of achieving novel functionalities and improved energy efficiencies. Current challenges associated

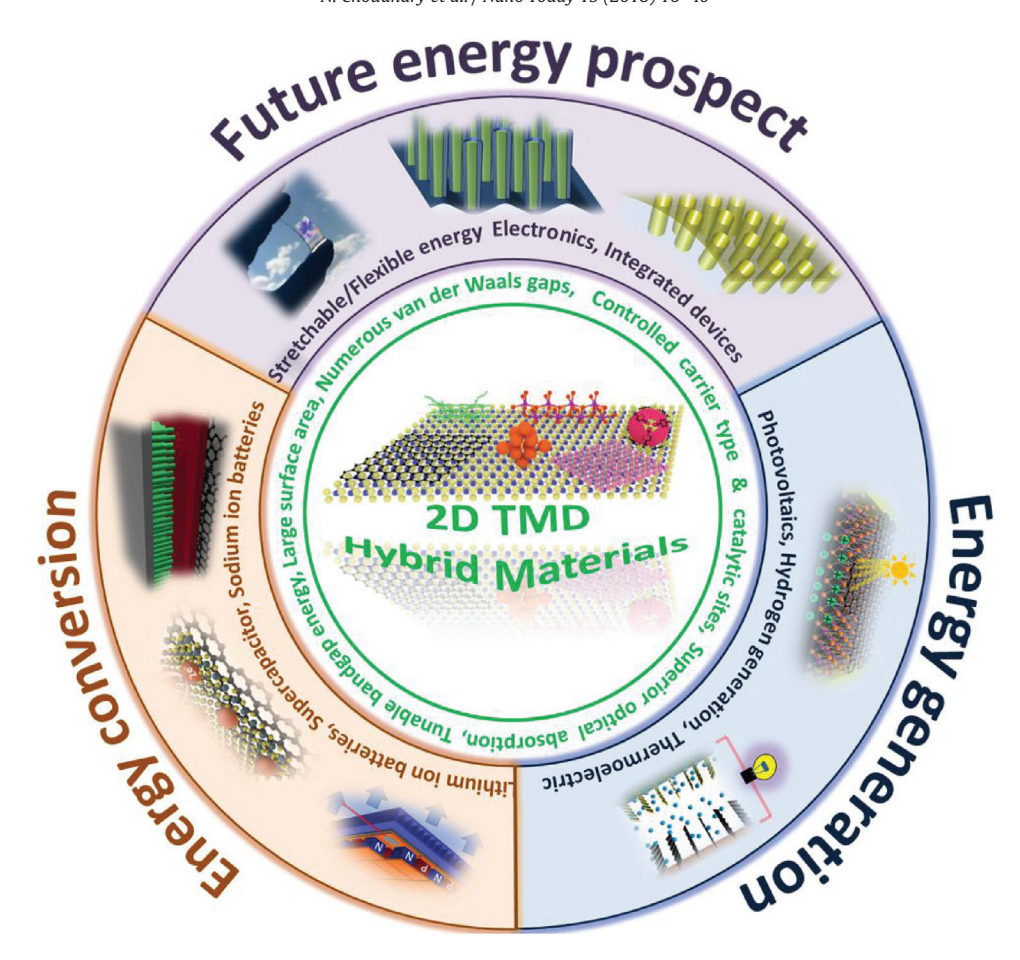


Fig. 1. Schematic illustration of 2D TMD hybrid materials for current energy applications and their prospect for future energy technologies.

with material development and forward-looking outlooks assessing unexplored research areas will also be suggested.

Classification and fabrication of 2D TMD hybrid energy materials

2D TMD hybrid materials can be broadly classified into two categories depending on the types of the materials to be incorporated with 2D TMDs; i.e., 2D TMD/inorganic hybrids, and 2D TMD/organic hybrids. The inorganic 2D TMD counterparts include noble metals, metal oxides, and metal chalcogenides, while the organic materials comprise conjugated polymers, carbonaceous nanomaterials, and metal organic frameworks (MOFs). Material components to be incorporated with 2D TMDs are determined by considering their intrinsic physical/chemical properties and projected functionalities after the incorporation as well as their mechanical stabilities upon interfacing with 2D TMDs. Depending on the type of constituting organic/inorganic components, their physical/chemical structures and the interaction/reaction mechanisms of binding with 2D TMDs vary. In most of 2D/2D hybrids such as TMD/TMD, TMD/graphene, and TMD/2D metal oxides, the interfacial interaction is dictated by the weak vdW forces which hold the atomic layers of distinct 2D materials together. In addition to the vdW attraction inherent to 2D materials, bindings of 2D TMDs with non-2D components were extensively pursued through various chemical functionalization methods [35,54]. For example, polymers, metal nanoparticles, and metal oxides covalently or non-covalently decorated 2D TMDs. Such functionalization/decorations were observed to preferably occur at the edges of 2D TMD layers rather than their chemically inert basal planes [55]. However, it is also noted that the intrinsic defects and impurities (e.g. sulfur vacancies or point defects) on 2D

TMD basal planes can also provide preferred binding sites for their interfacial covalent/ionic bonding with foreign materials [56]. In essence, further investigations are required to unveil the detailed interface chemistries behind the binding mechanism of 2D TMDs with various materials.

Successful integrations of 2D TMDs with inorganic/organic materials have been accomplished by a variety of physical/chemical methods and their combinatorial approaches. The physical methods include mechanical exfoliation/assembly, solution mixing, and physical deposition (sputtering and evaporation), whereas chemical methods employ in-situ reduction, hydro(solvo) thermal synthesis, high temperature calcination, chemical vapor transport, and surface-functionalization/anchoring. The application/versatilities of 2D TMD hybrids are strongly determined by the fabrication/integration methods of choice which significantly determine their material properties, qualities, and morphologies. For example, mechanical exfoliation methods generally produce structurally intact, high-quality 2D basal plane crystals which are most suited for fundamental electrical/optical researches. Liquid-phase exfoliation methods are desirable for the scalable integrations of 2D TMDs with various 2D or non-2D components. Accordingly, they are suitable for large-scale energy storage applications which do not require high charge carrier mobility in comparison to electronics-based applications. Meanwhile, they can often result in unwanted chemical functionalization and phase modifications in 2D TMDs. CVD methods allow for morphologycontrolled and scalable fabrication of 2D TMDs, as demonstrated in 2D TMD/2D TMD heterojunctions in lateral or vertical geometries with seamless atomic stitching of sub-atomic layers [57,58]. In contrast, 2D heterojunctions formed via mechanical exfoliations are limited to be small areas of 2D TMD vertical stacks with substantial impurities present at their interfaces [59]. However, the nature of the high temperature (typically,>600 °C) process inherent to CVD methods limits the incorporation of other temperature sensitive materials (e.g., polymers) into 2D TMDs, which often limit the versatilities of 2D TMD hybrid fabrications.

2D TMD-based inorganic hybrids

2D TMD/metal chalcogenide hybrids. 2D TMDs possess chemically inert/dangling bond-free 2D basal planes held via weak inter-layer vdW attraction, which allow for a facile integration of arbitrary 2D TMD layers circumventing the lattice match constraint demanded in conventional thin film crystal growths [60-62]. The novel 2D TMD/2D TMD hybrid materials with atomically sharp and high-quality interfaces provide unique functionalities for unconventional energy applications while retaining the intrinsic material properties of each constituent component. For example, combining two different 2D TMDs of distinct band gap energies and/or carrier types realizes 2D/2D electronic band structures with band offset/alignments (e.g. type II heterojunctions or p-n junctions) [63,64]. These hybrids can be utilized for extremely thin and optically transparent PVs owing to the facile collection/separation of photo-excited electron-hole pairs $(e^--(h)^+)$ at the 2D/2D interfaces. 2D TMD/2D TMD hybrids based on the combination of molybdenum (Mo) or tungsten (W)-based disulfides, diselenides, and ditellurides (e.g., MoS₂, WS₂, MoSe₂, WSe₂, MoTe₂, WTe₂) have been extensively explored [65-67]. For example, PV energy conversions have been demonstrated in 2D/2D p-n junctions by vertically stacking up one 2D TMD on top of the other such as stacked 2D WSe₂ (p-type)/2D MoS₂ (n-type) [68,69]. Despite the projected potential advantages (e.g., mechanical flexibility and optical tunability), the power conversion efficiencies of these 2D TMD/2D TMD hybrid materials at present remain very low to compete with matured PV technologies [70,71]. While a majority of planar 2D TMD/2D TMD hybrids focus on PV applications, other forms of TMDs such as 0D quantum dots and 1D nanowires were also developed for electrocatalytic and energy storage applications [72–75].

Besides Mo, W based sulfides and selenides, other metal chalcogenides incorporating Cd, Sn, Co, Bi, Ni, Zn, and Cu have been receiving significant interests in developing their own 2D structures and/or being incorporated into existing 2D TMDs [36,76,77]. Chalcogenides based on Co, Sn, and Ni are promising catalysts for HER and electrochemical energy storages (e.g., LIBs and supercapacitors) owing to their abundant active edge sites, defects, as well as structural similarities to other 2D TMDs [78,79]. For example, cadmium sulfide (CdS) integrated with 2D TMDs works as an efficient noble metal-free photocatalyst for water splitting since the CdS/2D TMD heterojunctions facilitate electron transfer with reduced charge recombination [80,81]. Bismuth selenide (Bi₂Se₃) in nearly 2D forms [82] combined with 2D MoS₂ layers demonstrated tunable optical and photoemission properties, making them highly intriguing for post silicon PV devices.

The fabrication of 2D TMD hybrids incorporating other layered/non-layered metal dichalcogenides has been pursued using various physical/chemical methods. Vertically-stacked layered 2D TMD/2D TMD hybrid materials (e.g., MoS₂/WS₂, MoSe₂/WS₂, etc.) were initially pursued with manual stacking of mechanically exfoliated 2D TMD flakes [83–85]. Fig. 2(a) shows an optical image of a typical 2D TMD/2D TMD hybrid material constructed by manually assembling mechanically exfoliated 2D MoS₂ and 2D WSe₂ flakes [86]. Despite the high quality of produced materials, this manual approach suffers from low-production yield and uncontrolled spatial integration, which makes it impractical for commercial usage. Another top-down fabrication approach involves solution-assisted exfoliation and assemblies of 2D TMDs [87,88]. Fig. 2(b) illustrates the solution-based production of 2D

MoS₂/2D WS₂ hybrid materials [89]. In this method, ammoniated (NH₃/NH₄⁺ ion intercalated) MS₂ (M=Mo, W) compounds were prepared to exfoliate stable MoS₂ and WS₂ dispersions in various solvents. 2D MoS₂/2D WS₂ hybrids were obtained by the sonication of the mixture of colloidal suspensions of MoS₂ and WS₂ sheets. The method can be extended to integrate 2D TMDs with other dimensional materials as demonstrated in 0D/2D MoS₂ hybrids where MoS₂ quantum dots were decorated in few-layer 2D MoS₂ flakes (Fig. 2(c)) [72]. Despite the intrinsic advantage of the facile production of large-scale 2D TMDs, this method suffers from unwanted introduction of defects/impurities and uses highly reactive lithium (Li) inherent to solution-based intercalation processes [90,91].

CVD has been employed as an alternative bottom-up technique to directly grow vertically-stacked 2D TMD/2D TMD hybrid materials. The co-evaporation of transition metals (e.g., Mo, W) and chalcogen (e.g., S, Se) precursors or sequential growth of one 2D TMD material on the top of the others have yielded a large family of 2D TMD/2D TMD hybrid materials including 2D WS2/2D MoS_2 , 2D $WSe_2/2D$ MoS_2 (or, 2D $MoS_2/2D$ WSe_2), and 2D $WSe_2/2D$ MoSe₂ [92–94]. Besides the vertically-stacked 2D TMD/2D TMD hybrids, these CVD approaches, under certain experimental conditions, have allowed for the fabrication of lateral 2D TMD/2D TMD hybrids with atomically stitching heterointerfaces [95,96]. Fig. 2(d, e) shows 2D WS₂ domains laterally grown from 2D MoS₂ edges forming in-plane 2D WS₂/2D MoS₂ heterointerfaces realized via one-step co-evaporation CVD process [58]. Successful growth of these lateral 2D MoS₂/2D MoSe₂ and 2D WS₂/2D WSe₂ were demonstrated via in-situ exchange of vapor phase reactants [97] along with via two-step epitaxial CVD growths [98]. The growth of lateral 2D TMD/2D TMD hybrids with in-plane interfaces is currently limited to high lattice matched materials and requires sophisticated experimental conditions and special precursors [99]. In addition to the co-evaporation-based CVD process, a two-step CVD synthesis employing the sulfurization/selenization of metal seed layers is emerging as an alternative to the growth of large-area 2D TMD/2D TMD hybrids with controlled interfacial morphologies [100]. In this approach, as shown in Fig. 2(f) [101], stacks of predeposited metal seeds (e.g., Mo/W) are subsequently sulfurized (or, selenized), which leads to the conversion of Mo/W to 2D MoS₂/2D WS₂ (or, 2D MoSe₂/2D WSe₂). Moreover, 2D TMD hybrids with TMD counterparts of non Mo- or W- sulfides/selenides were developed, including 3D hierarchical CoS₂/WS₂ hybrids by one-step sulfurization of Co and W precursors [102]. Various 2D TMD/TMD hybrids such as MoS₂/CdS, MoS₂/CoSe₂, and MoS₂/ZnS were also developed by hydrothermal synthesis (solvothermal) methods [103,104]. For example, a 3D porous flower-like MoS₂/CoSe₂ hybrid was synthesized via a two-step hydrothermal process [79]. Other growth techniques traditionally developed for thin film growth utilize molecular beam epitaxy (MBE), pulsed laser deposition (PLD), atomic layer deposition (ALD), and metal organic CVD (MOCVD) have been employed for various 2D TMD/TMD hybrids [105–107].

2D TMD/transition metal oxides. Transition metal oxides (TMOs) are extensively employed in a variety of energy generation/storage applications owing to their environmental benignity, low cost, and excellent catalytic activities [108,109]. TMOs such as titanium, zirconium, or zinc oxides (TiO₂, ZrO₂, and ZnO) are photocatalytic semiconductors employed for water splitting because of their suitable bandgap energies and redox potentials [110,111]. Upon sunlight illumination, TMOs generate e⁻-(h)⁺ which migrate to the reactive sites of their surfaces and in turn split water to evolve hydrogen gas (H₂) [112]. Amongst various TMOs, TiO₂ is one of the most extensively studied photocatalysts due to its intrinsically high photocatalytic activity and chemical stability in acidic/basic environments [113,114]. However, TiO₂ suffers from a few major technical bottlenecks; 1) limited optical absorption in ultravio-

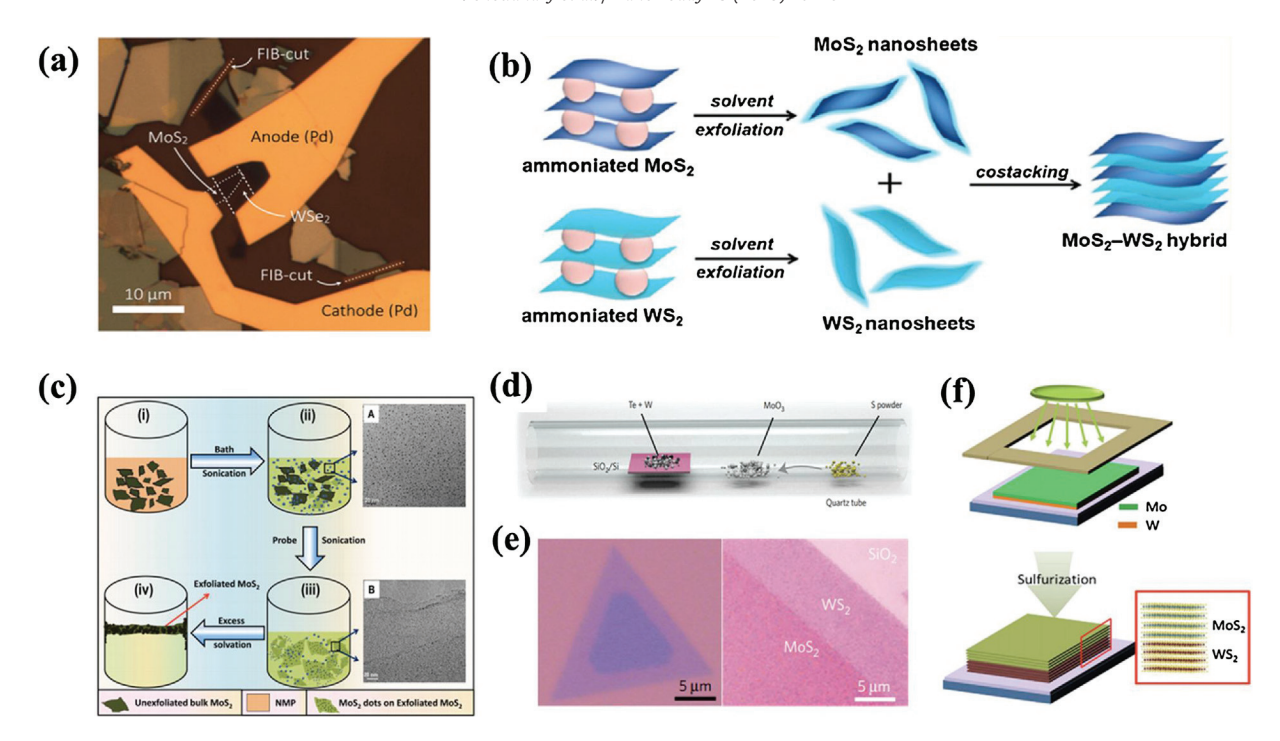


Fig. 2. (a) An optical image of 2D MoS₂/WSe₂ hybrid material constructed by a mechanical exfoliation. Reproduced with permission from Ref. [86]. Copyright 2014, the American Chemical Society. (b) Chemical exfoliation steps for the preparation of 2D MoS₂/WS₂ hybrids materials. Reproduced with permission from Ref. [89]. Copyright 2014, the American Chemical Society. (c) Synthetic procedures for the preparation of MoS₂ quantum dots dispersed in 2D MoS₂ layers using a liquid exfoliation approach. Reproduced with permission from Ref. [72]. Copyright 2014, the American Chemical Society. (d) Co-evaporation CVD process for the synthesis of 2D TMD hybrids and (e) Optical images of vertical and in-plane 2D MoS₂/WS₂ hybrids. Reproduced with permission from Ref. [58]. Copyright 2014, the Nature Publishing Group. (f) Schematic representation of a wafer-scale fabrication of 2D MoS₂/WS₂ vertical hybrid materials. Reproduced with permission from Ref. [101]. Copyright 2016, the Nature Publishing Group.

let (UV) regime corresponding to \sim 4% of total sunlight energy, 2) large overpotential for H₂ evolution, and 3) rapid recombination tendency of e⁻-(h)⁺ [115,116]. To circumvent these issues, TMOs have been incorporated with highly catalytic noble metals such as Pt, Pd, and Ru [117,118]. Despite the excellent catalytic activity, the intrinsically high cost and rarity of the noble metals hinders their sufficient usage. Recently, 2D TMDs have drawn substantive interests as promising co-catalysts for TMOs owing to following attributes; 1) Their bandgap energies (\sim 1.2–1.8 eV) match the visible regime, thereby broadening the energy harvesting range beyond the conventional UV regime in water splitting. 2) Suitable electronic band structures (e.g., rectifying junctions) formed at 2D TMD/TMO interfaces can facilitate the separation/collection of e⁻-(h) by efficiently inhibiting their recombination, which can lead to higher photocatalytic activity. 3) Large surface area and tailorable crystalline phases, i.e. semiconducting (2H) and metallic (1T) inherent to 2D TMDs coupled with their chemically reactive 2D edge sites can be utilized to enhance the photo catalytic activity of TMOs [42,119,120].

Fig. 3(a) illustrates how the photo catalytic efficacy of TiO_2 can be tailored and improved by incorporating 2D MoS_2 for HERs [121]. When TiO_2 is irradiated by sunlight, it generates e^-h^+ pairs which have higher chances of recombination without the presence of any co-catalyst, resulting in poor photocatalytic performance. However, in the presence of 2D MoS_2 co-catalysts, the photo generated electrons can be easily transferred from the conduction band of TiO_2 to MoS_2 surface, circumventing the possibility of e^--h^+ recombination so that electrons react with adsorbed H^+ to produce H_2 efficiently. 2D TMDs have also been functionally coupled with other TMOs and studied for energy storage applications (LIBs and supercapacitors) and electrocatalytic HERs. These materials include TMOs with d^n electronic configurations such as iron oxides of various oxidation states (Fe_2O_3 , Fe_3O_4), manganese oxide

 (Mn_3O_4) , cobalt oxide (Co_3O_4) and various metal dioxides like manganese dioxide (MnO_2) , ruthenium oxide (RuO_2) , and tin dioxide (SnO_2) [122,123]. In these hybrid structures, TMOs offer high specific capacitance, rich redox activity, and high reversible capacity as well as inhibiting the restacking of 2D TMDs [124]. In turn, 2D TMDs with large surface areas serve as supporting templates to anchor individual TMOs and confine their volume change during charge/discharge cycles [125]. Moreover, 2D TMD/TMO hybrids are expected to present wider operation voltage windows and higher ionic/electron conductivities over those stand-alone TMO materials, leading to enhanced energy density and rate capacitance performance in supercapacitors/LIBs applications [126,127].

Hydrothermal processes have been extensively used to produce a wide range of 2D TMD/TMO hybrids owing to their high simplicity and versatility [128,129]. For example, 3D hierarchical structures composed of 2D MoS2 decorated on TiO2 nanobelts were prepared by sequential hydrothermal processes [49]. Fig. 3(b) shows representative scanning electron microscope (SEM) images of TiO₂ nanobelts before (left) and after (right) the incorporation of 2D MoS₂. Similarly, ultrathin 2D MoS₂/TiO₂ hybrid materials using TiO₂ nanobelts were reported [130]. The resulted hybrids offer a significant enhancement of surface areas by more than an order of magnitude, leading to higher photocatalytic activities in both UV and visible regions compared to thicker TiO₂ nanobelt-based 2D MoS₂/TiO₂ nanocomposites. 2D MoS₂ was deposited on TMO nanofibers prepared by electrospinning through a hydrothermal deposition, resulting in 1D TMO/2D MoS₂ core/shell nanowires [42,131,132]. Fig. 3(c) shows 2D WS₂ sensitized TiO2 nanospheres which exhibit a wide range of optical absorption for enhanced photocatalytic activity [133]. In some cases, 2D TMDs serve as host materials incorporated with nanostructured TMOs such as copper, zinc, or tin oxides (CuO, ZnO, SnO) by hydrothermal processes [134,135]. For example, ultra-small

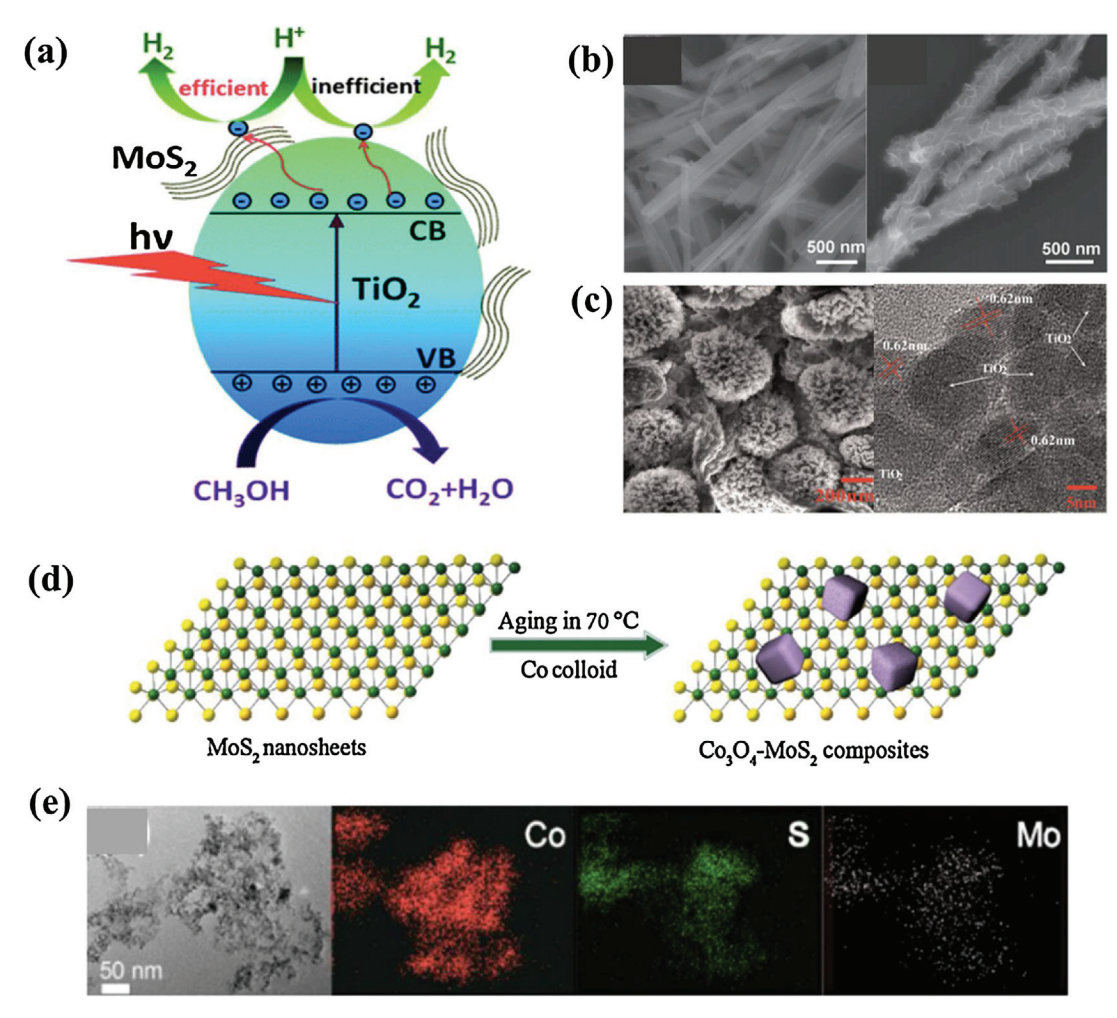


Fig. 3. (a) Schematic representation of the photocatalytic H₂ evolution activity and fast charge transfer mechanism in 2D MoS₂/TiO₂ hybrids. Reproduced with permission from Ref. [121]. Copyright 2015, the Royal Society of Chemistry. (b) SEM images of pristine TiO₂ nanobelts (left) and 2D MoS₂-coated TiO₂ hybrids (right). Reproduced with permission from Ref. [49]. Copyright 2013, the John Wiley and Sons. (c) SEM (left) and TEM (right) images of 2D MoS₂/TiO₂ nanospheres synthesized by a hydrothermal method. Reproduced with permission from Ref. [133]. Copyright 2015, Elsevier. (d) Schematic procedure for the fabrication of CoO₃-decorated 2D MoS₂ hybrids by a laser ablation in liquid (LAL) and (e) energy dispersive x-ray (EDX) mappings to show a spatial distribution of Co, S, and Mo. Reproduced with permission from Ref. [141]. Copyright

(~3.5 nm) iron oxide (Fe₃O₄) nanoparticles were uniformly decorated on the surfaces of 2D MoS₂ nanosheets [136]. Moreover, a hydrothermal synthesis of molybdenum trioxide (MoO₃) and ethylene glycol in the presence of 2D MoS₂ dispersions yields 2D MoS₂/MoO₂ hybrids *via* reciprocal hybridization [137]. However, hydrothermal methods suffer from some technical limitations such as complex/incomplete reduction reactions and the production of secondary phases, which led to the development of alternative methods. Mechano-chemistry approaches were extensively explored where 2D TMDs are mechanically/chemically sorted and assembled into TMOs. Simple sonication methods were developed to fabricate 2D MoS₂/TiO₂ hybrids in which chemically exfoliated metallic 1T-MoS₂ nanosheets were sonicated/bind with TiO₂ nanoparticles [138]. Ball milling methods offer advantages in terms of achieving uniform 2D TMD/TMO hybrids of high structural homogeneity [121]. Photon-assisted deposition and anion exchange reaction methods were also utilized to decorate TMOs on 2D TMDs and partially convert TMOs to 2D TMDs, respectively [139,140]. Laser ablation in liquid (LAL) was claimed to produce highly clean, small-sized reactive cobalt (Co) colloids [141] which were subsequently mixed with 2D MoS₂ and allowed for aging at low temperatures (Fig. 3(d)). Resulting MoS₂-Co₃O₄ hybrids were shown in Fig. 3(e). MoO₃/MoS₂ core/shell nanowires were fabricated by partially sulfurizing initial MoO₃ nanowires. The surface of the MoO₃ nanowires was converted to 2D MoS₂ *via* anion exchange reactions, and these novel 2D TMD/TMO hybrids exhibit excellent catalytic performances for HER applications [34].

2D TMD/noble metal hybrids. Noble metals such as Au, Pd, Pt, and Ag are attractive for a variety of energy applications including photocatalytic and electrochemical energy conversions owing to their high electrical conductivity coupled with their chemical inertness [142,143]. These properties can be facilely tailored just by controlling their shape/dimensions at nanoscales (1D, 2D, and 3D) as well as by tuning their compositions, which can render additional functionalities. Despite such excellent properties, the scarcity of noble metals and the associated high cost hinder their practical applications. Hence, significant efforts have been made on finding inexpensive/abundant materials that can achieve certain functionalities of precious noble metals. 2D TMDs have recently gained increasing interests as a low cost, non-metallic replacement of noble metals owing to their tunable electrical properties, intrinsic phase transformation, and electrochemically active 2D edge sites [144,145]. However, their electrical conductivity is significantly lower than that of pure metals, undermining their versatilities for many applications which require fast charge carrier transports (e.g., PVs). It is clear that either stand-alone noble metals or 2D TMDs cannot meet the aforementioned requirements of low

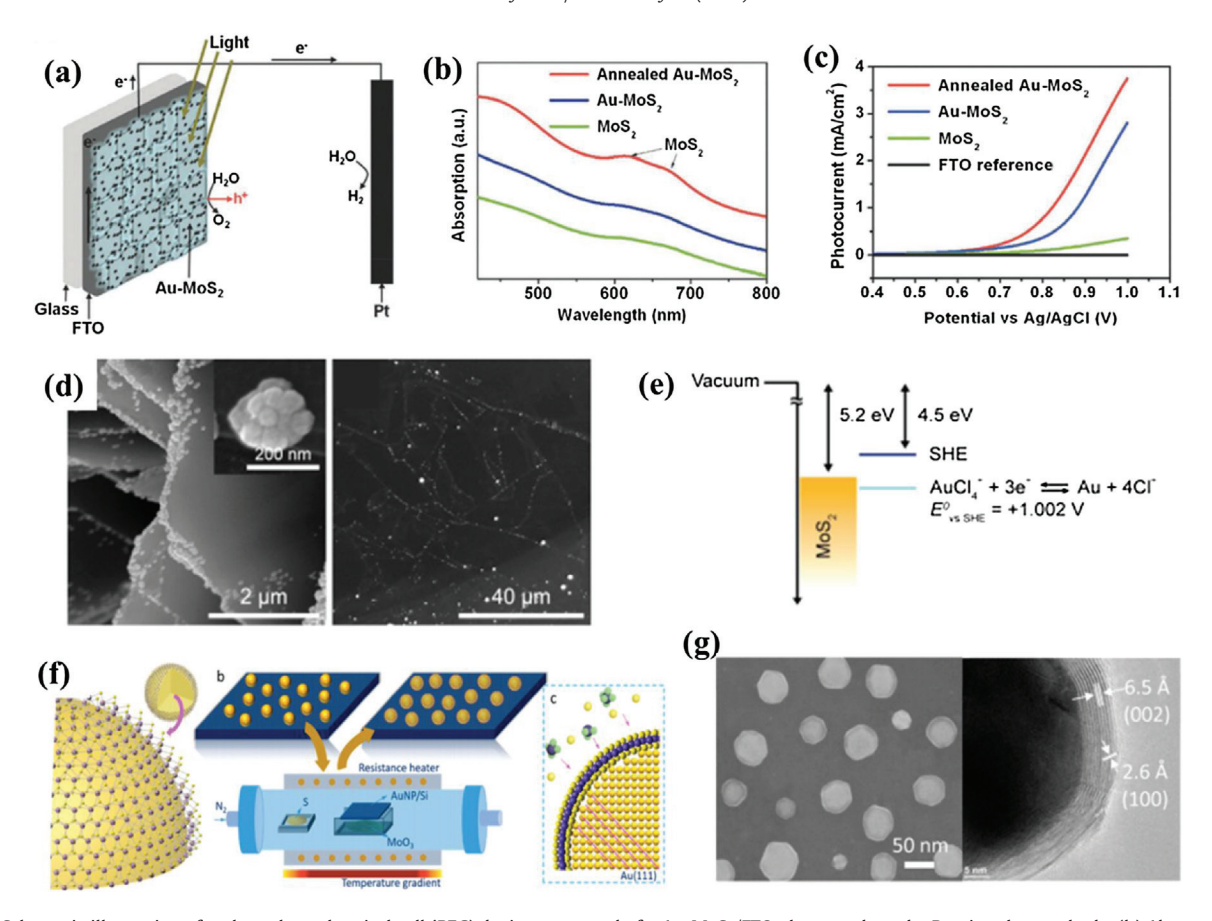


Fig. 4. (a) Schematic illustration of a photoelecrochemical cell (PEC) device composed of a Au-MoS₂/FTO photoanode and a Pt wire photocathode. (b) Absorption spectra of pristine MoS₂, Au-MoS₂ and annealed Au-MoS₂ hybrid. (c) Comparison of photocurrent in pristine MoS₂, Au-MoS₂, and FTO reference electrodes. Reproduced with permission from Ref. [147]. Copyright 2014, John Wiley and Sons. (d) SEM images showing Au nanoparticles preferentially decorated at the defect sites of 2D MoS₂ layers (e) An energy diagram for the Fermi level of MoS₂ above the reduction potential of Au³⁺ indicating a spontaneous redox reaction between 2D MoS₂ and HAuCl₄. Reproduced with permission from Ref. [156]. Copyright 2013, American Chemical Society. (f) Schematic of the Au@MoS2 core-shell heterostructure and its growth process setup using CVD. Au nanoparticle coated Si substrate placed on an alumina boat containing MoO3 reacts with sulfur vapors to form a MoS2 shell on the Au nanoparticles. (g) SEM (left) and TEM (right) images of Au/MoS₂ core/shell nanocrystals with few-layer 2D MoS₂ shells. Reproduced with permission from Ref. [160]. Copyright 2016, American Chemical Society.

cost and high electrical/chemical activity. This limitation drives the development of new 2D TMD/noble metal hybrids, which can alleviate the inherent weaknesses of each component and result in synergic positive effects. For example, the incorporation of a small amount of noble metals into 2D TMDs can create tunable and enhanced optical absorption through the light-trapping effect via 2D TMD/metal plasmonic coupling in a relatively inexpensive manner [146]. Fig. 4(a-c) are the representative images that show significant enhancement in the optical absorption and photocurrent of 2D MoS₂/Au composite electrodes when utilized in a photoelectrochemical cell (PEC) [147]. Fig. 4(a) is the schematic representation of PEC in which 2D MoS₂/Au on fluorine-doped tin oxide (FTO) and Pt wire was used as a photoanode and a photocathode, respectively. The UV-vis spectra in Fig. 4(b) reveal significantly high absorption in annealed 2D MoS₂/Au as compared to pristine 2D MoS₂ or non-annealed states. As a result, 2D MoS₂/Au-based PEC yields about 3.7 times higher photocurrent (\sim 370 μ A/cm²) compared to pristine 2D MoS₂ PEC (~100 µA/cm²), observed at 0.8 V under visible light illumination (Fig. 4(c)). Moreover, the metal/semiconductor Schottky junctions of noble metal/2D TMDs can be utilized for photon-assisted energy conversion/generation applications. Schottky junctions facilitate the separation/collection of photo-excited charges generated, thus efficiently suppress e--(h)⁺ recombination, leading to enhanced light harvesting activity of catalytic 2D TMDs [148,149]. Moreover, plasmon-excited hot electrons from the noble metals can further assist a direct reduction of water to form hydrogen. 2D TMD/noble metal hybrids have also exhibited a great promise to replace conventional poly(3,4-ethylenedioxythiophene) polystyrene sulfonate (PEDOT:PSS) hole transport layers (HTLs) for organic solar cells in which 2D TMDs act as a hole extraction material while noble metals function as a light trapping centers [150]. Moreover, noble metal nanoparticles anchored on defect-rich 2D TMD basal planes have exhibited excellent HER activities by modifying the surface electronic states of 2D TMDs while retaining their active edge sites [151].

Fabrications of 2D TMD/noble metal hybrids were initially pursued by directly depositing the metals on 2D TMDs, employing various vapor-deposition techniques including thermal/e-beam evaporation and ALD. Despite some successful demonstrations [152,153], these techniques suffer from low throughput and difficulties in controlling the size and spatial homogeneity of deposited metals [154]. Wet-chemical synthetic methods were alternatively pursued to directly grow 2D TMD/noble metal hybrids in an easier and more controlled manner accompanying high versatility to grow almost all noble metals. In-situ chemical reduction-based growths of noble metals were demonstrated on 2D MoS₂ [155,156]. Most of the noble metals (Pd, Pt) were epitaxially grown on the basal planes of 2D MoS₂ layers, while the SEM images in Fig. 4(d) show that Au nanoparticles (NPs) reduced from gold tetrachloride (AuCl₄) preferentially grow on the edge/defect sites of 2D MoS₂ layers. The edge/defect-oriented decorative growth of Au is due to the high work function of MoS₂ (i.e. 5.2 eV) that tends to locate its Fermi

level above the reduction potential of AuCl₄ (+1.002 V), allowing for 2D MoS₂ to donate electrons to reduce AuCl₄ into Au (Fig. 4(e)). Accordingly, Au NPs tends to grow at the edge- or line defect-sites of 2D MoS₂ as they are energetically more favorable. Controlled and selective decorations of Au NPs on the edge sites of CVD-grown 2D MoS₂ were also demonstrated using dip-casting methods by reducing AuCl₄ [55]. Anchoring of Au and Ag NPs to few-layer 2D MoS₂ was employed via microwave-assisted functionalization/reductions, which resulted in substantial enhancement in its electrical, thermal, and structural properties [157]. Moreover, a significant increase of photoluminescence (PL) was observed in Au NPs-incorporated 2D WS2 layers via a simple treatment of a chloroauric acid (HAuCl₄) aqueous solution in comparison to its pristine state [158]. Solvothermal methods, heating a mixture of metal precursors, chemical agents, and 2D TMDs in autoclaves were employed as a cost-effective and facile approach to synthesize 2D TMD/noble metal hybrids [159]. For example, Au/MoS₂ core/shell heterostructured NPs with uniformly surrounding few-layer 2D MoS₂ shells were developed [160]. Direct CVD co-evaporations of fullerene-like 2D MoS₂ onto the surface of Au nanoparticles were also employed, resulting in Au/2D MoS₂ core/shell nanoparticles (Fig. 4(f)). As-grown Au/2D MoS₂ core/shell nanoparticles with well-resolved \sim 5–10 atomic layers of 2D MoS₂ are presented in Fig. 4(g).

2D TMD-based organic hybrids

2D TMD/carbonaceous materials. Carbon-based nanomaterials such as activated carbon, carbon nanotubes (CNTs), carbon fibers, and graphene have been recognized as promising materials to produce 2D TMD hybrids owing to their high electrical conductivities, light weight, low toxicity, and ease of fabrication [161,162]. Integrating carbonaceous nanomaterials with 2D TMDs leads to following advantages for energy generation/storage applications; (1) Their high electrical conductivity (specially, CNT and graphene) alleviates the intrinsically low electrical conductivities of 2D TMDs. (2) Hierarchically-configurable carbonaceous materials such as carbon nanofibers and CNTs enhance the structural integrity of 2D TMDs and accommodate the volume change during their cyclic charge-discharge process in electrochemical energy storage applications. (3) The aggregation of 2D TMDs can be mitigated by dispersing carbonaceous materials, which will help to improve catalytic/electrochemical properties. (4) Graphene - 2D carbonaceous material - can be used as templates for the growth of 2D TMDs while providing conducting networks for the transportation/separation of charges/ions [163,164]. Similarly, 2D TMDs also reciprocate several advantages to the aforementioned carbonaceous materials; (1) 2D TMDs anchored/hybridized onto the surfaces of CNT or graphene offer electrocatalytically active sites which can facilitate the reduction of tri-iodide species, making these hybrids promising for counter electrodes (CEs) in dyesensitized solar cells (DSSCs). (2) 2D TMDs of tunable band gap energies (~1.2-1.8 eV) combined with graphene of low visible absorbance (\sim 2.3%) can produce electronic junctions which display significant light-matter interactions for ultrathin optoelectronics and photocatalytic HER applications. (3) 2D TMDs hybridized with graphene can circumvent its aggregation problem and maximize its surface area for enhanced electrochemical applications [165–167].

Hydrothermal method has been the main synthesis route for most of 2D TMDs/carbonaceous hybrid materials [168]. Fig. 5(a-c) schematically illustrate the procedure of in situ hydrothermal reactions of carbon precursors (resorcinol and formaldehyde) with molybdenum sol, ammonium tetrathiomolybdate ((NH₄)₂MoS₄). The hydrothermal reactions were performed at $180\,^{\circ}$ C, which leads to the formation of 2D MoS₂/carbon hybrids [169]. The TEM image in Fig. 5d clearly reveals that 2D MoS₂ layers are homogeneously embedded in the matrix of amorphous carbon with a lateral size

of ~40 nm. Similarly, 2D MoS₂/carbon nanosphere hybrids in 3D flower-like morphologies were prepared for high-performance sodium (Na) ion battery anodes [170]. A glucose-assisted reduction method to grow 2D MoS₂ layers on the surface of CNTs was developed [171]. In this approach, acid-treated CNTs were dispersed into glucose solutions by ultrasonication followed by an addition of sodium molybdate dihydrate (Na₂MoO₄·6H₂O), which results in highly crystalline 2D MoS₂/CNT hybrid nanostructures. Similarly, mixing CNTs with (NH₄)₂MoS₄ and HCl solutions yielded few-layer 2D MoS₂ coated multi-wall CNTs (MWNTs) [172]. However, such pretreatment of CNTs with strong acids to enhance their adhesions to 2D TMDs were found to be detrimental to the electrical properties of CNTs. An acid-free solvothermal method was alternatively developed to overcome this limitation [173], which involved the homogenous mixing of (NH₄)₂MoS₄ powders with MWCNTs in N, N-dimethylformamide (DMF) followed by heating in autoclaves. MoS_x/MWNTs coaxial hybrids were also developed and their fabrication is demonstrated in Fig. 5(e). MoS_x nanosheets were grown on the sidewall of MWNTs, whereas they started to protrude with increasing Mo/C ratio. Fig. 5(f) is a representative TEM image of the MoS_x/MWNTs coaxial hybrid, revealing highly interconnected MoS_x nanoflakes attached to MWNTs. Moreover, highly-crystalline phases of constituent MoS₂ and MWNTs were confirmed by the Raman spectroscopy characterization (Fig. 5(g)). 2D TMDs/carbon fiber hybrids were prepared by electrospinning or hydrothermal-combined electrospinning methods [174,175]. Electrospinning of (NH₄)₂MoS₄ and (poly(vinylpyrrolidone) (PVP) followed by thermal annealing in inert gas yielded thin carbon nanofibers embedded with ultra-small 2D MoS₂ flakes [176].

2D TMDs/graphene hybrids were initially pursued via a mechanical exfoliation and transfer of individual 2D layers [177,178]. This manual approach introduces unwanted gaps/wrinkles as well as residual contaminants between adjoining 2D layers, which is detrimental to the performances of resulting devices [179,180]. Chemical growth of 2D TMD/graphene hybrids was alternatively pursued for practical applications [181]. Direct growth of various 2D TMD layers on epitaxial graphene/silicon carbide (SiC) substrates were demonstrated by sulfurizing e-beam deposited Mo films on graphene [182]. In this approach, 2D MoS₂ and 2D WSe₂ layers were epitaxially grown on the basal planes of graphene (Fig. 5((h))), which was implemented either by co-evaporation CVD using powder precursors or by MOCVD process. Raman spectra (Fig. 5(i)) and scanning TEM images (Fig. 5(j)) show the structural integrity of 2D TMD/graphene hybrids achieved by these methods, indicating atomically sharp 2D TMD/graphene interfaces without noticeable interfacial diffusion. Growths of large-area (several µm) 2D MoS₂ layers on graphene were also demonstrated via thermal annealing of (NH₄)₂MoS₄ and sulfur precursors at relatively low temperature of 400 °C [60].

2D TMD/conductive polymers. Conductive polymers (CPs) including polyaniline (PANI), polypyrrole (PPy), polythiophene (PT), poly(3,4ethylenedioxythiophene) (PEDOT), and their derivatives have been increasingly employed for energy storage and conversion applications owing to their low cost, high electrical conductivity, facile process, light weight, and biodegradability [183,184]. However, their inherent weakness including poor mechanical strength and low heat resistance has demanded the use of filler materials to improve such properties in their matrices [185]. 2D TMDs, as fillers, have a variety of properties that can be utilized to engineer the physical properties of hosting polymers. The high mechanical strength of 2D TMDs (e.g. \sim 0.3 TPa for monolayer 2D MoS₂) is ideally suited to enhance the mechanical properties of CPs, making them an ideal reinforcing agent [186]. 2D TMDs can be easily dispersed and entangled into CPs to provide physical barriers of heat diffusion, thus enhance the thermal properties of the hybrids

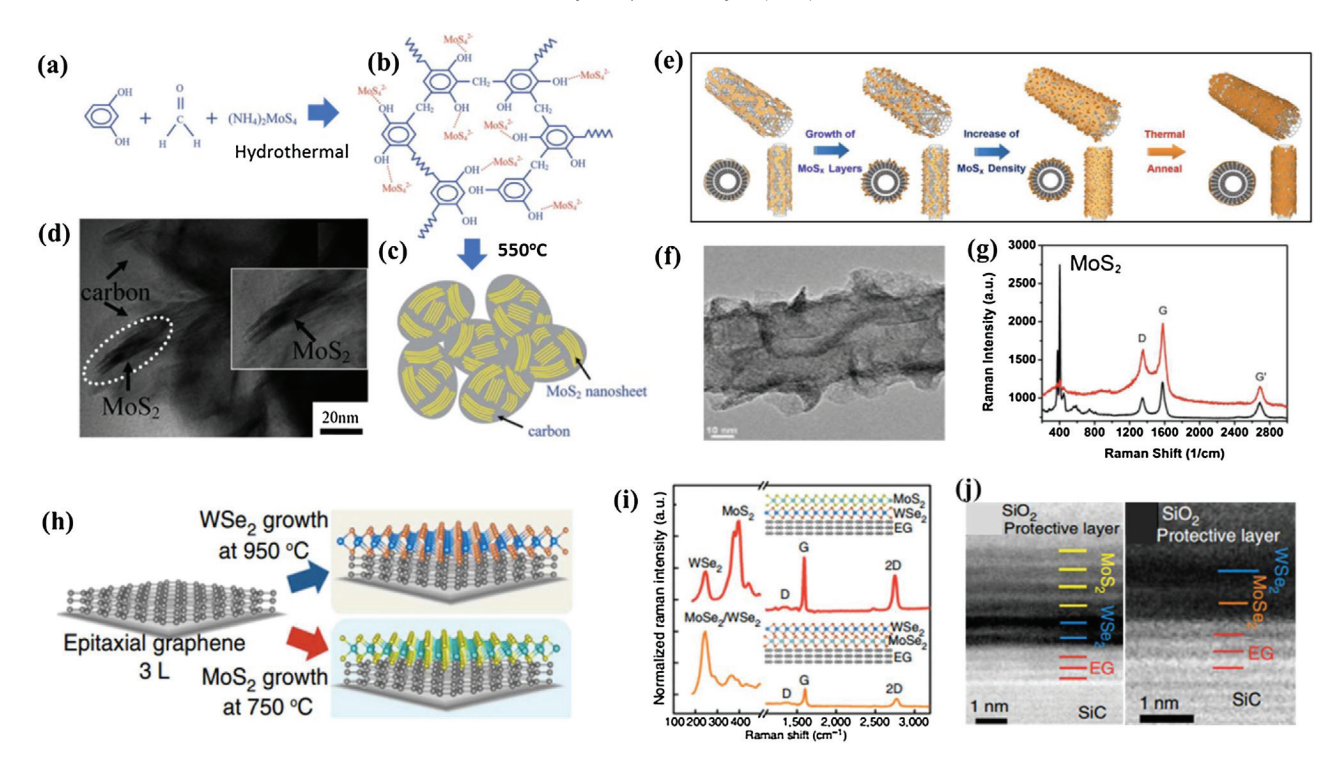


Fig. 5. (a–c) Synthetic procedure for the hydrothermal synthesis of 2D MoS₂/carbon hybrid materials. (d) TEM image showing 2D MoS₂ layers uniformly embedded in a carbon matrix. Reproduced with permission from Ref. [169]. Copyright 2012, the Royal Society of Chemistry. (e) Schematic procedure for the solvothermal growth of 2D MoS₂/MWNT hybrids. (f) TEM image and (g) Raman spectra of the 2D MoS₂/MWNT hybrids. Reproduced with permission from Ref. [173]. Copyright 2013, Nature Publishing Group. (h) CVD growth of 2D MoS₂ and 2D WSe₂ on epitaxial graphene to form 2D TMD/graphene hybrids. (i) Raman spectra showing the presence of 2D MoS₂/WSe₂ layers and graphene. (j) Scanning TEM (STEM) images showing the atomically sharp interfaces of 2D TMD/graphene hybrids. Reproduced with permission from Ref. [182]. Copyright 2015, Nature Publishing Group.

[187]. Most notably, 2D TMDs present variable oxidation states (e.g., +2 to +6 in MoS₂) [188], which can achieve reversible redox reactions combined with CPs enhancing their capacitive properties via pseudocapacitive reactions [189]. Such reversible redox reactions inherent to 2D TMDs can be applied to various inorganic/organic counterparts, generally improving the electrochemical performances of 2D TMD hybrids for energy storage applications. 2D TMDs like MoS₂ exist in different polymorphic forms such as 2H-(semiconducting), 1T-(metallic), and 3R-(semiconducting) which can be suitable for certain applications. For example, 1T-MoS₂ can significantly improve the electrical conductivity of PT [190], PPy [191] and PEDOT [189]. Since, most of 2D TMDs in their pristine form possesses low solubility in water and organic solvents, effective methods are required to make them compatible with polymer processing. Till date, several non-covalent and covalent approaches have been developed to efficiently incorporate 2D TMDs with polymers. These methods include (1) physical mixing of 2D TMDs and polymers via solution- and/or melting-based approaches, (2) in-situ polymerization of monomers in the presence of 2D TMDs, and (3) covalent functionalization of 2D TMDs with polymers using their precursors. The physical mixing of 2D TMDs were carried out in a variety of water-soluble (e.g. polyvinyl alcohol (PVA), polyethylene oxide (PEO), gelatin) and waterinsoluble polymers (e.g. epoxy resins, polyurethane, polystyrene) [192–195]. For example, mechanically exfoliated 2D MoS₂ layers were mixed with epoxy polymers via high speed sheer blending (Fig. 6(a)), which reinforced the polymers for structural applications [196]. Similarly, hydrothermally synthesized 2D MoS₂ layers were dispersed in poly(3,4-ethylenedioxythiophene)-poly(styrene sulfonate) (PEDOT-PSS) aqueous solutions via mechanical mixing [197]. The major common drawback of these approaches is the spontaneous restacking of individual 2D layers because of their intrinsic vdW interaction which results in poor dispersion in polymer solutions [198]. As alternatives methods, in-situ polymerizations of functionalized 2D TMDs were developed via solution mixing/blending approaches [199], which were proposed to achieve better dispersion of 2D TMDs. Various CPs including polypyrrole (PPy), polyaniline (PANI), and poly(3methylthiopene) (P3MT) were polymerized with 2D TMDs to develop 2D TMD/CP-based electrode materials for electrochemical energy storage/generations such as LIBs, supercapacitors, and electrocatalysts. For example, 2D MoS₂/PPy hybrids were produced by an in-situ oxidation-based polymerization of pyrrole in MoS₂ suspensions. As shown in Fig. 6(b) [200], 2D MoS₂ with intertwined layers was first formed by a hydrothermal synthesis. It was followed by the oxidative polymerization of pyrrole monomers adsorbed on the MoS₂ surface, which resulted in PPy-filled MoS₂ hybrids. Fig. 6(c) are the TEM images of the entangled/folded MoS₂ nanosheets (left) and MoS₂/PPy hybrids revealing PPy embedded in MoS₂ matrix (right). In another study, 2D MoS₂/PANI hybrids where PANI nanowires were vertically integrated on the surfaces of tubular 2D MoS₂ layers were produced via a simple chemical oxidative polymerization method [201]. Combining organic semiconductors (OSCs) with 2D TMDs was also pursued, aiming to develop large-scale, low-cost p-n junction PV devices. For example, ptype dioctylbenzothienobenzothiophene (C8-BTBT) and pentacene were incorporated with 2D MoS₂ layers (intrinsically n-type) by a vapor-deposition method, leading to OSC/2D MoS₂ p-n junction hybrids [202]. Similarly, poly(3-hexylthiophene) (P3HT) blended with phenyl-C61-butyric acid methyl ester (PCBM) OSCs were incorporated with CVD grown n-type MoS₂ layers (Fig. 6(d, e)) [203]. These hybrid materials coupled with Ag-based plasmonic metastructures exhibit ~6 fold enhancement of photo-carrier generation/absorption in comparison to stand-alone polymers.

In addition to conventional CPs, MOFs represent a new class of polymeric compounds comprising metal ions/clusters coordi-

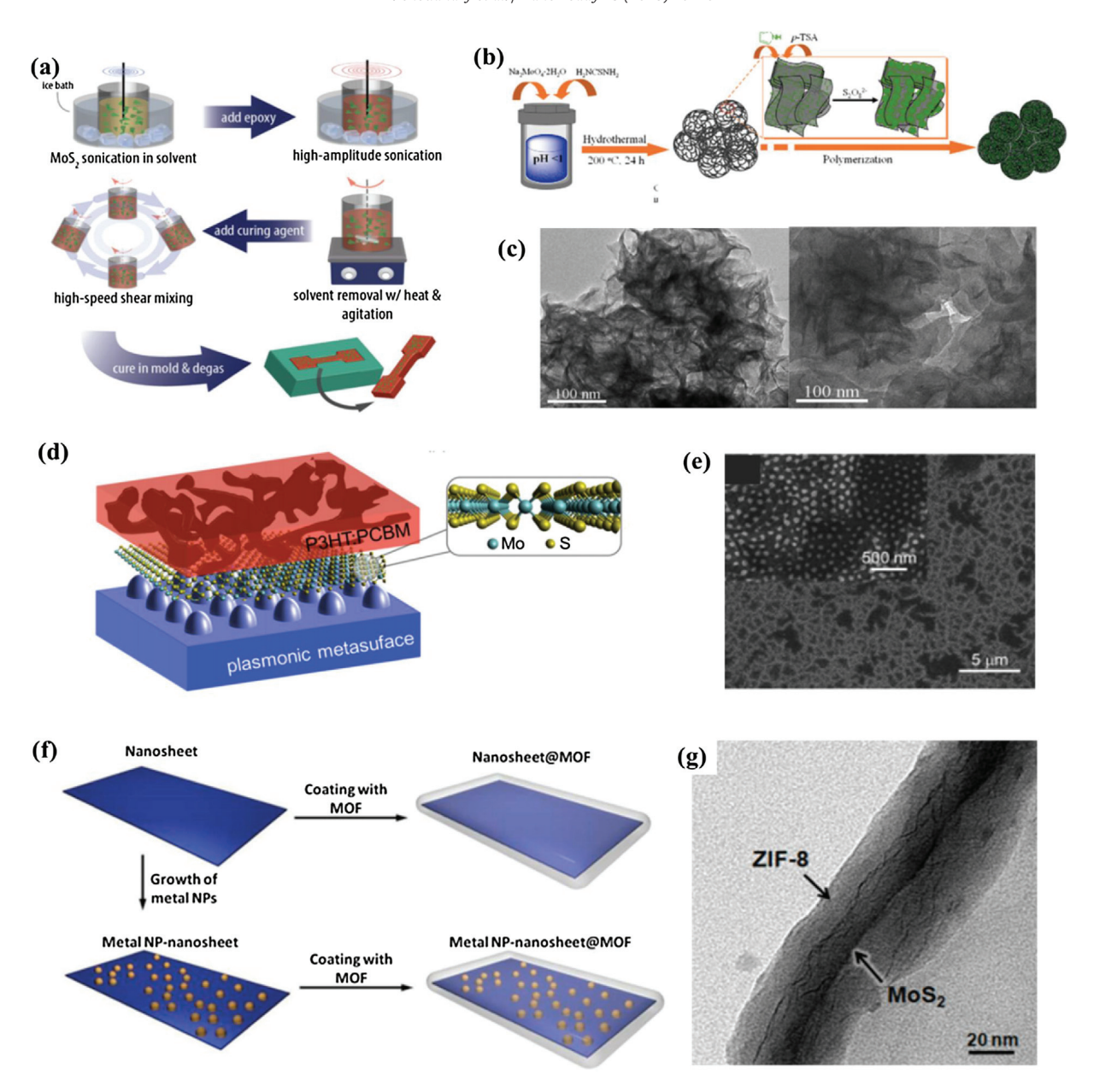


Fig. 6. (a) Solution mixing and high-speed shear blending methods to make 2D MoS₂/epoxy hybrids. Reproduced with permission from Ref. [196]. Copyright 2014, American Chemical Society. (b) In-situ polymerization method to synthesize PPy/MoS₂ hybrids. (c) TEM images showing folded/entangled 2D MoS₂ layers in an intertwined structure (left) and PPy embedded into 2D MoS₂ (right). Reproduced with permission from Ref. [200]. Copyright 2013, Elsevier. (d) Schematic representation and (e) SEM images of P3HT:PCBM/2D MoS₂ hybrids constructed on a plasmonic metasurface. Reproduced with permission from Ref. [203]. Copyright 2016, American Chemical Society. (f) Scheme procedures for the synthesis of 2D TMD/MOF hybrids. (g) TEM image of a 2D MoS₂/ZIF-8 hybrid, showing 2D MoS₂ core and ZIF-8 shell. Reproduced with permission from Ref. [206]. Copyright 2014, American Chemical Society.

nated to organic ligands which exhibit enriched surface active sites and tunable porosity (up to 90%) in highly versatile geometries [204]. Their unique functionalities, particularly structural flexibility and enormous porosity, make them promising for energy conversion/storage applications. However, their poor chemical stability and insufficient electrical conductivities severely limit their applicability. In order to mitigate these drawbacks, hybrid materials combining MOFs with other nanostructured active materials such as metals, polymers, oxides, and carbon materials have alternatively been pursued [205]. Particularly, 2D materials such as graphene and 2D TMDs are expected to improve MOFs' mechanical, electrical, and optical properties. Pt-dispersed 2D MoS₂ layers were incorporated into zeolitic imidazolate frameworks (ZIF-8) via an in-situ reduction (Fig. 6(f)) [206]. ZIF-8 was coated on the Pt/2D MoS₂ layers by a simple mixing of the aqueous solution of

2-methylimidazole and zinc acetate in the presence of the 2D templates where intimate contacts of ZIF-8/2D MoS₂ were achieved as shown in Fig. 6(g). Besides 2D MoS₂ layers, molybdenum polysulfide (MoS_x) anchored-MOF hybrids were developed for HER applications via a facile one-pot solvothermal reaction of MoS_x with a zirconium (Zr)-based MOF (i.e. UiO-66-NH₂) [207]. MOFs have also been utilized as precursors to synthesize various 2D TMD-based catalysts, including 2D MoS₂/TiO₂ [208].

Energy applications of 2D TMD hybrid materials

Energy generation

Photovoltaics. Semiconducting 2D TMD layers, particularly in their mono-to-few layer forms, have attracted significant attention for PV applications owing to their direct bandgap energies and broad

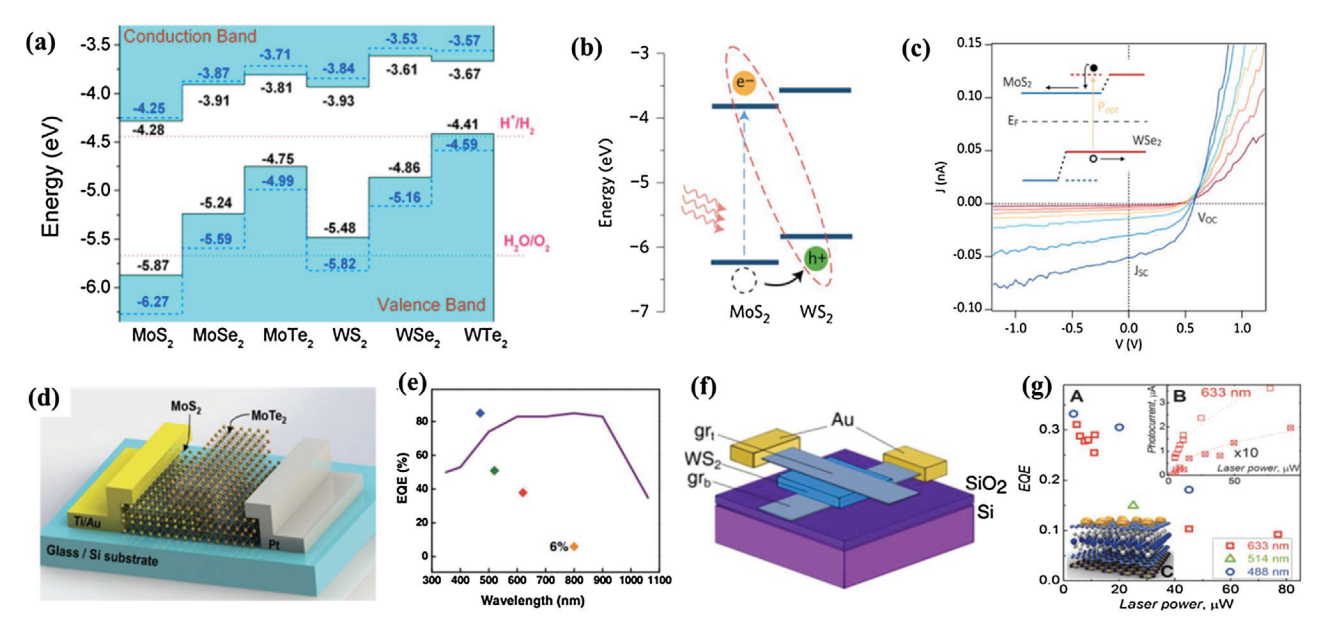


Fig. 7. (a) Calculated band alignments of various 2D TMD monolayers. Reproduced with permission from Ref. [210]. Copyright 2013, American Institute of Physics. (b) Band alignment of 2D MoS₂/WS₂ hybrids showing a type II heterojunction. Reproduced with permission from Ref. [15]. Copyright 2014, Nature Publishing Group. (c) Photo response from a vertically-stacked 2D WSe₂/MoS₂ p-n junction under varying illumination. Reproduced with permission from Ref. [86]. Copyright 2014, American Chemical Society. (d) Schematic of a 2D p-n junction diode based on vertically-stacked p-MoTe₂ and n-MoS₂ layers. (e) External quantum efficiency (EQE) of 85% observed in the MoS₂/MoTe₂ diode. Reproduced with permission from Ref. [211]. Copyright 2016, John Wiley and Sons. (f) Schematic illustration of a PV device based on 2D WS₂/graphene hybrid s. (g) Photo response of a 2D WS₂/graphene hybrid device exhibiting EQE of >30%. Reproduced with permission from Ref. [14]. Copyright 2013, AAAS.

optical absorptions in a range of infrared to visible light [209]. Applications of 2D TMDs in PV devices have been driven in two major directions. The first direction focuses on exploring novel PV devices by employing the excellent mechanical flexibility and optical absorption inherent to 2D TMDs. This approach was mainly pursued by integrating multiple 2D TMD layers of distinct electrical/optical functionalities. The second direction involves the incorporation of 2D TMDs into existing PV materials (e.g., Si or conductive polymers). This approach focuses on bestowing additional functionalities/merits into conventional PV devices such as cost reduction. In the former case, the simplest form of 2D TMDbased PV hybrid devices can be realized by combining two different 2D TMDs of distinct carrier types and/or appropriate band offsets. A large number of 2D TMDs form typical type-II band alignments when they are interfaced with each other, which enables fast and efficient separation of photo-excited e⁻-h⁺ via the built-in potentials at their 2D/2D interfaces. Fig. 7(a) shows the calculated band alignments formed by interfacing various 2D TMD monolayers, which indicates the suitability of 2D TMD/2D TMD hybrids for PV applications [210]. Fig. 7(b) represents a schematic diagram for the generation/separation of photo-excited e⁻-h⁺ at the junction of 2D MoS₂/2D WS₂ while both 2D monolayers present n-type transports [15]. Experimentally verified power conversion efficiencies (PCEs) of the 2D MoS₂/2D WS₂ hybrids presently remains below 2% [209]. Combining 2D TMDs of intrinsically distinct carrier types (i.e. p-type and n-type) was extensively pursued for p-n junction PV applications. Fig. 7(c) shows a typical photo response from a vertically-stacked 2D WSe₂ (p-type)/2D MoS₂(n-type) p-n junction under an illumination of varying amplitudes, indicating its substantive PV effect [86]. External quantum efficiency (EQE) of ~2.4% was reported in similarly prepared 2D WSe₂/2D MoS₂ p-n junction PV devices [40]. Recently, 2D MoTe₂ (p-type)/2D MoS₂ (n-type) hybrids in the form of vertically-stacked 2D monolayers were developed (Fig. 7(d)) [211]. These p-n junction diodes exhibited an excellent PV response with a high photoresponsivity of 322 mA/W, open-circuit voltage (V_{oc}) of \sim 0.3 and EQE of 85% (Fig. 7(e)). In addition to the manual stacking of distinguishable individual 2D layers, PV heterojunctions were also developed in single 2D TMD layers via monolithic approaches. For example, plasma-irradiation introduced p-doping in intrinsically n-type 2D MoS₂ was utilized to develop p-n junction in single 2D MoS₂ layers [212]. The p-n 2D MoS₂ PV devices composed of asymmetric contacts (Au/p-MoS₂ and ITO/n-MoS₂) yield a PCE of ~2.8%. In addition to 2D TMD/2D TMD hybrids, graphene/2D TMDs were explored for PV applications exploiting the extremely high electrical conductivity of metallic graphene which forms Schottky junctions with semiconducting 2D TMDs. One of the earliest examples is PV devices based on 2D WS₂ layers sandwiched between graphene (i.e. graphene/2D WS₂/graphene) (Fig. 7(f)) [14]. These 2D/2D hybrid devices achieved a high photoresponsivity of >0.1 A/W with an EQE of >30% (Fig. 7(g)). Similarly, PV devices based on few layer graphene/2D WS₂ [213] and graphene/2D MoS₂ [214] Schottky junctions achieved PCEs of \sim 3–4%.

2D TMD-based hybrids incorporating a wide range of conventional PV materials (inorganic or organic) were also developed and their PV performances were evaluated. Firstly, n-type 2D MoS₂ monolayers were directly integrated onto p-type Si substrates, realizing 2D/3D p-n heterojunction PV devices with PCEs of >5% [215]. Moreover, 2D MoS₂ layers interfaced with ITO (indium tin oxide) realized Schottky junction PV devices, benefiting from the high electrical conductivity and optical transparency of ITO [216]. Incorporating 2D TMDs into various functional materials were explored to improve the performances of PV device electrodes. MoS₂/CuS hybrids prepared by in-situ solvothermal methods worked as efficient counter electrodes for CdS/CdSe DSSCs, utilizing their enriched catalytic sites and reduced recombination rates at the electrode/electrolyte interfaces. A PCE of 5% with a fill factor of 0.48 were achieved in this case [217]. 2D MoS₂ layers incorporated with reduced graphene oxide (rGO) were used as counter electrodes in DSSCs, which leads to the enhancement of PCE by >6% in comparison to rGO-only electrodes [218]. 2D MoS₂ layers decorated with noble metals such as Pt were used as hole transport layers in organic PV devices [150]. 2D TMDs directly integrated with functional CPs were also explored as active components for

Table 1Performance comparison of various 2D TMD hybrids-based PV devices.

Composite	Solar cell type	J_{sc} (mAcm $^{-2}$)	$V_{oc}(V)$	FF (%)	PCE (%)	Ref.
Graphene/MoS ₂	Schottky	33.40	0.56	60.0	11.1	[221]
MoS ₂ /CNT	DSSC	15.82	0.77	65.0	7.92	[222]
Graphene/MoS ₂ /n-Si	Schottky	27.2	0.55	32	4.8	[223]
MoS ₂ /WS ₂ bilayer	Type II heterojunction	3.5	1.0	60.0	1.5	[209]
p-MoS ₂ /n-MoS ₂	p-n junction	20.9	0.28	47.0	2.8	[212]
WSe ₂ /MoSe ₂	p-n junction	_	0.05	-	0.12	[67]
$Mo_{1-x}W_xSe_2$	Schottky	92.0	0.44	32.0	16	[224]
MoO_3/MoS_2	Organic solar cell (OSC)	13.2	0.77	68.2	6.96	[225]
MoS ₂ /TiO ₂	Bulk heterojunction	4.7	0.56	-	1.7	[226]
MoS ₂ /TiO ₂	DSSC	17.72	0.60	77.8	8.96	[227]
Au/MOS ₂ /ITO	Schottky junction	5.37	0.59	55.0	1.8	[216]
Au NP@MOS ₂	Organic photovoltaic device (OPV)	13.4	0.69	53.0	4.91	[228]
Au-MoS ₂	OSC	15.4	0.72	65.2	7.25	[150]
MoSe ₂ /Mo	DSSC	16.71	0.74	72.2	9.00	[229]
PEDOT:PSS/MoS2-PAS	Perovskite	24.0	0.90	68.5	16.47	[230]
MoS ₂ /PTB ₇ :PC ₇₁ BM	OSC	15.86	0.72	71.0	8.11	[231]
Pentacene/MoS ₂	p-n junction	_	0.30	-	0.004	[220]
p-Si/MoS ₂	p-n junction	18.0	0.39	63.0	4.46	[232]
n-MoS ₂ /i-SiO ₂ /p-Si	n-i-p junction	5.5	0.30	-	4.5	[233]
Pd:MoS ₂ /Si	p-n junction	15.1	0.45	-	2.4	[234]
MoS ₂ /h-BN/GaAs	Schottky junction	21.1	0.76	56.3	9.03	[235]
TiO ₂ /CH ₃ NH ₃ PbI ₃ /MoS ₂ /Spiron-OMeTAD/Au	Perovskite	21.5	0.93	66.7	13.3	[236]

PV devices. For example, n-type 2D MoS_2 layers were directly integrated onto p-type rubrene to develop PV devices based on rubrene/2D MoS_2 p-n heterojunction vertical stacks [219]. Other examples include pentacene/2D MoS_2 p-n junction PV devices which exhibit gate-tunable PV responses [220]. Moreover, p-type organic semiconductors such as C8-BTBT were demonstrated to epitaxially grow on the top of n-type 2D MoS_2 monolayers, achieving PV p-n junctions [202]. Table 1 summarizes various solar cell parameters such as short-circuit photocurrent density (J_{sc}), open circuit voltage (V_{oc}), fill factor (FF), and PEC for 2D TMDs-based hybrid solar cells.

Hydrogen generation. Hydrogen (H₂) generation via a solar energydriven water splitting is recently gaining substantial interest as a new approach to generate renewable energy. This approach requires low-cost catalysts to initiate the HER accompanying high current densities at low over potentials. Traditionally, noble metals such as Pt have been utilized for this application, while their high cost is a major hurdle to hinder their commercial usage [237]. Researches have been looking for alternative catalytic materials which are chemically stable, non-toxic, earth abundant, and inexpensive. Recent studies have demonstrated that 2D TMDs are promising non-metallic catalysts owing to their large surface area coupled with the aforementioned attributes inherent to them, suggesting their potential as an alternative to Pt catalysts [238]. Theoretical and experimental studies conducted a decade ago demonstrated that the edge sites in 2D MoS₂ layers can drastically facilitate charge carrier transports associated with HER [29,239]. Since then, substantive researches have been driven toward utilizing the edge sites of 2D TMDs, which has focused on maximally/preferentially expose the 2D edge sites via controlled growths and structural modifications [30,240]. Along these efforts to engineer the structures of 2D TMD layers to achieve high catalytic activity, 2D TMDs themselves have been incorporated with noble metal catalytic NPs such as Pt, Pd, and Ag. The resulting hybrid materials can sustain the high electrical conductivity of the conventional catalyst (mostly, noble metals) while the 2D edge sites can further enhance HER. Fig. 8(a) shows the epitaxial/uniform growth of Pd NPs (5 nm in size) on the surface of 2D MoS2 layers [155]. The performances of 2D TMD/noble metal hybrid for catalytic HER applications were also evaluated. For example, Ptdecorated 2D MoS₂ layers exhibit significantly higher catalytic activity in comparison to pristine 2D MoS₂ layers (Tafel slopes of $40\,mVdec^{-1}$ vs. $94\,mVdec^{-1}$), as shown in Fig. 8(b). Similar studies also demonstrate that 2D MoS₂/Pd hybrid catalysts exhibit excellent HER activity accompanying the high turnover frequency (TOF) of $0.013\,s^{-1}$ and lower Tafel slope of $39\,mVdec^{-1}$ [241]. Drastic (\sim three fold) improvement of HER activity was observed in 2D MoS₂/Au hybrids in comparison to pristine 2D MoS₂ layers [242], which is mainly attributed to the increased carrier density resulted from the introduction of Au-plasmonic hot electrons.

In addition to the noble metals, 2D TMDs have also been incorporated with other functional materials (e.g. metal oxides and CPs) for HER applications. Fig. 8(c) shows molybdenum trioxide (MoO₃) nanowires coated with 2D MoS₂ layers and their HER performances [34]. A Tafel slope of 50–60 mVdec⁻¹ was demonstrated, which was claimed to be the combined consequence of the fast charge transports in the MoO₃ core and the enhanced catalytic activity contributed by the large surface area of the 2D MoS₂ shell. A wide range of 2D TMD/CP hybrid catalysts were developed owing to their intrinsic advantages of facile low-temperature solution fabrication process. 2D MoS₂/PPy hybrid films exhibited outstanding HER performances (Tafel slope as low as $29 \,\mathrm{mV} dec^{-1}$) nearly comparable to those of Pt catalysts [243]. Amongst many, carbonaceous nanomaterial (CNT or graphene) additives are particularly promising for HER because they can offer substantial enhancement in the electrical conductivity as well as provide large surface areas. 2D MoS₂ layers were incorporated with 3D-networked CNT forests [244] where largely exposed 2D edge sites contribute to achieving excellent HER performances (onset overpotential of 75 mV). Reduced graphene oxide (rGO) is an intriguing host material for 2D TMDs as it can efficiently disperse and anchor 2D TMDs maintaining their functionalities. Moreover, the oxygen-containing functional groups on the rGO surface serve as nucleation sites for 2D TMD growth. 2D MoS₂/rGO hybrids were initially developed using solvothermal processes. 2D MoS₂ layers were directly grown on the rGO surface using DMF as a surfactant (Fig. 8(d)), which achieved small 2D MoS₂ flakes uniformly distributed on rGO surfaces (Fig. 8(e)) [245]. The 2D MoS₂/rGO hybrid material exhibits excellent HER performances (Fig. 8(f), (g)); a very small overpotential \sim 0.1 V and a Tafel slope as small as 41 mVdec⁻¹. Besides 2D MoS₂, other 2D TMD layers such as 2D WS₂ and 2D MoSe₂ have been employed with rGO and their HER performances were evaluated. For example, 2H-WS₂/rGO hybrid exhibited a Tafel slope of 58 mVdec⁻¹ [45]. Moreover, highly porous MoSe₂/rGO/CNT stacked hybrids prepared by a spray pyrolysis demonstrated an overpotential of 0.24V and

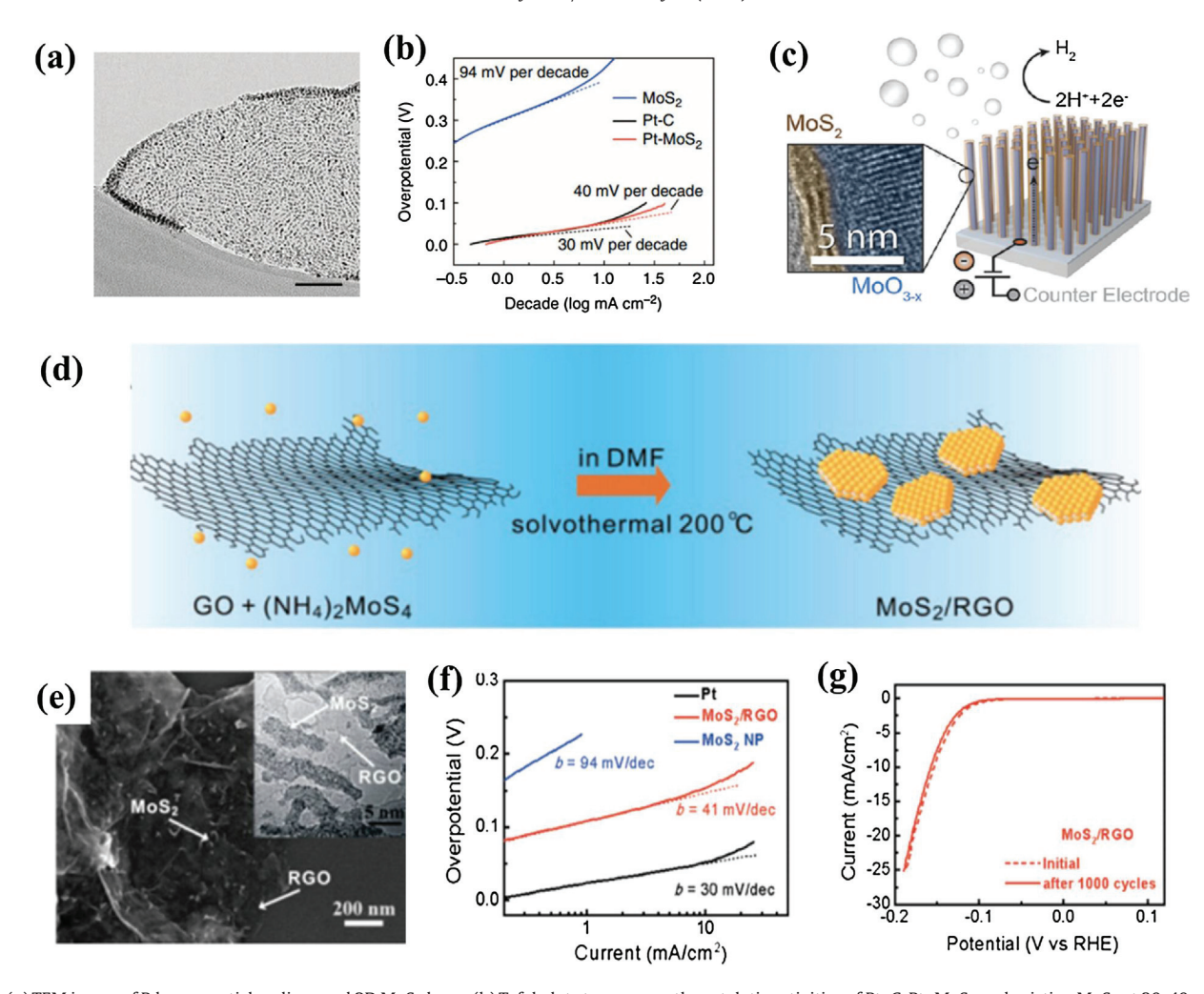


Fig. 8. (a) TEM image of Pd nanoparticles-dispersed 2D MoS₂ layer. (b) Tafel plots to compare the catalytic activities of Pt–C, Pt–MoS₂ and pristine MoS₂ at 30, 40 and 94 mV per decade. Reproduced with permission from Ref. [155]. Copyright 2013, Nature Publishing Group. (c) Schematic representation of MoO₃/MoS₂ core/shell nanowires and their catalytic reaction. Reproduced with permission from Ref. [34]. Copyright 2011, American Chemical Society. (d) Schematic representation of the solvothermal synthesis of 2D MoS₂/rGO hybrids. (e) SEM and TEM (inset) images of the 2D MoS₂/rGO hybrid. (f) Tafel plots showing a superior catalytic activity of the 2D MoS₂/rGO hybrid compared to pristine 2D MoS₂. (g) No HER current loss in the 2D MoS₂/rGO hybrid after 1000 cycles at current density of 100 mV/s. Reproduced with permission from Ref. [245]. Copyright 2011, American Chemical Society.

a Tafel slope 53 mVdec⁻¹, respectively [246]. 2D TMD hybrids containing non Mo- or W- metal chalcogenides also present promising HER performances [247,248]. For example, NiS₂-intercalated MoS₂ nanowires yielded a low onset potential of 76 mV and a Tafel slope of 70 mVdec⁻¹ [249]. Noticeably, MoS₂/CoSe₂ hybrid electrocatalysts prepared by solvothermal methods exhibited excellent HER performances; a small Tafel slope of 36 mVdec⁻¹ and no current loss even after repeated measurements, which surpasses the performances of nearly all noble metal-free HER electrocatalysts [250]. The underlying principles behind these performance advantages are attributed to the catalytically active sites and defects abundant in these hybrids as well as their large surface areas. 2D MoS₂incorporatd CdS nanorods were demonstrated to work as efficient metal-free photocatalysts under visible light, evolving H2 at a rate of $49.80 \,\mathrm{mmol}\,\mathrm{g}^{-1}\,\mathrm{h}^{-1}$ with a high quantum yield of 41.37% [103]. This performance advantage was attributed to the combined results of the co-catalytic activities of CdS and MoS2 and the efficient radical transfer with reduced charge recombination enabled by their intimate interfacial contacts.

Thermoelectrics. Sustainable energy requires technologies to effectively utilize all forms of energy including hydroelectricity, solar energy, wind energy, etc. Heat, a major source for electric-

ity, can be obtained from either green energy sources such as solar heat and geothermal energy, or raw energy sources (e.g., petroleum, natural gas, and coal). According to a report from Lawrence Livermore National Laboratory, out of about 98.3 Quads (1 Quad = 1.055×10^{18} joules) of energy used in US in 2014, 59.4 Quads were wasted as heat in power generation, transport, and utilization [251]. Effective recovery of waste heat is important in solving energy and environmental problems by providing supplemental electrical power without burning additional fossil fuel. The thermoelectric (TE) effect, a phenomenon that converts thermal energy directly into electric energy offers a reliable and environmentally friendly approach to utilize various types of waste heat. When a temperature gradient is generated in thermoelectric materials (usually semiconductors), electrons and holes with high thermal energy at the hot end diffuse to the cold end, creating a potential difference to power an external load. The efficiency of a thermoelectric material is represented by the Figure-of-merit, ZT, where $Z = \frac{S^2 \sigma}{\kappa}$ is a function of the electrical conductivity (σ), thermal conductivity (κ) and the Seebeck coefficient (S, a measure of thermoelectric voltage induced by a temperature difference across the hot and cold end), T is the average of the temperature at cold and hot ends. Improving ZT requires increasing the Seebeck coefficient and electrical conductivity, while minimizing the thermal conduc-

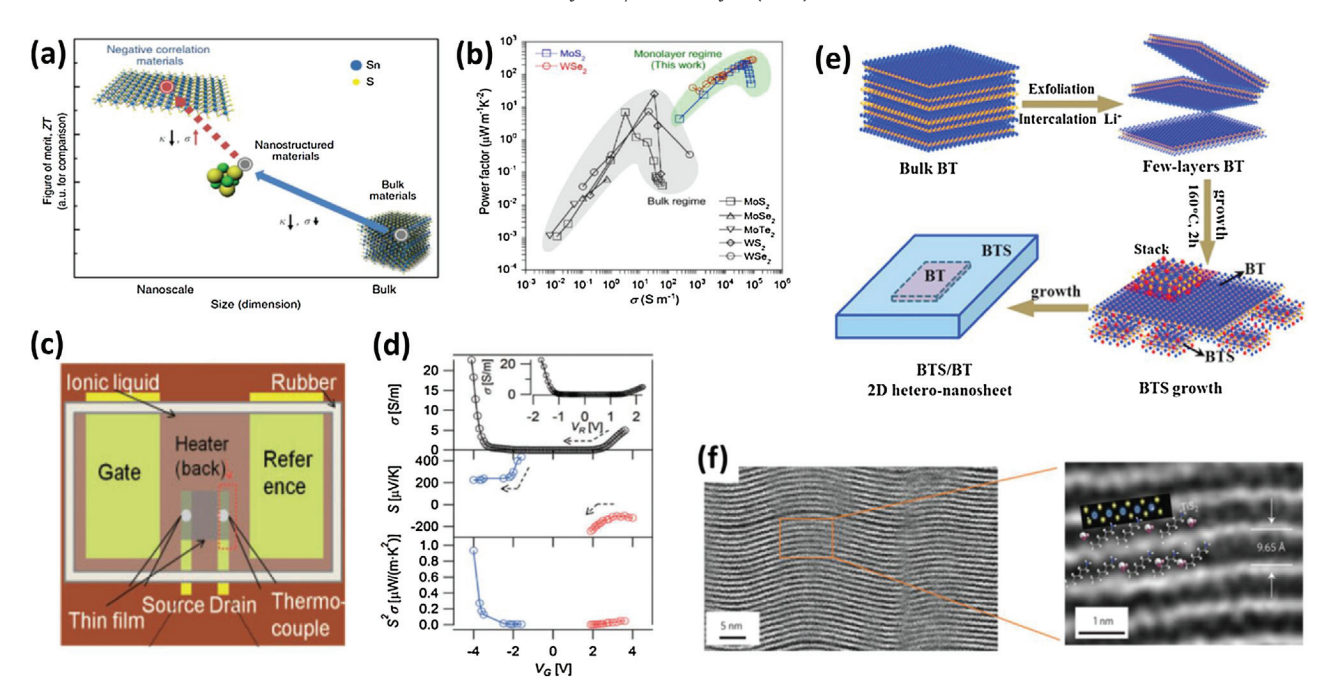


Fig. 9. (a) Evolution of thermoelectric properties in layered materials from their bulk counterparts to nanostructures. Reproduced with permission from Ref. [256]. Copyright 2016, Nature Publishing Group. (b) Comparison of power factor vs electrical conductivity in various 2D TMDs in bulk and monolayer forms. Reproduced with permission from Ref. [261]. Copyright 2016, American Physical Society. (c) Experimental setup for the measurement of thermoelectric properties in W52 nanotubes using electrolyte gating. (d) Variation of electrical conductivity (σ), Seebeck coefficient (S), and power factor ($S^2\sigma$) as a function of back gate voltage. Reproduced with permission from Ref. [262]. Copyright 2017, Institute of Physics. (e) Synthesis strategy for 2D Bi2Te2.7S0.3(BTS)/Bi2Te3(BT) hybrids. Reproduced with permission from Ref. [269]. Copyright 2016, Elsevier. (f) Low and high resolution STEM images of $TiS2[(HA)_x(H_2O)_y(DMSO)_z]$ hybrids. Reproduced with permission from Ref. [271]. Copyright 2015, Nature Publishing Group.

tivity at the same time [252]. It is important to note that electrical conductivity, Seebeck coefficient, and thermal conductivity are not independent, which makes it difficult to optimize one parameter without affecting the other parameters. Hence, substantive efforts on improving ZT focus on the development of new TE materials and/or their structural optimizations [253].

2D TMDs present promising electrical/thermal properties as efficient TE materials owing to their intrinsic quantum size effects which make the physical factors defining ZT free from the aforementioned interdependence [254,255]. Fig. 9(a) reveals how the ZT value changes with a structural evolution of TE materials from bulk materials to nanostructured/layered 2D materials [256]. Mono and few-layer 2D TMDs have exhibited great potential for improved TE conversion efficiencies [257,258]. Single crystalline 2D MoS₂ layers have exhibited a significantly large value of S \sim 105 μ VK⁻¹, measured in a field-effect-transistor (FET) configuration [259]. Mechanically-exfoliated few layer 2D WSe₂ layers also presented similar properties, measured via ionic gating [260]. However, these studies were carried out with 2D TMD flakes of very small sizes ($\leq 10 \,\mu\text{m}^2$), making them non-commensurate for reliable experimental determinations of the thermoelectric properties. In this regard, large-area CVD-grown 2D MoS₂ and 2D WSe₂ monolayers were investigated and their thermoelectric properties were determined in a FET configuration [261]. In this approach, a large FET channel length of 400 µm was maintained to ensure reliable thermoelectric measurements via uniformly large temperature gradient. As a result, large |S| (>200 μ VK⁻¹) and power factor $(>200 \,\mu\text{Wm}^{-1}\text{K}^{-2})$ were observed in both 2D MoS₂ and 2D WSe₂. Fig. 9(b) indicates an order of magnitude enhancement in the power factor as a function of $\boldsymbol{\sigma}$ in various 2D TMD monolayers compared to their bulk counterparts. Experimental efforts have been further driven to precisely determine the TE properties of various 2D TMD nanostructures. Fig. 9(c) shows the schematic setup for measuring the TE properties of WS2 nanotubes placed on an insulation

layer of parylene. A heater was attached at the back side to create the thermal gradient and the generated TE voltages were measured using electrolyte gating [262]. Fig. 9(d) presents the back gate (V_G) dependent electrical conductivity, Seebeck coefficient and power factor in the WS₂ nanotubes, revealing their ambipolar transports. In addition to the experimental efforts to measure the TE properties, it is predicted that metal chalcogenides and 2D TMD hybrids with other functional materials can achieve better TE properties compared to mono-component nanostructures. These projected advantages are attributed to the reduced thermal conductivity through phonon scattering at their hybrid interfaces [263]. Experimental efforts were pursed in developing 2D TMD hybrid TE materials to verify these merits [264,265]. Metallic 1T phased 2D MS₂ (M: Mo, W) layers were incorporated into rGO, which led to a maximum power factor of 15.1 and $17.4\,\mathrm{mW\,m^{-1}}$ K^{-2} in rGO/MoS₂ and rGO/WS₂, respectively [266]. 2D WS₂/PEDOT: PSS hybrids were also developed by sonicating 1T phase 2D WS₂ flakes into an aqueous solution of PEDOT: PSS [267]. The presence of PEDOT: PSS chains in WS₂ facilitated the transport of charge carriers and reduced the energy barrier within adjacent WS₂ flakes. A TE power factor of 45.2 μ W m⁻¹k⁻¹ was achieved in these hybrids, which reflects the enhanced electrical conductivity and the Seebeck coefficient. In another recent study, a simple oxygen doping strategy was employed to incorporate MoO2 nanoclusters into 2D MoS₂, which significantly improved the electrical conductivity and the Seebeck coefficient as well as suppressing the thermal conductivity. As a result, ~50 times enhancement in the TE efficiency was observed in comparison to the pristine state without doping [268].

Hierarchically structured $Bi_2Te_{2.7}S_{0.3}(BTS)/Bi_2Te_3(BT)$ hybrid nanosheets were realized by the layer-epitaxial growth of BTS on and along chemically exfoliated mono-to-few layer BT seed-crystals [269]. Fig. 9(e) shows the synthetic steps of BTS/BT hybrids. In these hybrid materials, the enhanced phonon scattering mostly pronounced at their interfaces resulted in ultralow thermal conduc-

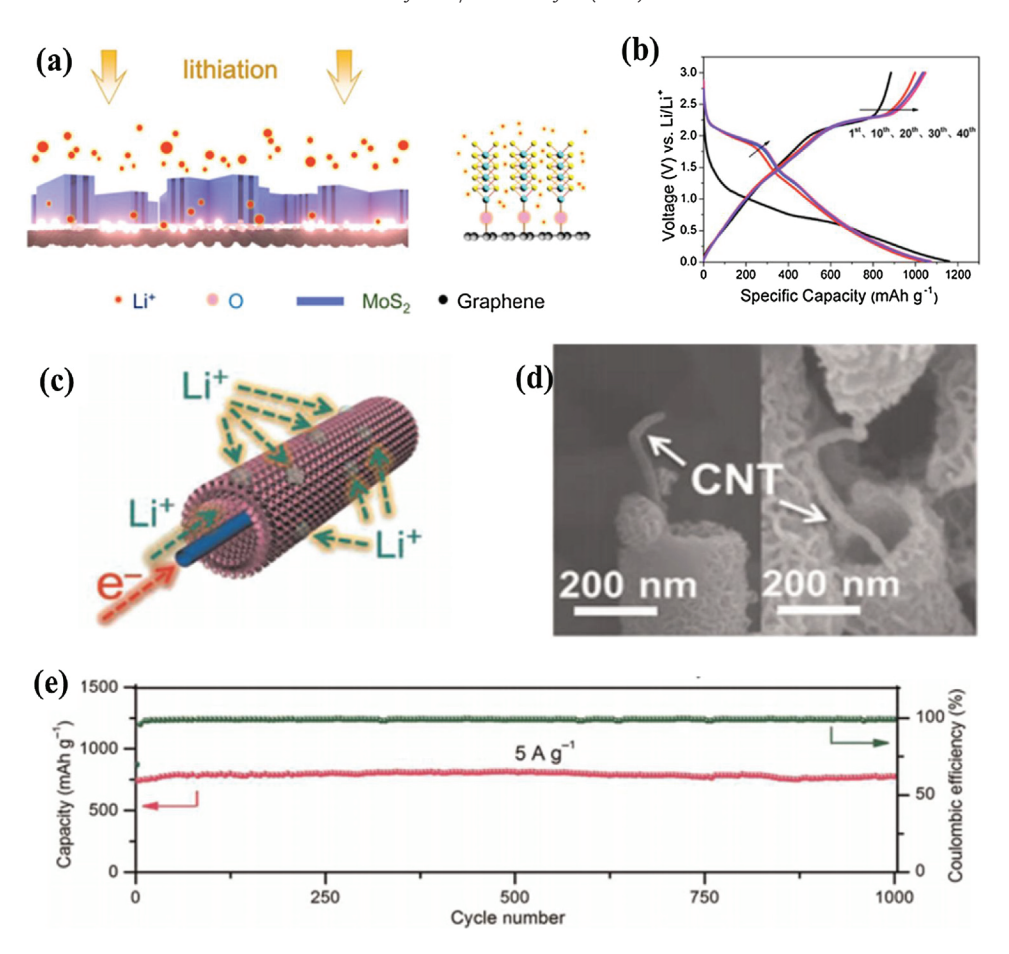


Fig. 10. (a) Schematic representation of Li⁺ diffusion into 2D MoS₂ layers vertically grown on top of graphene. (b) Charge–discharge curves of 2D MoS₂/graphene hybrid electrodes at different cycles at 100 mA g⁻¹. Reproduced with permission from Ref. [275]. Copyright 2016, American Chemical Society. (c) Schematic representation of transport paths for Li⁺ and electrons in CNT/MoS₂ tubular hybrid. (d) SEM images showing a single CNT wrapped with 2D MoS₂ tubular layers. (e) Cycle test of the 2D MoS₂/CNT hybrid electrode at 5 Ag⁻¹ showing an excellent cycling stability with nearly 100% coulombic efficiency after 1000 cycles. Reproduced with permission from Ref. [281]. Copyright 2016, AAAS.

tivity, which led to a maximum ZT of 1.17 at 450 K, approximately three times higher than that of pristine BT nanostructures. The intrinsically-layered structure of 2D TMDs allows for the incorporation of other functional materials into their vdW gaps. This intercalation-induced 2D structural change is predicted to enhance interfacial phonon scattering, which can lead to reduce the thermal conductivity [270]. For example, intercalation of hexylammonium ions into layered 2D TiS₂ crystals from an organic salt of dimethyl sulfoxide (DMSO) achieved an organic/inorganic hybrid of TiS₂[(HA)_x(H₂O)_y(DMSO)_z]. Fig. 9(f) shows the cross-sectional TEM image of the material, revealing its layered structure. These hybrid materials showed an eight-fold reduction in lattice thermal conductivity, leading to three times higher in-plane ZT value as compared to TiS₂ bulk materials [271].

Energy storage

Lithium ion batteries. Lithium ion batteries (LIBs) have become a major energy source for a large number of today's consumer electronic devices, including hybrid electric vehicles (HEVs), UPS systems, and power supplies for portable electronics. However, the low theoretical capacity (372 mAhg⁻¹) and the poor rate performance inherent to conventional graphite anode materials are not sufficient to fulfill the ever-increasing demand for higher power densities demanded in advanced LIBs [272]. 2D TMDs possess a great potential as LIB anode materials owing to their unique layered structures with highly dense vdW gaps which could efficiently facilitate Li* intercalation/de-intercalation, projecting the

advantage of extended cyclic stability. However, the major bottlenecks of 2D TMDs for LIB applications include their low electrical conductivity and the structural instability associated with the large volume expansion during Li+ intercalation events. To circumvent these issues, 2D TMDs have been incorporated with other capacitive and conductive materials, yielding 2D TMD hybrid LIB electrodes with improved performance and stability. In this context, carbonaceous nanomaterials, particularly, graphene and rGO have been extensively investigated. LIB anodes based on 2D MoS₂ layers directly grown on the surface of graphene exhibited a reversible capacity of 1290 mAhg-1 at a current density of $100 \,\mathrm{mAg^{-1}}$, with a capacity retention up to 50 cycles [273]. 2D MoS₂/graphene flower-like 3D structures were realized by the hydrolysis of lithiated MoS₂ (LiMoS₂), delivering a reversible capacity of 1300–1400 mAhg⁻¹ with a limited rate performance of \sim 500 mAhg⁻¹ at a current density of 1000 mAg⁻¹ [274]. Recently, a new type of 2D MoS₂/graphene hybrids were developed where individual 2D MoS₂ layers were vertically grown on top of the basal plane of graphene (Fig. 10(a)) [275]. The obtained vertical 2D MoS₂/graphene hybrids exhibited a high capacity of 1077 mAhg⁻¹ at $100 \,\mathrm{mAg^{-1}}$ up to 150 cycles (Fig. 10(b)). This performance improvement is attributed to the presence of C-O-Mo bonds which facilitate the transport of charged carriers and the ample free volumes between the vertical 2D MoS₂ layers which efficiently accommodate the volume expansion/shrinkage during the course of lithiation/de-lithiation events. A variety of 2D MoS₂/rGO hybrids were also developed for LIB anodes. 2D MoS₂/rGO hybrids produced

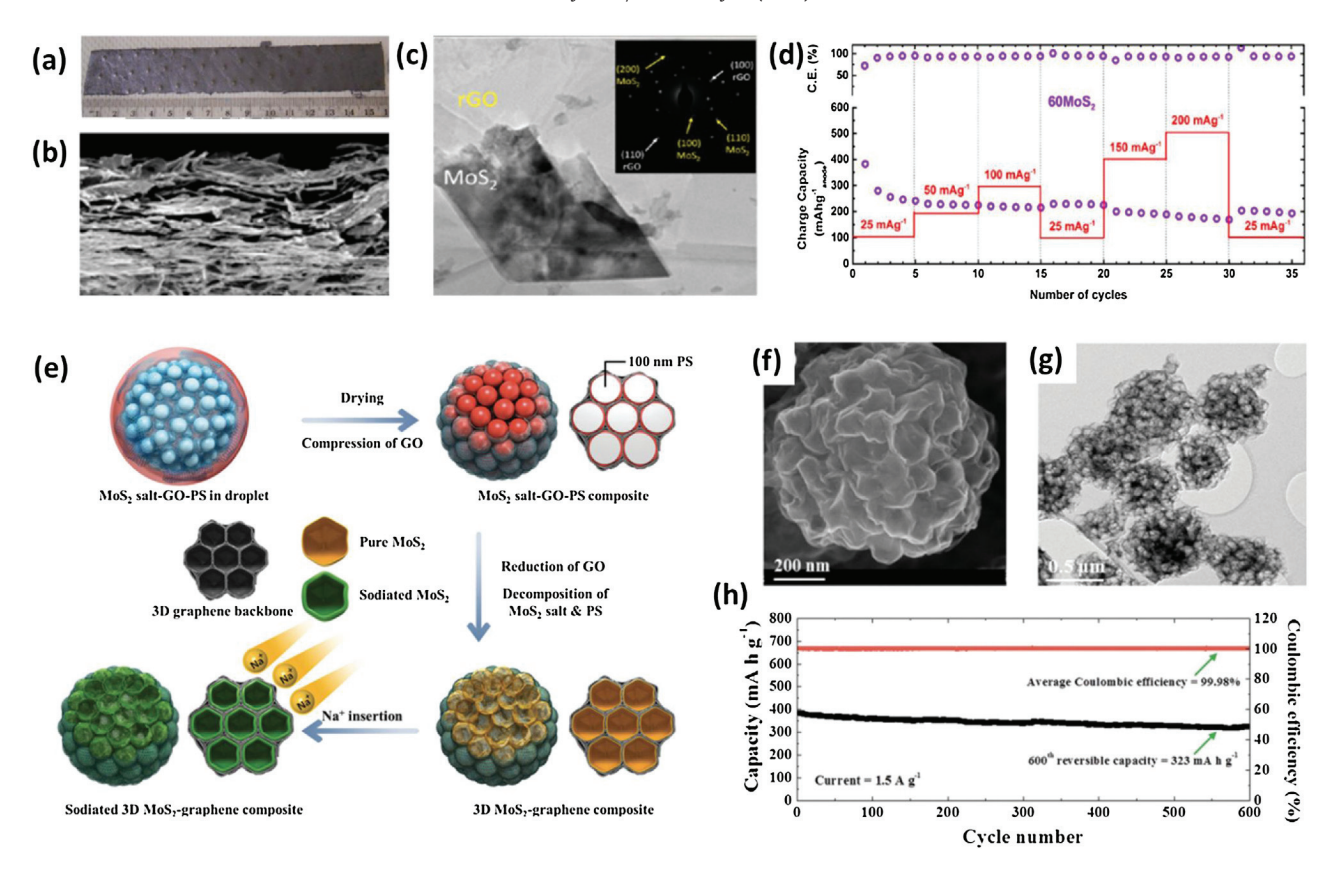


Fig. 11. (a) Image of a rGO/MoS_2 hybrid paper prepared using a vacuum filtration. (b) Cross-sectional SEM image of the rGO/MoS_2 hybrid paper showing its average thickness of \sim 20 μ m. (c) TEM image showing 2D MoS_2 layers wrapped with rGO flakes. TEM electron diffraction pattern (inset) shows the polycrystalline structure of rGO and 2D MoS_2 . (d) Charge capacity and coulombic efficiency of rGO/MoS_2 hybrid paper at different current densities. Reproduced with permission from Ref. [291]. Copyright 2014, American Chemical Society. (e) Schematic procedures for the pyrolysis synthesis of MoS_2 /graphene microspheres and the insertion of Na^+ . (f) SEM and (g) TEM images showing the 3D morphology of MoS_2 /graphene microspheres. ((h)) Cycle tests showing the specific capacity and coulombic efficiencies of the MoS_2 /graphene microspheres up to 600 cycles at a current density of 1.5 MoS_2 -graphene microspheres up to 600 cycles at a current density of 1.5 MoS_2 -graphene microspheres up to 600 cycles at a current density of 1.5 MoS_2 -graphene microspheres up to 600 cycles at a current density of 1.5 MoS_2 -graphene microspheres up to 600 cycles at a current density of 1.5 MoS_2 -graphene microspheres up to 600 cycles at a current density of 1.5 MoS_2 -graphene microspheres up to 600 cycles at a current density of 1.5 MoS_2 -graphene microspheres up to 600 cycles at a current density of 1.5 MoS_2 -graphene microspheres up to 600 cycles at a current density of 1.5 MoS_2 -graphene microspheres up to 600 cycles at a current density of 1.5 MoS_2 -graphene microspheres up to 600 cycles at a current density of 1.5 MoS_2 -graphene microspheres up to 600 cycles at a current density of 1.5 MoS_2 -graphene microspheres up to 600 cycles at a current density of 1.5 MoS_2 -graphene microspheres up to 600 cycles at a current density of 1.5 MoS_2 -graphene microspheres up to 600 cycles at a current density of 1.5 MoS_2 -graphene microspheres up to 600 cycles at a current density of 1.5 MoS_2 -

via a hydrothermal method exhibited a capacity of 1150 mAhg⁻¹ after 60 cycles and an excellent rate performance of \sim 890 mAhg⁻¹ at a current of 1A/g [276]. 2D MoS₂ layers integrated into 3D rGO foams reached a capacity of ~650 mAhg⁻¹ at a current rate of 0.1 C [277]. In addition to graphene and rGOs, CNTs have drawn particular attention owing to their very high electrical conductivity and facileness of integrating with 2D TMDs. Various forms of 2D MoS₂/CNT hybrids were exploited for LIB anodes which exhibited high capacities in the range of $\sim 400-1000 \,\mathrm{mAhg}^{-1}$. These materials include 2D MoS₂/CNTs in 3D networked structures [278], cylindrical 2D MoS₂/CNTs [279], coaxial CNTs with 2D MoS₂ on the their surfaces [280], and hierarchically integrated 2D MoS_x/MWNTs [173]. Most notably, hierarchically-structured 2D MoS₂/CNT hybrids were developed (Fig. 10(c,d)) [281], where individually networked CNTs were wrapped by tubular 2D MoS₂ layers which enhance the adsorption of Li+ while the internal CNTs provide pathways for charge carriers. These 2D MoS₂/CNT hybrids delivered an extraordinary high capacity of \sim 1320 mAhg⁻¹ (at $0.1 \,\mathrm{Ag^{-1}}$) with an impressive cyclic stability up to 1000 cycles (Fig. 10(e)).

Metal oxides are another promising class of materials that possess suitable material properties with a potential to replace conventional graphite electrodes in LIBs. For example, tin oxide (SnO₂) shows twice of the theoretical capacity (\sim 781 mAhg⁻¹) compared to graphite (\sim 372 mAhg⁻¹) in terms of intercalating Li⁺ [282]. These oxides can easily form hybrid materials with 2D TMDs while maintaining their structural suitability for LIB electrodes. 2D MoS₂/SnO₂ hybrids developed by the hydrothermal synthesis of SnO₂ NPs onto 2D MoS₂ layers delivered a reversible capacity

of 602 mAhg⁻¹ after 230 cycles [125]. The observed performance enhancement in these hybrid materials is endowed by the synergistic effects between 0D SnO₂ NPs and 2D MoS₂ layers, which complements each other to overcome their inherent weaknesses. For example, SnO₂ NPs incorporated into 2D MoS₂ layers served as "spacers" to prevent the restacking of individual 2D layers, whereas the structurally-retained 2D MoS₂ layers worked to prevent the agglomeration of SnO₂ NPs. Iron oxides of various oxidation states have been incorporated with 2D TMDs, aiming at utilizing their intrinsic advantages of high theoretical capacities, environmentalbenignity, and earth abundance [136]. Fe₂O₃ NPs (size \sim 4 nm) were decorated onto 2D MoS₂ layers to utilize the aforementioned property advantages as well as inhibit the restacking of 2D MoS₂ layers [283]. Specifically, 2D MoS₂ layers not only contribute to enhancing the total capacity of the hybrid anode but also support Fe₂O₃ to attain low irreversible capacity by converting irreversible Li₂O to Li⁺ through the formation of Mo metal clusters. Accordingly, this strong electrochemical coupling of Fe₂O₃ and MoS₂ resulted in excellent capacitive performances with a high reversible capacity of 864 mAhg⁻¹ at a current density of 2 Ag⁻¹ after 140 cycles. Similarly, structured 2D MoS₂/Co₃O₄ hybrids delivered a high discharge capacity of $1100\,\text{mAh}\,\text{g}^{-1}$ after 50 cycles at $200\,\text{mA}\,\text{g}^{-1}$ and a high reversible capacity of 946.6 mAhg⁻¹ after 50 cycles at a current density of $500 \,\mathrm{mA}\,\mathrm{g}^{-1}$ [284]. The synergetic effects as a result of combining 2D MoS₂ layers with Co₃O₄ NPs are multi-fold; A large amount of Co₃O₄ NPs acts as physical spacers for maintaining the structural integrity of 2D MoS₂ layers. Moreover, they provide short pathways for efficient ion transports while their agglomeration is, in turn, inhibited by surrounding 2D MoS₂ layers.

Sodium ion batteries. Extensive uses of LIBs in recent years following the explosive development of portable electronics and HEVs have been straining our Li resources to the extent where they approach the category of rare materials. In addition, LIBs tend to exhibit meager performances in harsh environments such as limited lifetimes mainly due to their safety concerns, which limits their versatility in emerging technologies such as flexible energy storage devices [285]. Recently, sodium ion batteries (SIBs) are representing a paradigm-shift for the safer and more sustainable battery technologies due to a huge abundance of sodium (Na) -4th most abundant element on earth. SIBs are projected to significantly lower the cost of rechargeable batteries as many as thirty times compared to LIBs while being free of safety concerns [286]. However, the major drawbacks associated with SIBs are the larger size of Na⁺ (1.02 Å) as compared Li⁺ (0.76 Å) and their high standard electrode potential (-2.71 V), which makes the storage of Na⁺ into conventional anode materials difficult, resulting in inferior storage capacity compared to LIBs. Incorporating 2D TMDs into SIB anode materials have been directed to mitigate these problems [287]. It is noted that most of the 2D TMD hybrids developed for SIB anodes till now incorporated carbonaceous additive materials [288], targeted at enhancing electrical conductivity as well as accommodating more Na⁺. Moreover, carbonaceous nanomaterials can buffer the substantial volume change of 2D TMDs during charge/discharge cycles [289], and improve the poor electrochemical performances inherent to pristine 2D TMDs at low operating voltages (e.g., 0.4V in case of 2D MoS₂) [290]. 2D MoS₂/rGO hybrids in the form of a paper were developed using a vacuum filtration method [291] (Fig. 11(a)), where individual 2D MoS₂/rGO hybrid layers were vertically stacked retaining numerous physical gaps (Fig. 11(b,c)). These hybrid SIB electrodes offered a capacity of \sim 230 mAhg⁻¹ and a coulombic efficiency reaching 99%. Additionally, the interleaved structure of porous rGO backbones provided a high mechanical support to 2D MoS₂ layers, resulting in good structural stability even after cycling at $200 \,\mathrm{mAg^{-1}}$, retaining 72% of the initial capacity (Fig. 11(d)). Other studies with similarly structured 2D MoS₂/rGO hybrids report a higher capacity of 352 mAhg⁻¹, where the high diffusivity of Na⁺ and the high electron transfer efficiency in 2D MoS2 interfaced with rGO were experimentally and computationally verified [292]. In addition to rGO, graphene were also extensively pursued as a host material for 2D TMDs, and 2D WS₂/graphene hybrids with 2D WS₂ layers anchored onto the graphene surface exhibited a capacity of ~590 mAhg⁻¹ [293]. A novel SIB anode material based on 3D MoS₂/graphene hybrids were developed using one-pot spray synthesis methods (Fig. 11(e)) [294]. A stable colloidal spray solution of polystyrene (PS) nanobeads, rGO, and (NH4)₂MoS₄ was used to form micrometer-sized droplets by an ultrasonic nebulizer. These droplets were then passed through a tube furnace at 800 °C and were converted to 3D MoS₂/graphene microspheres with a high porosity (Fig. 11(f,g)). These highly porous hybrid materials exhibited a high capacity of 797 mAhg⁻¹ at the 1st cycle and retained an average coulombic efficiency of 99.98% even after 600 cycles (Fig. 11(h)).

In addition to 2D MoS $_2$ and 2D WS $_2$, several other 2D TMDs have been explored to be incorporated into carbonaceous nanomaterials for SIB anodes. For example, 3D CNTs embedded with fullerenelike MoSe $_2$ prepared via spray pyrolysis and selenization processes exhibited much higher discharge capacity (296 mAhg $^{-1}$) as compared to stand-alone MoSe $_2$ (144 mAhg $^{-1}$) [295]. This enhanced Na $^+$ storage capacity is attributed to the synergetic effect from both constituting materials; Fullerene-like MoSe $_2$ provide large surface areas and ample reactive sites for efficient the intercalation/deintercalation of Na $^+$ with 3D CNTs. In parallel, 3D CNTs possess high structural porosity and electrical conductivities, which further contributes to increase the capacity. In another report, 2D

MoSe₂/MWCNT hybrids were formed by coating 2D MoSe₂ layers on MWCNTs exhibited a retention of 385 mAhg⁻¹ over 90 cycles at a current rate of 2000 mAhg⁻¹ [296], significantly higher than that of pristine 2D MoSe₂. It is due to the uniform distribution of MoSe₂ sheets onto MWNTs which shorten the electronic Na⁺ pathways while MWCNT flexible support prevents the electrode structure damage from volume expansion/contraction during cycling. Carbon nanofibers prepared by an electrospinning method were incorporated with 2D MoS₂ layers, and the resulting hybrids exhibited outstanding rate and cycling performances comparable to those of LIBs [297]. Porous hollow carbon spheres decorated with 2D MoSe₂ layers exhibited an excellent reversible capacity of 580 mA h g^{-1} after 100 cycles [298]. The synergic effects that lead to the high capacitive performance in these hybrids are attributed to following; High porosities of electrically conductive carbon spheres facilitate to accommodate/release the mechanical stress accumulated during charge-discharge cycles. Moreover, the uniformly coated individual 2D MoSe₂ layers provide percolation pathways for efficient Na⁺ diffusions. Other metal sulfides-based 2D TMDs have also been combined with carbon nanomaterials for SIB applications [287]. For example, electrodes based on 2D SnSe layers and carbon black fabricated by high-energy ball milling exhibited a high capacity of 324.9 mAhg⁻¹ at a high current density of 500 mAg⁻¹ over 200 cycles [299]. The high capacity/retention is also attributed to that the carbon black functions as a "buffer layer" to accommodate the volume change of the hybrid material, while enhanced electrical conductivity is offered by the uniformly dispersed 2D SnSe layers. Despite the successful storage of Na⁺ in these novel hybrid materials, the easy dissolution of reaction intermediates (i.e. Na₂S) into electrolytes during continued charging/discharging cycles severely limits the retention stabilities of SIBs [170]. The deposition of passivation layers to electrode/electrolyte interfaces has been explored to circumvent this structural loss-associated performance degradation. Atomic layer depositions of metal oxide layers were extensively pursued [300,301]. For example, the deposition of TiO₂ resulted in ~53% enhancement in the discharge capacity (i.e. 1392 mAh g^{-1}) and $\sim 1.3 \text{ time increase in the capaci-}$ tance retention of 2D MoS₂/carbon cloth hybrids. Table 2 represents the characteristics of 2D TMD hybrids based Li⁺ and Na⁺ battery electrodes comparing their key parameters, i.e., discharge capacity, coulombic efficiency, and cycle performance.

Supercapacitors. 2D TMDs have been increasingly employed in various energy conversion devices as overviewed above, while their applications to supercapacitors remain sparse for now. Although their intrinsic structural uniqueness of large surface area and numerous vdW gaps is projected to be ideal for supercapacitor applications [321], their relatively low electrical conductivity and structural instabilities are the major concerns making them uncompetitive with conventional LIBs [322,323]. Integrating 2D TMDs with other capacitive materials for supercapacitors has been directed to mitigate these issues while realizing additional functionalities (e.g., high mechanical flexibility) as well as retaining the intrinsic advantages of supercapacitors over LIBs (e.g., high power density and air stability). Most studies on 2D TMD hybrids for supercapacitors have focused on developing new electrode materials to alleviate their intrinsic weakness (e.g. low energy density) over LIBs. The presence of the numerous vdW gaps in 2D TMD layers is ideally suitable for efficient charge transports driven by the electrical double layer capacitance (EDLC) mechanism, while combining 2D TMDs with other pseudocapacitive materials can further improve the energy density. Traditionally, various TMOs such as NiO, Co₃O₄, and Fe₂O₃ have been used for supercapacitor electrodes [324] as they present various oxidation states suitable for pseudocapacitive reactions. The integration of 2D TMDs with these pseudocapacitive materials can further improve the supercapac-

Table 2Performance comparisons of Li⁺ and Na⁺ batteries based on 2D TMDs hybrids with various organic/inorganic components.

Classification	Hybrid electrode	Battery Type	1st discharge capacity (mAhg ⁻¹)	Coulombic efficiency (%)	Cycle performance (mAhg ⁻¹)/Current density (mAg ⁻¹)/Cycles	Ref.
TMDs/Carbon materials	MoS ₂ /CNT nanohybrid	LIB	1747	83.6	1679/1000/425	[302]
	ReS ₂ /CNT		1513	65.0	793/215/100	[303]
	MoS ₂ /Graphene		1483	91.1	1351/100/200	[274]
	MoSe ₂ /Carbon fibre	SIB	887.9	85.5	452.6/200/100	[304]
	SnS ₂ /rGO		839	75.0	628/200/100	[305]
	Sb ₂ S ₅ /Graphene foam		1156	73.6	748/200/300	[306]
TMD/Metal	MoS2-G/Ag nanoclusters	LIB	1605	66.0	1300/500/200	[307]
	Sb/MoS ₂ /C		1046.7		679.5/200/250	[308]
TMDs/Polymers	SnS2@PANI nanoplates	LIB	1395.8	69.4	730.8/100/80	[309]
	SnS/PPy		1828	59.4	703/1000/500	[310]
	MoS ₂ /PANI nanowires		1062.7	_	952.6/100/50	[52]
	MoS ₂ /PEO	SIB	242	99.0	148/50/70	[311]
	MoS ₂ /PANI		888	83.2	456/300/100	[312]
TMD/TMO	Fe_3O_4/MoS_2	LIB	1237	99.4	1200/500/560	[136]
	SnS_2/Co_3O_4		1344	73.0	715/100/100	[313]
	TiO ₂ @MoS ₂ /C		1083.9	78.0	457/100/100	[314]
	WS _x /WO ₃ thorn bush	SIB	1213	_	600/100/100	[315]
	$Na_2Ti_2O_5/VS_2$		575	99.8	203/100/100	[316]
	HfO2-coated MoS2		1058	_	636/100/50	[300]
TMD/TMD	MoS_2/WS_2	LIB	1157	90.0	998/100/100	[317]
	Ce_2S_3/MoS_2		225.5	99.1	459.2/100/500	[318]
	SnS-MoS ₂	SIB	555	_	396//100	[319]
	MoS ₂ /SnS ₂ -Gr		840	60.0	655/150/100	[320]

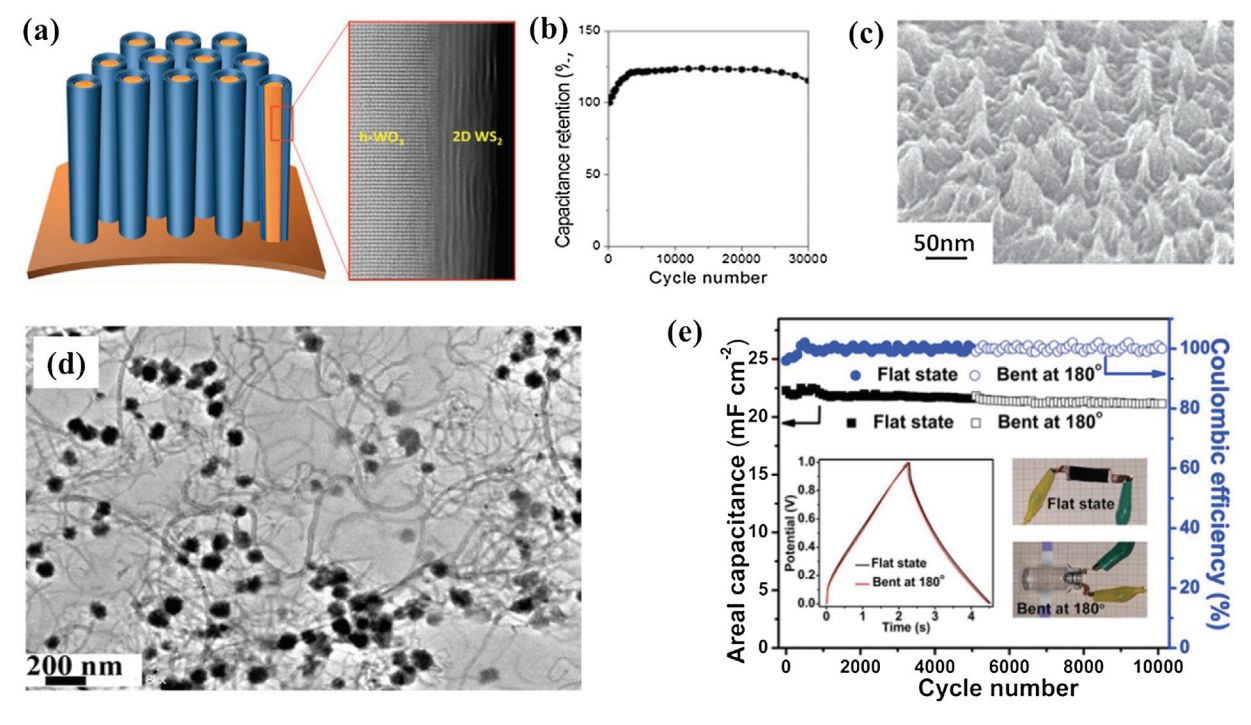


Fig. 12. (a) Schematic representation of an array of WO₃/WS₂ core/shell nanowires and their WO₃/WS₂ interface morphology. (b) Cycle test of the WO₃/WS₂ core/shell nanowire electrode showing an excellent stability up to 30,000 charge/discharge cycles. Reproduced with permission from Ref. [325]. Copyright 2016, American Chemical Society. (c) SEM image of 2D MoS₂/PANI hybrids showing the needle-like structure. Reproduced with permission from Ref. [328]. Copyright 2015, John Wiley and Sons. (d) TEM image of 3D MoS₂/CNT/rGO hybrids. (e) Long-term cyclic stability of the 3D MoS₂/CNT/rGO hybrids up to 10,000 cycles under mechanical bending at a current density of 10 mAcm⁻². The insets show the galvanostatic charge/discharge curve and the image of 3D MoS₂/CNT/rGO hybrids supercapacitors in flat and bent states. Reproduced with permission from Ref. [334]. Copyright 2017, John Wiley and Sons.

itor performances (mainly *via* enhanced EDLC). For example, 2D MoS₂/porous NiO hybrids with vertically-aligned 2D layers exhibited a high capacitance of $1080\,\mathrm{Fg^{-1}}$ at $1\,\mathrm{Ag^{-1}}$ [126]. Recently, core/shell hybrid nanowires based on single-crystalline tungsten trioxide (WO₃) core nanowires and 2D WS₂ shell layers were developed and integrated onto W foils [325]. These nanowires possess atomically sharp 2D WS₂/WO₃ interfaces and tailored functionalities specific to each constituting components (i.e., adsorption

and transport of charges through shell and core, respectively) (Fig. 12(a)). The core/shell hybrid nanowires exhibited an outstanding charging/discharging cyclic stability up to 30,000 cycles owing to their excellent chemical/mechanical stability (Fig. 12(b)), and achieved high energy densities exceeding a majority of conventional energy storage devices.

2D TMDs were also incorporated with a variety of carbonaceous materials including CPs, graphene, and CNTs, targeted at achieving

 Table 3

 Electrochemical performances of 2D TMD hybrids based supercapacitor electrodes.

TMD Hybrid electrode	Capacitance/Scan rate	Capacitance Retention (%)/Scan rate	Cycles	Energy density	Operation voltage (V)	Ref.
WS ₂ /rGO	350 Fg ⁻¹ /2 mV/s	$100/3\mathrm{Ag^{-1}}$	1000	49 WhKg ⁻¹	-	[335]
MoS ₂ /rGO	$265 \mathrm{Fg^{-1}} / 10 \mathrm{mV} \mathrm{s^{-1}}$	$92/20 \text{mV s}^{-1}$	1000	63 WhKg ⁻¹	0.25-0.8	[336]
MoS ₂ /MWCNT	$452.7 \mathrm{Fg^{-1}} / 1 \mathrm{Ag^{-1}}$	95.8/1 Ag ⁻¹	1000	-	-0.75-0.25	[329]
3D Graphene/MoS ₂	$169.37 \mathrm{Fg^{-1}} / 1 \mathrm{Ag^{-1}}$	90/100 mVs ⁻¹	1400	24.59 Wh/Kg	-0.9-0.2	[337]
Porous C/MoS ₂	$210 \mathrm{Fg^{-1}} / 1 \mathrm{Ag^{-1}}$	$105/4\mathrm{Ag^{-1}}$	1000	_	0.0-0.5	[338]
Carbon fiber cloth/WS2	$399 \mathrm{Fg^{-1}} / 1 \mathrm{Ag^{-1}}$	99/1 Ag ⁻¹	500	_	-0.8-0.2	[339]
MoS ₂ -NiO	$1080.6\mathrm{Fg^{-1}}/1\mathrm{Ag^{-1}}$	$101.9/2\mathrm{Ag^{-1}}$	9000	$39.6 \mathrm{Whkg^{-1}}$	0.0-0.5	[126]
MoS ₂ /NiCo ₂ O ₄	7.1 Fcm ⁻² /2 mVs ⁻¹	98.2/6 Ag ⁻¹	8000	18.4 Whkg ⁻¹	0.0-0.6	[340]
WS_2/WO_3	47.5 mFcm ⁻² /5 mV s ⁻¹	$\geq 100/100 mVs^{-1}$	30,000	0.06 Whcm ⁻³	-0.3-0.5	[325]
MoS ₂ -CoSe ₂	2577 Fg ⁻¹ / 1Ag ⁻¹	$91.03/20\mathrm{Ag^{-1}}$	5000	60.5 Whkg ⁻¹	-0.2-0.8	[79]
MoS ₂ /Bi ₂ S ₃	$1258 \mathrm{Fg^{-1}}/30 \mathrm{Ag^{-1}}$	$92.8/10\mathrm{Ag^{-1}}$	5000	_	-0.2-0.6	[341]
MoS_2/CoS_2	142 mFcm ⁻² /1 mAcm ⁻²	92.7/1 mAcm ⁻²	1000	$11.11 \mathrm{Whkg^{-1}}$	-0.6-0.2	[342]
NiSe@MoSe ₂	$223 \mathrm{Fg^{-1}} / 1 \mathrm{Ag^{-1}}$	$91.4/5\mathrm{Ag^{-1}}$	5000	$32.6 \mathrm{Whkg^{-1}}$	-0.1-0.6	[343]
MoS ₂ @3D-Ni-foam	3400 mFcm ⁻² /3 mAcm ⁻²	80/50 mAcm ⁻²	4500	-	0.0.0.6	[344]
Ag@MoS ₂	$980 \mathrm{Fg^{-1}} / 1 \mathrm{Ag^{-1}}$	97/1 Ag ⁻¹	5000	_	-0.1-0.6	[345]
3D tubular MoS ₂ /PANI	$552 \mathrm{Fg^{-1}} / 0.5 \mathrm{Ag^{-1}}$	79/1 Ag ⁻¹	6000	_	-0.1-0.6	[201]
1H-MoS ₂ @Oleylamine	50.65 mFcm ⁻² /0.37 Ag ⁻¹	240/2.75 mAcm ⁻²	5000	$1-7 \mu Whcm^{-2}$	0.0-1.0	[346]
MoS ₂ /PPy	$700\mathrm{Fg^{-1}}/10\mathrm{mV}\mathrm{s^{-1}}$	$85/1 \mathrm{Ag^{-1}}$	4000	83.3 Whkg ⁻¹	0.0-0.9	[327]
MoS ₂ /RGO@PANI	$1224{\rm Fg^{-1}}$ at $1{\rm Ag^{-1}}$	$82.5/10\mathrm{Ag^{-1}}$	3000	$22.3 \mathrm{Whkg^{-1}}$	-0.2 - 0.8	[347]
1D PANI/2D MoS ₂	812 Fg ⁻¹ /1 mAcm ⁻²	-	-	112 Whkg ⁻¹	0.0-1.0	[188]

high capacitance and energy density using low-temperature solution mixing processes. 2D MoS₂/PANI hybrids synthesized using an in-situ polymerization method exhibited a capacitance of $575 \,\mathrm{Fg}^{-1}$ at 1 Ag⁻¹ and energy density of 265 WhKg⁻¹ [326]. 2D MoS₂/PPy hybrids prepared by the similar methods achieved an impressive capacitance of \sim 700 Fg⁻¹ at a scan rate of 10 mV s⁻¹, surpassing nearly all previously developed stand-alone PPy-based supercapacitors [327]. These materials also presented a significantly high energy density of 83.3 Whkg⁻¹ at a power density of 3332 WKg⁻¹ while their cyclic stability is presently limited. 2D MoS₂/PANI hybrids developed in the form of "nanoneedles" (Fig. 12(c)) [328] presented an improved cyclic stability with a capacitance retention of 91% after 4000 cycles, while delivering a high energy density of 106 Wh kg⁻¹ and a capacitance of 669 Fg⁻¹ at 1 Ag⁻¹. Various 2D MoS₂/carbon nanomaterial hybrids including 2D MoS₂/CNT and 2D MoS₂/graphene were developed and their performances were evaluated. 2D MoS₂/MWNT hybrids developed by a onepot L-cysteine-assisted hydrothermal method exhibited a high capacitance of 452.7 Fg⁻¹ with 4.2% capacitance loss after 1000 cycles [329]. Flexible fibrous supercapacitors based on aligned 2D MoS₂/CNT hybrids delivered a capacitance of 135 Fcm⁻³ [330]. 3D sphere-like MoS₂/graphene hybrids obtained by a solution phase method exhibited a maximum capacitance up to 243 Fg⁻¹ with an excellent energy density of 73.5 Wh kg⁻¹ [27]. 2D MoS₂/graphene hybrid membranes achieved capacitance of 11 mFcm⁻² at 5 mV s⁻¹ [331]. Interestingly, a significant enhancement of capacitance up to 800% was observed in cyclic charging/discharging events, which was attributed to the continued exfoliation of the layered materials. More complex hybrids based on the ternary components of 2D TMDs, CPs, and metal oxides (or carbonaceous materials) have recently drawn attentions toward further improving supercapacitor performances [332]. 2D MoS₂/PANI/MWNT hybrids prepared by an in-situ polymerization method reached a capacitance of 350 Fg^{-1} and high energy density of 7.77 WhKg⁻¹ [333]. Moreover, large-scale 3D networked 2D MoS₂/CNT/rGO hybrids were developed for flexible supercapacitor devices (Fig. 12(d)) [334]. These novel supercapacitor electrode materials offered a capacitance of 129 mF cm⁻² at 0.1nmAcm⁻². Flexible supercapacitor devices based on these electrodes exhibited a remarkably long cycle stability of 94.7% and capacitance retention under severe mechanical bending even at 10,000 cycles (Fig. 12(e)). Table 3 compares the energy storage capacities of various 2D TMD hybrids based supercapacitor electrodes. 2D TMDs incorporated with carbonaceous materials or conductive polymers presently present superior per-

formances over 2D TMD hybrids with metal oxides and/or other TMDs.

Conclusion and outlook

The onset of the energy crisis caused by the exhaustive use of fossil fuels has driven exploration into novel materials which could replace or complement traditional non-renewable energy resources and realize alternative energy generation/storage systems with improved performances, 2D TMDs hold high promise in these endeavors as they offer a variety of structural, chemical, electrical, and optical properties uniquely suited to energy applications as well as being usable for emerging energy technologies of unconventional form factors such as flexible devices. Despite their projected potentials, pristine 2D TMDs offer unsatisfactory performance as stand-alone energy device components due to their intrinsic weaknesses associated with their structural fragility and defect-mediated limited carrier transports. These challenges have motived the study of 2D TMD hybrid materials which can benefit from both the unprecedented material properties inherent to 2D TMDs and the robust and established functionalities of traditional energetic materials in a highly synergistic manner. This review comprehensively summarizes the recent advancements in the development of a wide range of 2D TMD hybrid materials and their applications to energy generation, conversion, and storage systems. The material property advantages of 2D TMDs for energy applications has been utilized in two broadly defined directions; 1) To compensate the intrinsic demerits of the counterpart energy materials while maintaining or improving the performances of traditional energy systems. 2) To realize functionalities that cannot be achieved with traditional materials for next-generation energy systems. One example of the former case is to incorporate 2D MoS₂ with ample edge sites into noble metals to mitigate their high cost of in catalytic applications. Various 2D TMD hybrids have been developed with similar motivations and have been applied to energy conversion systems, including hydrogen generation, batteries, and supercapacitors. One example of the latter case is to combine 2D TMDs and other non-traditional nanomaterials such as graphene. For example, 2D TMD/graphene hybrids containing semiconductor (2D TMD)-metal (graphene) Schottky junctions can efficiently generate/separate photo-excited charge carriers upon solar illumination. These unique electrical properties of 2D TMDs coupled with their extremely small thickness were utilized to develop highly flexible and semi-transparent PV devices that are

unachievable with traditional materials/approaches, although their energy conversion efficiencies presently remain very low.

Despite the tremendous potential of 2D TMD hybrids and the increasing interest in their fundamental researches, their properties still need much improvement for practical energy applications. Some major directions are suggested as following:

- (1) Phase engineering of 2D TMDs. 2D TMDs possess multiple crystalline phases (e.g., semiconducting 2H- and metallic 1T-), and each phase is required to be engineered to meet the specific needs for energy applications. For example, maximizing 2H-phase is desirable for PV applications to avoid unwanted Schottky barrier formation, while enriching 1T-phase is essential for certain applications (e.g., HER and LIB) which only require the high electrical conductivities of 2D TMDs. A few strategies for the phase engineering have been explored including the intercalations of Li⁺ [348], but more rigorous, controllable and scalable approaches are demanded.
- (2) Controlled and scalable integration of 2D TMDs. Manual stacking of individually exfoliated 2D TMD layers was initially applied to integrate multiple 2D TMDs. Although it was proven to be successful in integrating 2D TMDs with other 2D materials such as graphene, this manual approach is not technically viable and practical because of the lack of scalability and structural control. For the integration of 2D TMDs with other 2D materials, it is highly demanded to develop reliable integration strategies such as chemical vapor deposition process which can grow morphology-controlled 2D TMD hybrids accompanying wafer-level scalability and atomic level precision. Moreover, the morphology-controlled integration of 2D TMDs with other functional materials of more pronounced structural/dimensional dissimilarity is another demanding challenging. Convention solution-based integrations or hydrothermal synthesis methods often result in randomly-oriented assemblies of 2D TMDs with their counterpart functional materials, leading to uncontrolled interfacial morphologies and degraded material properties. For example, integrating 2D TMDs with polymers employs adhesive "binders" in many cases, which can cause the chemical and/or mechanical instability at the 2D TMD/polymer interfaces, limiting their performances for energy applications. It is highly demanded to develop scalable methods which can maintain the structural integrity of constituent materials at nanoscales and transfer their resulting functionalities to practical-level devices.
- (3) Fundamental understanding of the performance-property relationships in 2D hybrid materials. In parallel to the efforts directed to developing practical devices, the fundamental understanding of structural property-energy performance relationships in 2D hybrid materials is critically essential. A large number of important questions have remained unanswered. For example, how would the performances of energy conversion devices be affected by the intrinsic structural variations (e.g., crystallinity, layer number/orientation, etc.) of 2D TMDs? What are the fundamental factors that determine these structural variations, and would they be adjustable to leverage the material properties and device functionalities of 2D TMD hybrids? What are the atomistic mechanisms for the mechanical/chemical "binding" of 2D TMDs with other interacting materials and what would the atomistic views of the interfacial morphologies of 2D TMD hybrids be? Addressing these questions would greatly broaden and deepen the material sciences of 2D TMDs as well as provide technical guidance for optimizing the performances of 2D TMD hybrid energy devices. Some of these questions would be only possible to answer via advanced material characterization techniques such as in-situ spectroscopies and electron microscopies.

(4) New energy conversion devices and concepts. Lastly, the continued exploration of 2D TMDs beyond traditionally developed materials could project new venues for relatively less investigated energy applications. Examples of such applications include thermophotovoltaics (TPV) which directly converts the heat energy from the solar radiation to electricity. A basic TPV system consists of a thermal emitter and a PV diode where thermally radiated photons are absorbed and converted into electricity by the same principle for PV. Accordingly, the materials of high thermal stability and broadband optical absorption - from near infrared to visible light - are highly desired to ensure high energy conversion efficiency. Some 2D TMDs are identified to be highly promising for these applications when they are heterogeneously integrated with other 2D materials or optical metamaterials [349,350]. A large number of unprecedented yet promising opportunities is to follow as more 2D TMDs are developed and their fundamental sciences interfacing with other functional materials are better elucidated.

Acknowledgement

Y. J gratefully acknowledges support from National Science Foundation (CMMI-1728309). N.C. acknowledges the partial support from the Preeminent Postdoctoral Program (P3) at University of Central Florida.

References

- [1] M.J. Allen, V.C. Tung, R.B. Kaner, Chem. Rev. 110 (2010) 132-145.
- [2] K.S. Novoselov, A.K. Geim, S.V. Morozov, D. Jiang, Y. Zhang, S.V. Dubonos, I.V. Grigorieva, A.A. Firsov, Science 306 (2004) 666–669.
- [3] W. Choi, N. Choudhary, G.H. Han, J. Park, D. Akinwande, Y.H. Lee, Mater. Today 20 (2017) 116–130.
- [4] S.Z. Butler, S.M. Hollen, L. Cao, Y. Cui, J.A. Gupta, H.R. Gutiérrez, T.F. Heinz, S.S. Hong, J. Huang, A.F. Ismach, E. Johnston-Halperin, M. Kuno, V.V. Plashnitsa, R.D. Robinson, R.S. Ruoff, S. Salahuddin, J. Shan, L. Shi, M.G. Spencer, M. Terrones, W. Windl, J.E. Goldberger, ACS Nano 7 (2013) 2898–2926.
- [5] P. Johari, V.B. Shenoy, ACS Nano 6 (2012) 5449-5456.
- [6] R. Lv, J.A. Robinson, R.E. Schaak, D. Sun, Y. Sun, T.E. Mallouk, M. Terrones, Acc. Chem. Res. 48 (2015) 56–64.
- [7] A. Splendiani, L. Sun, Y. Zhang, T. Li, J. Kim, C.Y. Chim, G. Galli, F. Wang, Nano Lett. 10 (2010) 1271–1275.
- [8] B. Radisavljevic, A. Radenovic, J. Brivio, V. Giacometti, A. Kis, Nat. Nanotechnol. 6 (2011) 147.
- [9] H. Wang, H. Feng, J. Li, Small 10 (2014) 2165-2181.
- [10] D. Lembke, S. Bertolazzi, A. Kis, Acc. Chem. Res. 48 (2015) 100–110.
- [11] R. Dominko, D. Arčon, A. Mrzel, A. Zorko, P. Cevc, P. Venturini, M. Gaberscek, M. Remskar, D. Mihailovic, Adv. Mater. 14 (2002) 1531–1534.
- [12] W. Wu, D. De, S.-C. Chang, Y. Wang, H. Peng, J. Bao, S.-S. Pei, Appl. Phys. Lett. 102 (2013), 142106.
- [13] N. Choudhary, J. Park, J.Y. Hwang, W. Choi, ACS Appl. Mater. Interfaces 6 (2014) 21215–21222.
- [14] L. Britnell, R. Ribeiro, A. Eckmann, R. Jalil, B. Belle, A. Mishchenko, Y.-J. Kim, R. Gorbachev, T. Georgiou, S. Morozov, Science 340 (2013) 1311–1314.
- [15] X. Hong, J. Kim, S.-F. Shi, Y. Zhang, C. Jin, Y. Sun, S. Tongay, J. Wu, Y. Zhang, F. Wang, Nat. Nanotechnol. 9 (2014) 682–686.
- [16] K. He, C. Poole, K.F. Mak, J. Shan, Nano Lett. 13 (2013) 2931–2936.
- [17] H.J. Conley, B. Wang, J.I. Ziegler, R.F. Haglund Jr, S.T. Pantelides, K.I. Bolotin, Nano Lett. 13 (2013) 3626–3630.
- [18] J. Wu, H. Schmidt, K.K. Amara, X. Xu, G. Eda, B. Özyilmaz, Nano Lett. 14 (2014) 2730–2734.
- [19] G. Huai-Hong, Y. Teng, T. Peng, Z. Zhi-Dong, Chin. Phys. B 23 (2013) 017201.
- [20] A. Jäger-Waldau, M.C. Lux-Steiner, E. Bucher, Solid State Phenomena 37 (1994) 479–484.
- [21] X. Zhou, B. Xu, Z. Lin, D. Shu, L. Ma, J. Nanosci. Nanotechnol. 14 (2014) 7250–7254.
- [22] J. Xiao, D. Choi, L. Cosimbescu, P. Koech, J. Liu, J.P. Lemmon, Chem. Mater. 22 (2010) 4522–4524.
- [23] X. Duan, C. Wang, A. Pan, R. Yu, X. Duan, Chem. Soc. Rev. 44 (2015) 8859–8876.
- [24] K. Kośmider, J. Fernández-Rossier, Phys. Rev. B Condens. Matter Mater. Phys. 87 (2013) 075451.
- [25] A.K. Geim, I.V. Grigorieva, Nature 499 (2013) 419.
- [26] X. Wang, F. Xia, Nat. Mater. 14 (2015) 264.
- [27] K.-J. Huang, L. Wang, Y.-J. Liu, Y.-M. Liu, H.-B. Wang, T. Gan, L.-L. Wang, Int. J. Hydrogen Energy 38 (2013) 14027–14034.
- [28] L. Hu, Y. Ren, H. Yang, Q. Xu, ACS Appl. Mater. Interfaces 6 (2014) 14644–14652.

- [29] T.F. Jaramillo, K.P. Jørgensen, J. Bonde, J.H. Nielsen, S. Horch, I. Chorkendorff, Science 317 (2007) 100–102.
- [30] J. Kibsgaard, Z. Chen, B.N. Reinecke, T.F. Jaramillo, Nat. Mater. 11 (2012) 963.
- [31] M. Chhowalla, Z. Liu, H. Zhang, Chem. Soc. Rev. 44 (2015) 2584–2586.
- [32] D. Voiry, J. Yang, M. Chhowalla, Adv. Mater. 28 (2016) 6197-6206.
- [33] K. Chang, Z. Mei, T. Wang, Q. Kang, S. Ouyang, J. Ye, ACS Nano 8 (2014) 7078–7087.
- [34] Z. Chen, D. Cummins, B.N. Reinecke, E. Clark, M.K. Sunkara, T.F. Jaramillo, Nano Lett. 11 (2011) 4168–4175.
- [35] C. Tan, H. Zhang, Chem. Soc. Rev. 44 (2015) 2713-2731.
- [36] M.-R. Gao, Y.-F. Xu, J. Jiang, S.-H. Yu, Chem. Soc. Rev. 42 (2013) 2986–3017.
- [37] K.C. Kwon, S. Choi, K. Hong, C.W. Moon, Y.-S. Shim, D.H. Kim, T. Kim, W. Sohn, J.-M. Jeon, C.-H. Lee, Energy Environ. Sci. 9 (2016) 2240–2248.
- [38] H. Tian, Z. Tan, C. Wu, X. Wang, M.A. Mohammad, D. Xié, Y. Yang, J. Wang, L.-J. Li, J. Xu, Sci. Rep. 4 (2014) 5951.
- [39] J. Yoon, W. Park, G.Y. Bae, Y. Kim, H.S. Jang, Y. Hyun, S.K. Lim, Y.H. Kahng, W.K. Hong, B.H. Lee, Small 9 (2013) 3295–3300.
- [40] C.-H. Lee, G.-H. Lee, A.M. Van Der Zande, W. Chen, Y. Li, M. Han, X. Cui, G. Arefe, C. Nuckolls, T.F. Heinz, Nat. Nanotechnol. 9 (2014) 676–681.
- [41] N. Huo, J. Kang, Z. Wei, S.S. Li, J. Li, S.H. Wei, Adv. Funct. Mater. 24 (2014) 7025–7031.
- [42] C. Liu, L. Wang, Y. Tang, S. Luo, Y. Liu, S. Zhang, Y. Zeng, Y. Xu, Appl. Catal. B 164 (2015) 1–9.
- [43] D. Xie, D. Wang, W. Tang, X. Xia, Y. Zhang, X. Wang, C. Gu, J. Tu, J. Power Sources 307 (2016) 510–518.
- [44] J.N. Coleman, M. Lotya, A. O'Neill, S.D. Bergin, P.J. King, U. Khan, K. Young, A. Gaucher, S. De, R.J. Smith, Science 331 (2011) 568–571.
- [45] J. Yang, D. Voiry, S.J. Ahn, D. Kang, A.Y. Kim, M. Chhowalla, H.S. Shin, Angew. Chem. Int. Ed. 52 (2013) 13751–13754.
- [46] M.A. Lukowski, A.S. Daniel, F. Meng, A. Forticaux, L. Li, S. Jin, J. Am. Chem. Soc. 135 (2013) 10274–10277.
- [47] S. Wang, X. Wang, J.H. Warner, ACS Nano 9 (2015) 5246-5254.
- [48] S. Mao, Z. Wen, S. Ci, X. Guo, K.K. Ostrikov, J. Chen, Small 11 (2015) 414–419.
- [49] W. Zhou, Z. Yin, Y. Du, X. Huang, Z. Zeng, Z. Fan, H. Liu, J. Wang, H. Zhang, Small 9 (2013) 140–147.
- [50] I. Tacchini, E. Terrado, A. Anson, M. Martinez, Micro Nano Lett. 6 (2011) 932–936.
- [51] M.-W. Lin, L. Liu, Q. Lan, X. Tan, K.S. Dhindsa, P. Zeng, V.M. Naik, M.M.-C. Cheng, Z. Zhou, J. Phys. D Appl. Phys. 45 (2012) 345102.
- Cheng, Z. Zhou, J. Phys. D Appl. Phys. 45 (2012) 345102. [52] L. Yang, S. Wang, J. Mao, J. Deng, Q. Gao, Y. Tang, O.G. Schmidt, Adv. Mater.
- 25 (2013) 1180–1184. [53] A.V. Murugan, M. Quintin, M.-H. Delville, G. Campet, C.S. Gopinath, K.
- Vijayamohanan, J. Power Sources 156 (2006) 615–619. [54] J. Liu, Z. Zeng, X. Cao, G. Lu, L.-H. Wang, Q.-L. Fan, W. Huang, H. Zhang, Small 8 (2012) 3517–3522.
- [55] Y. Shi, J.-K. Huang, L. Jin, Y.-T. Hsu, S.F. Yu, L.-J. Li, H.Y. Yang, Sci. Rep. 3 (2013) 1839.
- [56] C.M. Smyth, R. Addou, S. McDonnell, C.L. Hinkle, R.M. Wallace, J. Phys. Chem. C 120 (2016) 14719–14729.
- [57] M.-Y. Li, Y. Shi, C.-C. Cheng, L.-S. Lu, Y.-C. Lin, H.-L. Tang, M.-L. Tsai, C.-W. Chu, K.-H. Wei, J.-H. He, W.-H. Chang, K. Suenaga, L.-J. Li, Science 349 (2015) 524–528
- [58] Y. Gong, J. Lin, X. Wang, G. Shi, S. Lei, Z. Lin, X. Zou, G. Ye, R. Vajtai, B.I. Yakobson, Nat. Mater. 13 (2014) 1135–1142.
- [59] A. Pant, Z. Mutlu, D. Wickramaratne, H. Cai, R.K. Lake, C. Ozkan, S. Tongay, Nanoscale 8 (2016) 3870–3887.
- [60] Y. Shi, W. Zhou, A.-Y. Lu, W. Fang, Y.-H. Lee, A.L. Hsu, S.M. Kim, K.K. Kim, H.Y. Yang, L.-J. Li, Nano Lett. 12 (2012) 2784–2791.
- [61] H. Fang, C. Battaglia, C. Carraro, S. Nemsak, B. Ozdol, J.S. Kang, H.A. Bechtel, S.B. Desai, F. Kronast, A.A. Unal, Proc. Natl. Acad. Sci. U. S. A. 111 (2014) 6198–6202.
- [62] F. Withers, O. Del Pozo-Zamudio, A. Mishchenko, A. Rooney, A. Gholinia, K. Watanabe, T. Taniguchi, S. Haigh, A. Geim, A. Tartakovskii, Nat. Mater. 14 (2015) 301–306.
- [63] M.-H. Chiu, C. Zhang, H.-W. Shiu, C.-P. Chuu, C.-H. Chen, C.-Y.S. Chang, C.-H. Chen, M.-Y. Chou, C.-K. Shih, L.-J. Li, Nat. Commun. 6 (2015) 7666.
- [64] R. Cheng, D. Li, H. Zhou, C. Wang, A. Yin, S. Jiang, Y. Liu, Y. Chen, Y. Huang, X. Duan, Nano Lett. 14 (2014) 5590–5597.
- [65] Á. Szabó, S.J. Koester, M. Luisier, IEEE Electron. Device Lett. 36 (2015) 514–516.
- [66] A. Nourbakhsh, A. Zubair, M.S. Dresselhaus, Ts. Palacios, Nano Lett. 16 (2016) 1359–1366.
- [67] Y. Gong, S. Lei, G. Ye, B. Li, Y. He, K. Keyshar, X. Zhang, Q. Wang, J. Lou, Z. Liu, Nano Lett. 15 (2015) 6135–6141.
- [68] J.H. Yu, H.R. Lee, S.S. Hong, D. Kong, H.-W. Lee, H. Wang, F. Xiong, S. Wang, Y. Cui, Nano Lett. 15 (2015) 1031–1035.
- [69] B. Peng, G. Yu, X. Liu, B. Liu, X. Liang, L. Bi, L. Deng, T.C. Sum, K.P. Loh, 2D Mater. 3 (2016) 025020.
- [70] M.-L. Tsai, W.-C. Tu, L. Tang, T.-C. Wei, W.-R. Wei, S.P. Lau, L.-J. Chen, J.-H. He, Nano Lett. 16 (2016) 309–313.
- [71] L. Ye, H. Li, Z. Chen, J. Xu, ACS Photonics 3 (2016) 692-699.
- [72] D. Gopalakrishnan, D. Damien, M.M. Shaijumon, ACS Nano 8 (2014) 5297–5303.
- [73] Y. Pi, Z. Li, D. Xu, J. Liu, Y. Li, F. Zhang, G. Zhang, W. Peng, X. Fan, ACS Sustain. Chem. Eng. 5 (2017) 5175–5182.
- [74] T. Wang, S. Chen, H. Pang, H. Xue, Y. Yu, Adv. Sci. 4 (2017) 1600289.

- [75] A.Y. Polyakov, L. Yadgarov, R. Popovitz-Biro, V.A. Lebedev, I. Pinkas, R. Rosentsveig, Y. Feldman, A.E. Goldt, E.A. Goodilin, R. Tenne, J. Phys. Chem. C 118 (2014) 2161–2169.
- [76] L. Wang, Y. Ma, M. Yang, Y. Qi, RSC Adv. 5 (2015) 89069-89075.
- [77] P.T. Gomathi, P. Sahatiya, S. Badhulika, Adv. Funct. Mater. 27 (2017) 1701611.
- [78] C. An, J. Feng, J. Liu, G. Wei, J. Du, H. Wang, S. Jin, J. Zhang, Inorg. Chem. Front. 4 (2017) 1042–1047.
- [79] L. Fang, Y. Qiu, W. Li, F. Wang, M. Lan, K. Huang, Q. Jing, J. Colloid Interface Sci. 512 (2018) 282–290.
- [80] X. Zong, G. Wu, H. Yan, G. Ma, J. Shi, F. Wen, L. Wang, C. Li, J. Phys. Chem. C 114 (2010) 1963–1968.
- [81] J. Ji, B. Sun, F. Shan, Q. Li, F. Huang, Y. Song, F. Wang, RSC Adv. 6 (2016) 100115–100121.
- [82] A. Vargas, F. Liu, C. Lane, D. Rubin, I. Bilgin, Z. Hennighausen, M. DeCapua, A. Bansil, S. Kar, Sci. Adv. 3 (2017) e1601741.
- [83] H. Li, J. Wu, Z. Yin, H. Zhang, Acc. Chem. Res. 47 (2014) 1067-1075.
- [84] P. Rivera, J.R. Schaibley, A.M. Jones, J.S. Ross, S. Wu, G. Aivazian, P. Klement, K. Seyler, G. Clark, N.J. Ghimire, J. Yan, D.G. Mandrus, W. Yao, X. Xu, Nat. Commun. 6 (2015) 6242.
- [85] C.-J. Shih, Q.H. Wang, Y. Son, Z. Jin, D. Blankschtein, M.S. Strano, ACS Nano 8 (2014) 5790–5798.
- [86] M.M. Furchi, A. Pospischil, F. Libisch, J. Burgdörfer, T. Mueller, Nano Lett. 14 (2014) 4785–4791.
- [87] V. Nicolosi, M. Chhowalla, M.G. Kanatzidis, M.S. Strano, J.N. Coleman, Science 340 (2013) 1226419.
- [88] G.S. Bang, K.W. Nam, J.Y. Kim, J. Shin, J.W. Choi, S.-Y. Choi, ACS Appl. Mater. Interfaces 6 (2014) 7084–7089.
- [89] A. Anto Jeffery, C. Nethravathi, M. Rajamathi, J. Phys. Chem. C 118 (2014) 1386–1396.
- [90] R.J. Smith, P.J. King, M. Lotya, C. Wirtz, U. Khan, S. De, A. O'Neill, G.S. Duesberg, J.C. Grunlan, G. Moriarty, Adv. Mater. 23 (2011) 3944–3948.
- [91] L. Niu, J.N. Coleman, H. Zhang, H. Shin, M. Chhowalla, Z. Zheng, Small 12 (2016) 272–293.
- [92] X. Zhang, F. Meng, J.R. Christianson, C. Arroyo-Torres, M.A. Lukowski, D. Liang, J.R. Schmidt, S. Jin, Nano Lett. 14 (2014) 3047–3054.
- [93] X. Ling, Y.-H. Lee, Y. Lin, W. Fang, L. Yu, M.S. Dresselhaus, J. Kong, Nano Lett. 14 (2014) 464–472.
- [94] Y. Shi, H. Li, L.-J. Li, Chem. Soc. Rev. 44 (2015) 2744-2756.
- [95] C. Huang, S. Wu, A.M. Sanchez, J.J.P. Peters, R. Beanland, J.S. Ross, P. Rivera, W. Yao, D.H. Cobden, X. Xu, Nat. Mater. 13 (2014) 1096.
- [96] M. Mahjouri-Samani, M.-W. Lin, K. Wang, A.R. Lupini, J. Lee, L. Basile, A. Boulesbaa, C.M. Rouleau, A.A. Puretzky, I.N. Ivanov, Nat. Commun. 6 (2015) 7749.
- [97] X. Duan, C. Wang, J.C. Shaw, R. Cheng, Y. Chen, H. Li, X. Wu, Y. Tang, Q. Zhang, A. Pan, Nat. Nanotechnol. 9 (2014) 1024–1030.
- [98] K. Chen, X. Wan, J. Wen, W. Xie, Z. Kang, X. Zeng, H. Chen, J.-B. Xu, ACS Nano 9 (2015) 9868–9876.
- [99] X.-Q. Zhang, C.-H. Lin, Y.-W. Tseng, K.-H. Huang, Y.-H. Lee, Nano Lett. 15 (2014) 410–415.
- [100] Y. Zhan, Z. Liu, S. Najmaei, P.M. Ajayan, J. Lou, Small 8 (2012) 966–971.
- [101] N. Choudhary, J. Park, J.Y. Hwang, H.-S. Chung, K.H. Dumas, S.I. Khondaker, W. Choi, Y. Jung, Sci. Rep. 6 (2016) 25456.
- [102] X. Zhou, X. Yang, H. Li, M.N. Hedhili, K.-W. Huang, L.-J. Li, W. Zhang, J. Mater. Chem. A 5 (2017) 15552–15558.
- [103] X.-L. Yin, L.-L. Li, W.-J. Jiang, Y. Zhang, X. Zhang, L.-J. Wan, J.-S. Hu, ACS Appl. Mater. Interfaces 8 (2016) 15258–15266.
 [104] R.M. Clark, B.J. Carey, T. Daeneke, P. Atkin, M. Bhaskaran, K. Latham, I.S. Cole,
- [104] R.M. Clark, B.J. Carey, T. Daeneke, P. Atkin, M. Bhaskaran, K. Latham, I.S. Cole, K. Kalantar-zadeh, Nanoscale 7 (2015) 16763–16772.
- [105] K. Aretouli, P. Tsipas, D. Tsoutsou, J. Marquez-Velasco, E. Xenogiannopoulou, S. Giamini, E. Vassalou, N. Kelaidis, A. Dimoulas, Appl. Phys. Lett. 106 (2015) 143105.
- [106] H.C. Diaz, R. Chaghi, Y. Ma, M. Batzill, 2D Mater. 2 (2015) 044010.
- [107] K.E. Aretouli, D. Tsoutsou, P. Tsipas, J. Marquez-Velasco, S. Aminalragia Giamini, N. Kelaidis, V. Psycharis, A. Dimoulas, ACS Appl. Mater. Interfaces 8 (2016) 23222-23229.
- [108] P.-L. Taberna, S. Mitra, P. Poizot, P. Simon, J.-M. Tarascon, Nat. Mater. 5 (2006) 567.
- [109] C. Yuan, H.B. Wu, Y. Xie, X.W.D. Lou, Angew. Chem. Int. Ed. 53 (2014) 1488–1504.
- [110] E. Formo, E. Lee, D. Campbell, Y. Xia, Nano Lett. 8 (2008) 668–672.
- [111] Z.L. Wang, R829, J. Phys. Condens. Matter 16 (2004).
- [112] B. Rausch, M.D. Symes, G. Chisholm, L. Cronin, Science 345 (2014) 1326–1330.
- [113] J. Jitputti, S. Pavasupree, Y. Suzuki, S. Yoshikawa, Jpn. J. Appl. Phys. 47 (2008) 751.
- [114] Y.K. Kho, A. Iwase, W.Y. Teoh, L. M\u00e4dler, A. Kudo, R. Amal, J. Phys. Chem. C 114 (2010) 2821–2829.
- [115] C. Burda, Y. Lou, X. Chen, A.C. Samia, J. Stout, J.L. Gole, Nano Lett. 3 (2003) 1049–1051.
- [116] A. Galińska, J. Walendziewski, Energy Fuels 19 (2005) 1143–1147.
- [117] A. Dawson, P.V. Kamat, J. Phys. Chem. B 105 (2001) 960–966.
- [118] C. Wang, H. Yin, S. Dai, S. Sun, Chem. Mater. 22 (2010) 3277–3282.
- [119] H. He, J. Lin, W. Fu, X. Wang, H. Wang, Q. Zeng, Q. Gu, Y. Li, C. Yan, B.K. Tay, Adv. Energy Mater. 6 (2016) 1600464.

- [120] Y. Hou, A.B. Laursen, J. Zhang, G. Zhang, Y. Zhu, X. Wang, S. Dahl, I. Chorkendorff, Angew. Chem. Int. Ed. 52 (2013) 3621-3625
- [121] Y. Zhu, Q. Ling, Y. Liu, H. Wang, Y. Zhu, PCCP 17 (2015) 933-940.
- [122] S. Ravula, C. Zhang, J.B. Essner, J.D. Robertson, J. Lin, G.A. Baker, ACS Appl. Mater. Interfaces 9 (2017) 8065-8074.
- [123] S.-S. Ding, W.-Q. Huang, Y.-C. Yang, B.-X. Zhou, W.-Y. Hu, M.-Q. Long, P. Peng, G.-F. Huang, J. Appl. Phys. 119 (2016) 205704.
- [124] X. Wang, Y. Zheng, J. Yuan, J. Shen, A.-j. Wang, L. Niu, S. Huang, Electrochim. Acta 212 (2016) 890-897.
- [125] Y. Chen, J. Lu, S. Wen, L. Lu, J. Xue, J. Mater. Chem. A 2 (2014) 17857-17866.
- [126] K. Wang, J. Yang, J. Zhu, L. Li, Y. Liu, C. Zhang, T. Liu, J. Mater. Chem. A 5 (2017) 11236-11245.
- [127] Q. Pan, F. Zheng, X. Ou, C. Yang, X. Xiong, Z. Tang, L. Zhao, M. Liu, ACS Sustain. Chem. Eng. 5 (2017) 4739-4745
- [128] A. Hamdi, L. Boussekey, P. Roussel, A. Addad, H. Ezzaouia, R. Boukherroub, Y. Coffinier, Mater. Des. 109 (2016) 634-643.
- [129] H. Li, K. Yu, X. Lei, B. Guo, H. Fu, Z. Zhu, J. Phys. Chem. C 119 (2015) 22681-22689.
- [130] H. Li, Y. Wang, G. Chen, Y. Sang, H. Jiang, J. He, X. Li, H. Liu, Nanoscale 8 2016) 6101-6109.
- [131] M. Shen, Z. Yan, L. Yang, P. Du, J. Zhang, B. Xiang, Chem. Commun. 50 (2014) 15447-15449
- [132] Y. Huang, Y.-E. Miao, L. Zhang, W.W. Tjiu, J. Pan, T. Liu, Nanoscale 6 (2014) 10673-10679.
- [133] S. Cao, T. Liu, S. Hussain, W. Zeng, X. Peng, F. Pan, Physica E 68 (2015)
- [134] H. Li, K. Yu, X. Lei, B. Guo, C. Li, H. Fu, Z. Zhu, Dalton Trans. 44 (2015) 10438-10447.
- [135] N. Tian, Z. Li, D. Xu, Y. Li, W. Peng, G. Zhang, F. Zhang, X. Fan, Ind. Eng. Chem. Res. 55 (2016) 8726-8732
- [136] Y. Chen, B. Song, X. Tang, L. Lu, J. Xue, Small 10 (2014) 1536-1543.
- [137] M. Yousaf, A. Mahmood, Y. Wang, Y. Chen, Z. Ma, R.P. Han, J. Electr. Eng. 4 (2016) 58-74.
- [138] S. Bai, L. Wang, X. Chen, J. Du, Y. Xiong, Nano Res. 8 (2015) 175-183.
- [139] S. Kanda, T. Akita, M. Fujishima, H. Tada, J. Colloid Interface Sci. 354 (2011) 607-610.
- [140] C. Meng, Z. Liu, T. Zhang, J. Zhai, Green Chem. 17 (2015) 2764-2768.
- [141] D. Liang, Z. Tian, J. Liu, Y. Ye, S. Wu, Y. Cai, C. Liang, Electrochim. Acta 182 (2015) 376–382.
- [142] H. You, S. Yang, B. Ding, H. Yang, Chem. Soc. Rev. 42 (2013) 2880-2904.
- [143] S.K. Mohapatra, N. Kondamudi, S. Banerjee, M. Misra, Langmuir 24 (2008) 11276-11281.
- [144] U. Maitra, U. Gupta, M. De, R. Datta, A. Govindaraj, C. Rao, Angew. Chem. Int. Ed. 52 (2013) 13057-13061.
- [145] C. Lee, H. Yan, L.E. Brus, T.F. Heinz, J. Hone, S. Ryu, ACS Nano 4 (2010) 2695-2700.
- [146] F. Koppens, T. Mueller, P. Avouris, A. Ferrari, M. Vitiello, M. Polini, Nat. Nanotechnol. 9 (2014) 780-793.
- [147] Z. Yin, B. Chen, M. Bosman, X. Cao, J. Chen, B. Zheng, H. Zhang, Small 10 (2014) 3537-3543.
- [148] P. Zuo, L. Jiang, X. Li, B. Li, Y. Xu, X. Shi, P. Ran, T. Ma, D. Li, L. Qu, ACS Appl. Mater. Interfaces 9 (2017) 7447-7455.
- [149] N. Kaushik, A. Nipane, F. Basheer, S. Dubey, S. Grover, M.M. Deshmukh, S.
- Lodha, Appl. Phys. Lett. 105 (2014) 113505. [150] X. Yang, W. Liu, M. Xiong, Y. Zhang, T. Liang, J. Yang, M. Xu, J. Ye, H. Chen, J. Mater. Chem. A 2 (2014) 14798-14806.
- [151] Y. Sun, S. Gao, F. Lei, Y. Xie, Chem. Soc. Rev. 44 (2015) 623–636.
- [152] S. Shin, Z. Jin, D.H. Kwon, R. Bose, Y.-S. Min, Langmuir 31 (2015) 1196–1202.
- [153] S. Najmaei, A. Mlayah, A. Arbouet, C. Girard, J. Léotin, J. Lou, ACS Nano 8 (2014) 12682-12689.
- [154] C. Gong, C. Huang, J. Miller, L. Cheng, Y. Hao, D. Cobden, J. Kim, R.S. Ruoff, R.M. Wallace, K. Cho, ACS Nano 7 (2013) 11350-11357.
- [155] X. Huang, Z. Zeng, S. Bao, M. Wang, X. Qi, Z. Fan, H. Zhang, Nat. Commun. 4 (2013) 1444.
- [156] J. Kim, S. Byun, A.J. Smith, J. Yu, J. Huang, J. Phys. Chem. Lett. 4 (2013) 1227-1232
- [157] T. Sreeprasad, P. Nguyen, N. Kim, V. Berry, Nano Lett. 13 (2013) 4434-4441.
- [158] S.Y. Choi, C.T. Yip, G.-C. Li, D.Y. Lei, K.H. Fung, S.F. Yu, J. Hao, AIP Adv. 5 (2015) 067148.
- [159] J. Huang, Z. Dong, Y. Li, J. Li, W. Tang, H. Yang, J. Wang, Y. Bao, J. Jin, R. Li, Mater. Res. Bull. 48 (2013) 4544-4547.
- [160] Y. Li, J.D. Cain, E.D. Hanson, A.A. Murthy, S. Hao, F. Shi, Q. Li, C. Wolverton, X. Chen, V.P. Dravid, Nano Lett. 16 (2016) 7696-7702.
- [161] T.D. Burchell, Carbon Materials for Advanced Technologies, Elsevier, Netherlands, 1999.
- [162] R.H. Baughman, A.A. Zakhidov, W.A. De Heer, Science 297 (2002) 787-792.
- [163] D. Chen, G. Ji, B. Ding, Y. Ma, B. Qu, W. Chen, J.Y. Lee, Nanoscale 5 (2013) 7890-7896
- [164] Y. Liu, X. He, D. Hanlon, A. Harvey, J.N. Coleman, Y. Li, ACS Nano 10 (2016) 8821-8828.
- [165] F. Bonaccorso, L. Colombo, G. Yu, M. Stoller, V. Tozzini, A.C. Ferrari, R.S. Ruoff, V. Pellegrini, Science 347 (2015) 1246501.
- [166] S. Xu, Z. Lei, P. Wu, J. Mater. Chem. A 3 (2015) 16337-16347.
- [167] J. He, N. Kumar, M.Z. Bellus, H.-Y. Chiu, D. He, Y. Wang, H. Zhao, Nat. Commun. 5 (2014) 5622.

- [168] K. Chang, W. Chen, L. Ma, H. Li, H. Li, F. Huang, Z. Xu, Q. Zhang, J.-Y. Lee, J. Mater. Chem. 21 (2011) 6251-6257.
- [169] S.K. Das, R. Mallavajula, N. Jayaprakash, L.A. Archer, J. Mater. Chem. 22 (2012) 12988-12992.
- [170] H. Kang, Y. Liu, K. Cao, Y. Zhao, L. Jiao, Y. Wang, H. Yuan, J. Mater. Chem. A 3 (2015) 17899-17913.
- [171] S. Ding, J.S. Chen, X.W.D. Lou, Chem. Eur. J. 17 (2011) 13142-13145.
- [172] S.-Y. Tai, C.-J. Liu, S.-W. Chou, F.S.-S. Chien, J.-Y. Lin, T.-W. Lin, J. Mater. Chem. 22 (2012) 24753-24759.
- [173] Y. Shi, Y. Wang, J.I. Wong, A.Y.S. Tan, C.-L. Hsu, L.-J. Li, Y.-C. Lu, H.Y. Yang, Sci. Rep. 3 (2013) 2169.
- [174] C. Zhao, J. Kong, X. Yao, X. Tang, Y. Dong, S.L. Phua, X. Lu, ACS Appl. Mater. Interfaces 6 (2014) 6392-6398
- [175] F. Zhou, S. Xin, H.W. Liang, L.T. Song, S.H. Yu, Angew. Chem. Int. Ed. 53 (2014) 11552-11556.
- [176] C. Zhu, X. Mu, P.A. van Aken, Y. Yu, J. Maier, Angew. Chem. Int. Ed. 53 (2014) 2152-2156.
- [177] R. Moriya, T. Yamaguchi, Y. Inoue, S. Morikawa, Y. Sata, S. Masubuchi, T. Machida, Appl. Phys. Lett. 105 (2014) 083119.
- [178] H. Xu, J. Wu, Q. Feng, N. Mao, C. Wang, J. Zhang, Small 10 (2014) 2300-2306.
- [179] Y. Liu, Y. Guo, S. Sonam, S.K. Hong, M.H. Nai, C.T. Nai, L. Gao, J. Chen, B.J. Cho, C.T. Lim, Adv. Funct. Mater. 25 (2015) 5492-5503.
- [180] P. Huang, C. Ruiz-Vargas, A. van der Zande, W. Whitney, Nature 469 (2011) 389-392.
- [181] J.A. Miwa, M. Dendzik, S.S. Grønborg, M. Bianchi, J.V. Lauritsen, P. Hofmann, S. Ulstrup, ACS Nano 9 (2015) 6502-6510. [182] Y.-C. Lin, R.K. Ghosh, R. Addou, N. Lu, S.M. Eichfeld, H. Zhu, M.-Y. Li, X. Peng,
- M.J. Kim, L.-J. Li, Nat. Commun. 6 (2015) 7311.
- [183] Y. Shi, L. Peng, Y. Ding, Y. Zhao, G. Yu, Chem. Soc. Rev. 44 (2015) 6684-6696.
- [184] R. Liu, S.B. Lee, J. Am. Chem. Soc. 130 (2008) 2942–2943.
- [185] X. Cheng, V. Kumar, T. Yokozeki, T. Goto, T. Takahashi, J. Koyanagi, L. Wu, R. Wang, Compos. Part A 82 (2016) 100-107.
- [186] T. Alamro, M.K. Ram, Electrochim. Acta 235 (2017) 623–631.
- [187] A. Sajedi-Moghaddam, E. Saievar-Iranizad, M. Pumera, Nanoscale 9 (2017) 8052-8065.
- [188] M.S. Nam, U. Patil, B. Park, H.B. Sim, S.C. Jun, RSC Adv. 6 (2016) 101592-101601.
- [189] J. Wang, Z. Wu, H. Yin, W. Li, Y. Jiang, RSC Adv. 4 (2014) 56926-56932.
- [190] B.-Z. Lin, C. Ding, B.-H. Xu, Z.-J. Chen, Y.-L. Chen, Mater. Res. Bull. 44 (2009) 719-723.
- [191] T. Wang, W. Liu, J. Tian, X. Shao, D. Sun, Polym. Compos. 25 (2004) 111-117.
- [192] F. Jiang, J. Xiong, W. Zhou, C. Liu, L. Wang, F. Zhao, H. Liu, J. Xu, J. Mater. Chem. A 4 (2016) 5265-5273.
- [193] R. Bissessur, W. White, Mater. Chem. Phys. 99 (2006) 214-219.
- [194] X. Zhao, Y. Mai, H. Luo, D. Tang, B. Lee, C. Huang, L. Zhang, Appl. Surf. Sci. 288 (2014) 736-741.
- [195] Y.-J. Huang, M.-S. Fan, C.-T. Li, C.-P. Lee, T.-Y. Chen, R. Vittal, K.-C. Ho, Electrochim. Acta 211 (2016) 794-803.
- [196] O. Eksik, J. Gao, S.A. Shojaee, A. Thomas, P. Chow, S.F. Bartolucci, D.A. Lucca, N. Koratkar, ACS Nano 8 (2014) 5282-5289.
- [197] D. Song, M. Li, Y. Jiang, Z. Chen, F. Bai, Y. Li, B. Jiang, J. Photochem. Photobiol. A 279 (2014) 47-51.
- [198] K. Zhou, J. Liu, P. Wen, Y. Hu, Z. Gui, Appl. Surf. Sci. 316 (2014) 237-244.
- [199] X. Wang, E.N. Kalali, D.-Y. Wang, J. Mater. Chem. A 3 (2015) 24112–24120.
 [200] G. Ma, H. Peng, J. Mu, H. Huang, X. Zhou, Z. Lei, J. Power Sources 229 (2013)
- 72 78.
- [201] L. Ren, G. Zhang, Z. Yan, L. Kang, H. Xu, F. Shi, Z. Lei, Z.-H. Liu, ACS Appl. Mater. Interfaces 7 (2015) 28294-28302.
- [202] D. He, Y. Pan, H. Nan, S. Gu, Z. Yang, B. Wu, X. Luo, B. Xu, Y. Zhang, Y. Li, Z. Ni, B. Wang, J. Zhu, Y. Chai, Y. Shi, X. Wang, Appl. Phys. Lett. 107 (2015) 183103.
- [203] C.E. Petoukhoff, M.B.M. Krishna, D. Voiry, I. Bozkurt, S. Deckoff-Jones, M. Chhowalla, D.M. O'Carroll, K.M. Dani, ACS Nano 10 (2016) 9899-9908.
- [204] H. Furukawa, N. Ko, Y.B. Go, N. Aratani, S.B. Choi, E. Choi, A.Ö. Yazaydin, R.Q. Snurr, M. O'Keeffe, J. Kim, O.M. Yaghi, Science 329 (2010) 424–428
- [205] S. Liu, L. Sun, F. Xu, J. Zhang, C. Jiao, F. Li, Z. Li, S. Wang, Z. Wang, X. Jiang, H. Zhou, L. Yang, C. Schick, Energy Environ. Sci. 6 (2013) 818-823.
- [206] X. Huang, B. Zheng, Z. Liu, C. Tan, J. Liu, B. Chen, H. Li, J. Chen, X. Zhang, Z. Fan, W. Zhang, Z. Guo, F. Huo, Y. Yang, L.-H. Xie, W. Huang, H. Zhang, ACS Nano 8 (2014) 8695-8701.
- [207] X. Dai, M. Liu, Z. Li, A. Jin, Y. Ma, X. Huang, H. Sun, H. Wang, X. Zhang, J. Phys. Chem. C 120 (2016) 12539-12548.
- [208] B. Ma, P.-Y. Guan, Q.-Y. Li, M. Zhang, S.-Q. Zang, ACS Appl. Mater. Interfaces 8 (2016) 26794–26800.
- [209] M. Bernardi, M. Palummo, J.C. Grossman, Nano Lett. 13 (2013) 3664–3670.
- [210] J. Kang, S. Tongay, J. Zhou, J. Li, J. Wu, Appl. Phys. Lett. 102 (2013) 012111.
- [211] A. Pezeshki, S.H.H. Shokouh, T. Nazari, K. Oh, S. Im, Adv. Mater. 28 (2016) 3216-3222.
- [212] S. Wi, H. Kim, M. Chen, H. Nam, L.J. Guo, E. Meyhofer, X. Liang, ACS Nano 8 (2014) 5270-5281
- [213] M. Shanmugam, R. Jacobs-Gedrim, E.S. Song, B. Yu, Nanoscale 6 (2014) 12682-12689.
- [214] J. Meng, H.-D. Song, C.-Z. Li, Y. Jin, L. Tang, D. Liu, Z.-M. Liao, F. Xiu, D.-P. Yu, Nanoscale 7 (2015) 11611-11619.
- [215] M.-L. Tsai, S.-H. Su, J.-K. Chang, D.-S. Tsai, C.-H. Chen, C.-I. Wu, L.-J. Li, L.-J. Chen, J.-H. He, ACS Nano 8 (2014) 8317-8322.
- [216] M. Shanmugam, C.A. Durcan, B. Yu, Nanoscale 4 (2012) 7399–7405.

- [217] C.K. Kamaja, R.R. Devarapalli, M.V. Shelke, ChemElectroChem 4 (2017) 1984-1989
- [218] C.-J. Liu, S.-Y. Tai, S.-W. Chou, Y.-C. Yu, K.-D. Chang, S. Wang, F.S.-S. Chien, J.-Y. Lin, T.-W. Lin, J. Mater. Chem. 22 (2012) 21057-21064
- [219] F. Liu, W.L. Chow, X. He, P. Hu, S. Zheng, X. Wang, J. Zhou, Q. Fu, W. Fu, P. Yu, Q. Zeng, H.J. Fan, B.K. Tay, C. Kloc, Z. Liu, Adv. Funct. Mater. 25 (2015) 5865-5871.
- [220] D. Jariwala, S.L. Howell, K.-S. Chen, J. Kang, V.K. Sangwan, S.A. Filippone, R. Turrisi, T.J. Marks, L.J. Lauhon, M.C. Hersam, Nano Lett. 16 (2016) 497-503.
- [221] Y. Tsuboi, F. Wang, D. Kozawa, K. Funahashi, S. Mouri, Y. Miyauchi, T. Takenobu, K. Matsuda, Nanoscale 7 (2015) 14476-14482.
- [222] G. Yue, W. Zhang, J. Wu, Q. Jiang, Electrochim. Acta 112 (2013) 655-662.
- [223] K. Jiao, C. Duan, X. Wu, J. Chen, Y. Wang, Y. Chen, PCCP 17 (2015) 8182-8186. [224] S.-G. Yi, S.H. Kim, S. Park, D. Oh, H.Y. Choi, N. Lee, Y.J. Choi, K.-H. Yoo, ACS
- Appl. Mater. Interfaces 8 (2016) 33811-33820. [225] J.-M. Yun, Y.-J. Noh, C.-H. Lee, S.-I. Na, S. Lee, S.M. Jo, H.-I. Joh, D.-Y. Kim, Small 10 (2014) 2319-2324.
- [226] M. Shanmugam, T. Bansal, C.A. Durcan, B. Yu, Appl. Phys. Lett. 100 (2012)
- [227] R. Tang, R. Yin, S. Zhou, T. Ge, Z. Yuan, L. Zhang, L. Yin, J. Mater. Chem. A 5 (2017) 4962–4971.
- [228] M.-K. Chuang, S.-S. Yang, F.-C. Chen, Materials 8 (2015) 5252.
- [229] L.T.L. Lee, J. He, B. Wang, Y. Ma, K.Y. Wong, Q. Li, X. Xiao, T. Chen, Sci. Rep. 4 (2014) 4063.
- [230] R. Dai, Y. Wang, J. Wang, X. Deng, ChemSusChem 10 (2017) 2869-2874.
- [231] X. Gu, W. Cui, H. Li, Z. Wu, Z. Zeng, S.-T. Lee, H. Zhang, B. Sun, Adv. Energy Mater. 3 (2013) 1262-1268.
- [232] S.K. Pradhan, B. Xiao, A.K. Pradhan, Sol. Energy Mater. Sol. Cells 144 (2016)
- [233] L.Z. Hao, W. Gao, Y.J. Liu, Z.D. Han, Q.Z. Xue, W.Y. Guo, J. Zhu, Y.R. Li, Nanoscale 7 (2015) 8304-8308.
- [234] L.Z. Hao, Y.J. Liu, W. Gao, Y.M. Liu, Z.D. Han, Q.Z. Xue, J. Zhu, RSC Adv. 6 (2016) 1346-1350.
- [235] S. Lin, X. Li, P. Wang, Z. Xu, S. Zhang, H. Zhong, Z. Wu, W. Xu, H. Chen, Sci. Rep. 5 (2015) 15103.
- [236] A. Capasso, F. Matteocci, L. Najafi, M. Prato, J. Buha, L. Cinà, V. Pellegrini, A.D. Carlo, F. Bonaccorso, Adv. Energy Mater. 6 (2016) 1600920.
- [237] J.R. McKone, E.L. Warren, M.J. Bierman, S.W. Boettcher, B.S. Brunschwig, N.S. Lewis, H.B. Gray, Energy Environ. Sci. 4 (2011) 3573-3583.
- [238] A.-Y. Lu, X. Yang, C.-C. Tseng, S. Min, S.-H. Lin, C.-L. Hsu, H. Li, H. Idriss, J.-L. Kuo, K.-W. Huang, L.-J. Li, Small 12 (2016) 5530-5537.
- [239] B. Hinnemann, P.G. Moses, J. Bonde, K.P. Jørgensen, J.H. Nielsen, S. Horch, I. Chorkendorff, J.K. Nørskov, J. Am. Chem. Soc. 127 (2005) 5308-5309.
- [240] D. Kong, H. Wang, J.J. Cha, M. Pasta, K.J. Koski, J. Yao, Y. Cui, Nano Lett. 13 (2013) 1341-1347.
- [241] B.B. Li, S.Z. Qiao, X.R. Zheng, X.J. Yang, Z.D. Cui, S.L. Zhu, Z.Y. Li, Y.Q. Liang, J. Power Sources 284 (2015) 68-76.
- [242] Y. Shi, J. Wang, C. Wang, T.-T. Zhai, W.-J. Bao, J.-J. Xu, X.-H. Xia, H.-Y. Chen, J. Am. Chem. Soc. 137 (2015) 7365–7370.
- [243] T. Wang, J. Zhuo, K. Du, B. Chen, Z. Zhu, Y. Shao, M. Li, Adv. Mater. 26 (2014) 3761-3766.
- [244] D.J. Li, U.N. Maiti, J. Lim, D.S. Choi, W.J. Lee, Y. Oh, G.Y. Lee, S.O. Kim, Nano Lett. 14 (2014) 1228-1233.
- [245] Y. Li, H. Wang, L. Xie, Y. Liang, G. Hong, H. Dai, J. Am. Chem. Soc. 133 (2011) 7296-7299.
- [246] G.D. Park, J.H. Kim, S.-K. Park, Y.C. Kang, ACS Appl. Mater. Interfaces 9 (2017) 10673-10683
- [247] B. Han, Y.H. Hu, Energy Sci. Eng. 4 (2016) 285-304.
- [248] X.-L. Yin, G.-Y. He, B. Sun, W.-J. Jiang, D.-J. Xue, A.-D. Xia, L.-J. Wan, J.-S. Hu, Nano Energy 28 (2016) 319-329.
- [249] T. An, Y. Wang, J. Tang, W. Wei, X. Cui, A.M. Alenizi, L. Zhang, G. Zheng, J. Mater. Chem. A 4 (2016) 13439-13443.
- [250] M.-R. Gao, J.-X. Liang, Y.-R. Zheng, Y.-F. Xu, J. Jiang, Q. Gao, J. Li, S.-H. Yu, Nat. Commun. 6 (2015) 5982.
- [251] Lawrence Livermore National Laboratory, Energy Flow Charts: Charting the Complex Relationships among Energy, Water, and Carbon, (2015) https:// flowcharts.llnl.gov/, (accessed 5 Jan 2018).
- [252] G.J. Snyder, E.S. Toberer, Nat. Mater. 7 (2008) 105.
- [253] D.-Y. Chung, T.P. Hogan, M. Rocci-Lane, P. Brazis, J.R. Ireland, C.R. Kannewurf, M. Bastea, C. Uher, M.G. Kanatzidis, J. Am. Chem. Soc. 126 (2004) 6414–6428.
- [254] G. Zhang, Y.-W. Zhang, J. Mater. Chem. C 5 (2017) 7684-7698.
- [255] D. Wickramaratne, F. Zahid, R.K. Lake, J. Chem. Phys. 140 (2014) 124710.
- [256] M.-J. Lee, J.-H. Ahn, J.H. Sung, H. Heo, S.G. Jeon, W. Lee, J.Y. Song, K.-H. Hong, B. Choi, S.-H. Lee, M.-H. Jo, Nat. Commun. 7 (2016) 12011.
- [257] Z. Jin, Q. Liao, H. Fang, Z. Liu, W. Liu, Z. Ding, T. Luo, N. Yang, Sci. Rep. 5 (2015) 18342.
- [258] S. Kumar, U. Schwingenschlögl, Chem. Mater. 27 (2015) 1278-1284.
- [259] M. Buscema, M. Barkelid, V. Zwiller, H.S.J. van der Zant, G.A. Steele, A. Castellanos-Gomez, Nano Lett. 13 (2013) 358-363.
- [260] M. Yoshida, T. Iizuka, Y. Saito, M. Onga, R. Suzuki, Y. Zhang, Y. Iwasa, S. Shimizu, Nano Lett. 16 (2016) 2061-2065.
- [261] J. Pu, K. Kanahashi, N.T. Cuong, C.-H. Chen, L.-J. Li, S. Okada, H. Ohta, T. Takenobu, Phys. Rev. B Condens. Matter Mater. Phys. 94 (2016) 014312.
- [262] K. Hideki, S. Mitsunari, O. Ryotaro, M. Yutaka, Y. Yohei, Y. Kazuhiro, Appl. Phys. Express 10 (2017) 015001.
- [263] Z. Zhang, Y. Xie, Q. Peng, Y. Chen, Sci. Rep. 6 (2016) 21639.

- [264] S. Yang, J. Si, Q. Su, H. Wu, Mater. Lett. 193 (2017) 146–149.
- [265] X. Yannan, C. Ting-Mao, Y. Weifeng, H. Minghui, Z. Yingru, L. Ning, L. Zong-Hong, Semicond. Sci. Technol. 32 (2017) 044003.
- [266] T. Wang, C. Liu, F. Jiang, Z. Xu, X. Wang, X. Li, C. Li, J. Xu, X. Yang, PCCP 19 (2017) 17560-17567.
- [267] T. Wang, C. Liu, X. Wang, X. Li, F. Jiang, C. Li, J. Hou, J. Xu, J. Polym. Sci. B Polym. Phys. 55 (2017) 997-1004.
- [268] S. Kong, T. Wu, M. Yuan, Z. Huang, Q.-L. Meng, Q. Jiang, W. Zhuang, P. Jiang, X. Bao, J. Mater. Chem. A 5 (2017) 2004-2011.
- [269] S. Li, C. Xin, X. Liu, Y. Feng, Y. Liu, J. Zheng, F. Liu, Q. Huang, Y. Qiu, J. He, J. Luo, F. Pan, Nano Energy 30 (2016) 780-789.
- [270] C. Wan, Y. Wang, N. Wang, W. Norimatsu, M. Kusunoki, K. Koumoto, J. Electron. Mater. 40 (2011) 1271-1280.
- [271] C. Wan, X. Gu, F. Dang, T. Itoh, Y. Wang, H. Sasaki, M. Kondo, K. Koga, K. Yabuki, G.J. Snyder, R. Yang, K. Koumoto, Nat. Mater. 14 (2015) 622
- [272] Y. Xu, R. Yi, B. Yuan, X. Wu, M. Dunwell, Q. Lin, L. Fei, S. Deng, P. Andersen, D. Wang, H. Luo, J. Phys. Chem. Lett. 3 (2012) 309-314.
- [273] K. Chang, W. Chen, Chem. Commun. 47 (2011) 4252-4254.
- [274] Y. Liu, Y. Zhao, L. Jiao, J. Chen, J. Mater. Chem. A 2 (2014) 13109-13115.
- [275] Y. Teng, H. Zhao, Z. Zhang, Z. Li, Q. Xia, Y. Zhang, L. Zhao, X. Du, Z. Du, P. Lv, K. Świerczek, ACS Nano 10 (2016) 8526–8535.
- [276] H. Li, K. Yu, H. Fu, B. Guo, X. Lei, Z. Zhu, J. Phys. Chem. C 119 (2015) 7959-7968.
- [277] J. Yao, B. Liu, S. Ozden, J. Wu, S. Yang, M.-T.F. Rodrigues, K. Kalaga, P. Dong, P. Xiao, Y. Zhang, R. Vajtai, P.M. Ajayan, Electrochim. Acta 176 (2015) 103-111.
- [278] D.P. Mumukshu, C. Eunho, C. Nitin, K. Chiwon, L. Wonki, H. Jun Yeon, C. Wonbong, Nanotechnology 27 (2016) 495401.
- [279] H. Yoo, A.P. Tiwari, J. Lee, D. Kim, J.H. Park, H. Lee, Nanoscale 7 (2015) 3404-3409.
- [280] Q. Wang, J. Li, J. Phys. Chem. C 111 (2007) 1675-1682.
- [281] Y.M. Chen, X.Y. Yu, Z. Li, U. Paik, X.W. Lou, Sci. Adv. 2 (2016) e1600021.
- [282] Y. Idota, T. Kubota, A. Matsufuji, Y. Maekawa, T. Miyasaka, Science 276 (1997) 1395-1397.
- [283] B. Qu, Y. Sun, L. Liu, C. Li, C. Yu, X. Zhang, Y. Chen, Sci. Rep. 7 (2017) 42772.
- [284] Y. Lou, D. He, Z. Wang, Y. Hu, Y. Shen, J. Ming, J. Chen, Chem. Eng. J. 313 (2017) 1269-1277.
- [285] N. Nitta, F. Wu, J.T. Lee, G. Yushin, Mater. Today 18 (2015) 252-264.
- [286] M.D. Slater, D. Kim, E. Lee, C.S. Johnson, Adv. Funct. Mater. 23 (2013) 947-958
- [287] Y. Liu, H. Kang, L. Jiao, C. Chen, K. Cao, Y. Wang, H. Yuan, Nanoscale 7 (2015) 1325-1332.
- [288] S. Wenzel, T. Hara, J. Janek, P. Adelhelm, Energy Environ. Sci. 4 (2011) 3342-3345
- [289] Z. Zhang, X. Yang, Y. Fu, RSC Adv. 6 (2016) 12726–12729.
 [290] Z. Hu, L. Wang, K. Zhang, J. Wang, F. Cheng, Z. Tao, J. Chen, Angew. Chem. 126 (2014) 13008-13012.
- [291] L. David, R. Bhandavat, G. Singh, ACS Nano 8 (2014) 1759-1770.
- [292] X. Xie, Z. Ao, D. Su, J. Zhang, G. Wang, Adv. Funct. Mater. 25 (2015) 1393-1403.
- [293] D. Su, S. Dou, G. Wang, Chem. Commun. 50 (2014) 4192–4195.[294] S.H. Choi, Y.N. Ko, J.-K. Lee, Y.C. Kang, Adv. Funct. Mater. 25 (2015) 1780-1788
- [295] S.H. Choi, Y.C. Kang, Nanoscale 8 (2016) 4209-4216.
- [296] Z. Zhang, X. Yang, Y. Fu, K. Du, J. Power Sources 296 (2015) 2–9.
- [297] X. Xiong, W. Luo, X. Hu, C. Chen, L. Qie, D. Hou, Y. Huang, Sci. Rep. 5 (2015) 9254.
- [298] X. Yang, Z. Zhang, Y. Fu, Q. Li, Nanoscale 7 (2015) 10198-10203.
- [299] Z. Zhang, X. Zhao, J. Li, Electrochim. Acta 176 (2015) 1296-1301.
- [300] B. Ahmed, D.H. Anjum, M.N. Hedhili, H.N. Alshareef, Small 11 (2015) 4341-4350.
- [301] W. Ren, W. Zhou, H. Zhang, C. Cheng, ACS Appl. Mater. Interfaces 9 (2017) 487-495
- [302] J. Li, Y. Hou, X. Gao, D. Guan, Y. Xie, J. Chen, C. Yuan, Nano Energy 16 (2015) 10 - 18
- [303] F. Qi, J. He, Y. Chen, B. Zheng, Q. Li, X. Wang, B. Yu, J. Lin, J. Zhou, P. Li, W.
- Zhang, Y. Li, Chem. Eng. J. 315 (2017) 10–17. [304] Y. Zhang, Z. Liu, H. Zhao, Y. Du, RSC Adv. 6 (2016) 1440–1444.
- [305] B. Qu, C. Ma, G. Ji, C. Xu, J. Xu, Y.S. Meng, T. Wang, J.Y. Lee, Adv. Mater. 26 (2014) 3854-3859.
- [306] Y. Lu, N. Zhang, S. Jiang, Y. Zhang, M. Zhou, Z. Tao, L.A. Archer, J. Chen, Nano Lett. 17 (2017) 3668-3674.
- [307] G. Ji, Y. Yu, Q. Yao, B. Qu, D. Chen, W. Chen, J. Xie, J.Y. Lee, NPG Asia Mater. 8 (2016) e247.
- [308] Y. Huang, C. Ji, Q. Pan, X. Zhang, J. Zhang, H. Wang, T. Liao, Q. Li, J. Alloys Compd. 728 (2017) 1139-1145.
- [309] G. Wang, J. Peng, L. Zhang, J. Zhang, B. Dai, M. Zhu, L. Xia, F. Yu, J. Mater. Chem. A 3 (2015) 3659-3666.
- [310] J. Liu, M. Gu, L. Ouyang, H. Wang, L. Yang, M. Zhu, ACS Appl. Mater. Interfaces 8 (2016) 8502-8510.
- [311] Y. Li, Y. Liang, F.C. Robles Hernandez, H. Deog Yoo, Q. An, Y. Yao, Nano Energy 15 (2015) 453-461. [312] H. Wang, H. Jiang, Y. Hu, N. Li, X. Zhao, C. Li, J. Mater. Chem. A 5 (2017)
- 5383-5389 [313] Y. Zhu, Y. Chu, J. Liang, Y. Li, Z. Yuan, W. Li, Y. Zhang, X. Pan, S.-L. Chou, L.
- Zhao, R. Zeng, Electrochim. Acta 190 (2016) 843-851. [314] G. Li, L. Yu, H. Hu, Q. Zhu, Y. Wang, Y. Yu, Electrochim. Acta 212 (2016) 59-67.

- [315] W.-H. Ryu, H. Wilson, S. Sohn, J. Li, X. Tong, E. Shaulsky, J. Schroers, M. Elimelech, A.D. Taylor, ACS Nano 10 (2016) 3257–3266.
- [316] J.-Y. Liao, A. Manthiram, Nano Energy 18 (2015) 20-27.
- [317] D. Chen, G. Ji, B. Ding, Y. Ma, B. Qu, W. Chen, J.Y. Lee, Ind. Eng. Chem. Res. 53 (2014) 17901–17908.
- [318] B. Hou, X. Wang, J. Wang, J. Yao, H. Zhang, W. Yu, G. Liu, X. Dong, L. Wang, RSC Adv. 7 (2017) 6309–6314.
- [319] S.H. Choi, Y.C. Kang, ACS Appl. Mater. Interfaces 7 (2015) 24694–24702.
- [320] Y. Jiang, Y. Guo, W. Lu, Z. Feng, B. Xi, S. Kai, J. Zhang, J. Feng, S. Xiong, ACS Appl. Mater. Interfaces 9 (2017) 27697–27706.
- [321] B. Mendoza-Sánchez, Y. Gogotsi, Adv. Mater. 28 (2016) 6104-6135.
- [322] J.M. Soon, K.P. Loh, Electrochem. Solid-State Lett. 10 (2007) A250-A254.
- [323] Y. Yang, H. Fei, G. Ruan, C. Xiang, J.M. Tour, Adv. Mater. 26 (2014) 8163–8168.
- [324] N. Choudhary, C. Li, J. Moore, N. Nagaiah, L. Zhai, Y. Jung, J. Thomas, Adv. Mater. 29 (2017) 1605336.
- [325] N. Choudhary, C. Li, H.-S. Chung, J. Moore, J. Thomas, Y. Jung, ACS Nano 10 (2016) 10726–10735.
- [326] K.-J. Huang, L. Wang, Y.-J. Liu, H.-B. Wang, Y.-M. Liu, L.-L. Wang, Electrochim. Acta 109 (2013) 587–594.
- [327] H. Tang, J. Wang, H. Yin, H. Zhao, D. Wang, Z. Tang, Adv. Mater. 27 (2015) 1117–1123.
- [328] J. Zhu, W. Sun, D. Yang, Y. Zhang, H.H. Hoon, H. Zhang, Q. Yan, Small 11 (2015) 4123–4129.
- [329] K.-J. Huang, L. Wang, J.-Z. Zhang, L.-L. Wang, Y.-P. Mo, Energy 67 (2014)
- [330] Y. Luo, Y. Zhang, Y. Zhao, X. Fang, J. Ren, W. Weng, Y. Jiang, H. Sun, B. Wang, X. Cheng, H. Peng, J. Mater. Chem. A 3 (2015) 17553–17557.
- [331] M.A. Bissett, I.A. Kinloch, R.A.W. Dryfe, ACS Appl. Mater. Interfaces 7 (2015) 17388–17398.
- [332] L. Zijiong, Z. Ying, Z. Weiyang, Mater. Res. Express 4 (2017) 055018.
- [333] A.K. Thakur, A.B. Deshmukh, R.B. Choudhary, I. Karbhal, M. Majumder, M.V. Shelke, Mater. Sci. Eng. B 223 (2017) 24–34.
- [334] S. Wang, J. Zhu, Y. Shao, W. Li, Y. Wu, L. Zhang, X. Hao, Chem. Eur. J. 23 (2017) 3438–3446.
- [335] S. Ratha, C.S. Rout, ACS Appl. Mater. Interfaces 5 (2013) 11427–11433.
- [336] E.G. da Silveira Firmiano, A.C. Rabelo, C.J. Dalmaschio, A.N. Pinheiro, E.C. Pereira, W.H. Schreiner, E.R. Leite, Adv. Energy Mater. 4 (2014) 1301380.
- [337] K. Singh, S. Kumar, K. Agarwal, K. Soni, V. Ramana Gedela, K. Ghosh, Sci. Rep. 7 (2017), 9458.
- [338] B. Hu, X. Qin, A.M. Asiri, K.A. Alamry, A.O. Al-Youbi, X. Sun, Electrochim. Acta 100 (2013) 24–28.
- [339] X. Shang, J.-Q. Chi, S.-S. Lu, J.-X. Gou, B. Dong, X. Li, Y.-R. Liu, K.-L. Yan, Y.-M. Chai, C.-G. Liu, Appl. Surf. Sci. 392 (2017) 708–714.
- [340] S. Wen, Y. Liu, F. Zhu, R. Shao, W. Xu, Appl. Surf. Sci. 428 (2018) 616–622.
- [341] L. Fang, Y. Qiu, T. Zhai, F. Wang, M. Lan, K. Huang, Q. Jing, Colloids Surf. A 535 (2017) 41–48.
- [342] L. Wang, X. Zhang, Y. Ma, M. Yang, Y. Qi, J. Phys. Chem. C 121 (2017) 9089–9095.
- [343] H. Peng, J. Zhou, K. Sun, G. Ma, Z. Zhang, E. Feng, Z. Lei, ACS Sustain. Chem. Eng. 5 (2017) 5951–5963.
- [344] D.K. Nandi, S. Sahoo, S. Sinha, S. Yeo, H. Kim, R.N. Bulakhe, J. Heo, J.-J. Shim, S.-H. Kim, ACS Appl. Mater. Interfaces 9 (2017) 40252–40264.
- [345] Z. Wu, L. Xie, Y. Xiao, D. Wang, J. Alloys Compd. 708 (2017) 763–768.
- [346] N. Savjani, E.A. Lewis, M.A. Bissett, J.R. Brent, R.A.W. Dryfe, S.J. Haigh, P. O'Brien, Chem. Mater. 28 (2016) 657–664.
- [347] X. Li, C. Zhang, S. Xin, Z. Yang, Y. Li, D. Zhang, P. Yao, ACS Appl. Mater. Interfaces 8 (2016) 21373–21380.
- [348] M. Chhowalla, D. Voiry, J. Yang, H.S. Shin, K.P. Loh, MRS Bull. 40 (2015) 585–591.
- [349] D. Huo, J. Zhang, H. Wang, X. Ren, C. Wang, H. Su, H. Zhao, Nanoscale Res. Lett. 12 (2017) 465.
- [350] M. Xie, S. Zhang, B. Cai, Y. Gu, X. Liu, E. Kan, H. Zeng, Nano Energy 38 (2017) 561–568.



Nitin Choudhary is currently a postdoctoral scholar in Dr. Jung's group at the NanoScience Technology Center of the University of Central Florida. He graduated from the Indian Institute of Technology (India) in experimental condensed matter physics. His current research focus is on the large area growth of 2D materials for electronics and energy applications.



Md Ashraful Islam received his Master's degree in Electrical Engineering from University of Tulsa, Oklahoma, USA (2015). He is currently a Ph.D. candidate of Electrical Engineering at the University of Central Florida, USA under the supervision of Dr. Jung. His research interests include the growth, fabrication, and characterization of 2D materials for stretchable electronics and bio applications.



Jung Han Kim received his Ph.D. degree in Materials Science and Engineering from Seoul National University in South Kore. Currently, he is a post-doctoral research scholar working with Dr. Jung at the NanoScience Technology Center, University of Central Florida. His research interests include studying nanoscale structure-property relationships in various nanomaterials and developing 2D TMDs-based flexible electronic devices.



Tae-Jun Ko is currently a postdoctoral scholar in Dr. Jung's group at the NanoScience Technology Center of the University of Central Florida. He received his Ph.D. degree in Materials Science and Engineering from Seoul National University, South Korea. His current research focus is on the growth control and characterizations of 2D materials for electronics and oil-water separation applications.



Anthony Schropp is an undergraduate in the Chemistry Department at the University of Central Florida. His focus area is in electrochemical and semiconducting nanomaterials. Currently, he performs research at the Nanoscience Technology Center under the supervision of Dr. Jung



Luis Hurtado is an undergraduate student at the University of Central Florida with major in Electrical Engineering. He works on the synthesis of 2D TMDs, focusing on their electrochemical properties for high performing energy storage devices.



Dylan Weitzman is pursuing a Bachelor's in Physics from the University of Central Florida College of Sciences. He is currently working with Dr. Jung at the Nanoscience Technology Center, and his research interests are in 2D MoS_2 growth on exotic substrates for oil/water separation, sensors and supercapacitors.



Dr. Lei Zhai is currently a professor at the NanoScience Technology Center, University of Central Florida with joint appointments in the departments of Chemistry and Materials Science & Engineering. He obtained his Ph.D. at Carnegie Mellon University and worked at Massachusetts Institute of Technology as a postdoctoral associate before joining UCF in 2005. He is an NSF CAREER awardee. His research focuses on conjugated polymer supramolecular structures and composites for energy conversion and storage, and polymer derived ceramics.



Dr. Yeonwoong Jung is an assistant professor at the NanoScience Technology Center with joint appointments in Materials Science & Engineering and Electrical & Computer Engineering of the University of Central Florida. He obtained his Ph.D. in Materials Science & Engineering from the University of Pennsylvania and completed postdoctoral training at the Yale University. His research focuses on the growth and characterization of low dimensional (1D, 2D) materials to explore their extraordinary properties for transformative technologies in energy and electronic applications.